FINITE ELEMENT INVESTIGATION OF A COMPOSITE CYLINDRICAL SHELL UNDER TRANSVERSE LOAD WITH THROUGH THICKNESS SHEAR AND SNAPPING

THESIS

Kevin J. Silva
Captain, USAF

AFIT/GAE/ENY/89D-35

DEPARTMENT OF THE AIR FORCE
AIR UNIVERSITY
AIR FORCE INSTITUTE OF TECHNOLOGY

Wright-Patterson Air Force Base, Ohio

AFIT/GAE/ENY/89D-35

FINITE ELEMENT INVESTIGATION OF A COMPOSITE CYLINDRICAL SHELL UNDER TRANSVERSE LOAD WITH THROUGH THICKNESS SHEAR AND SNAPPING

THESIS

Kevin J. Silva
Captain, USAF

AFIT/GAE/ENY/89D-35

AFIT/GAE/ENY/89D-35

FINITE ELEMENT INVESTIGATION OF A COMPOSITE CYLINDRICAL SHELL UNDER TRANSVERSE LOAD WITH THROUGH THICKNESS SHEAR AND SNAPPING

THESIS

Presented to the faculty of the School of Engineering

of the Air Force Institute of Technology

Air University

in Partial Fulfillment of the Requirements

for the Degree of

Master of Science in Aeronautical Engineering

Kevin J. Silva, B.S.

Captain, USAF

December 1989

Acknowledgements

This thesis is part of a research project on the static and dynamic response of composite shells sponsored by the Air Force Office of Scientific Research, Dr. Anthonoy Amos contract monitor, Dr. Anthony Palazotto, AFIT/ENY, principal investigator.

Thanks go to Dr. Palazotto for his patient guidance in this research; Captain Scott Dennis (Ph.D.) who authored the computer code used in my investigations; and Dr. C.T. Tsai who both programmed the solution algorithm and provided helpful hints on its operation. Special thanks go to my wife and daughters for keeping me in touch with reality at home.

Contents

	Page
Acknowledgements	ii
List of Figures	iv
List of Tables	vi
List of Symbols	vii
Abstract	ix
I. Introduction	1-1
Analytical Method	1-2
Previous Work	1-3
Current Work	1-9
II. Theory	2-1
Geometry and Assumptions	2-2
Constitutive Development	2-3
Kinematic Development	2-9
Potential Energy	2-16
The 36 DOF Element	2-18
Finite Element Formulation	2-21
Solution Algorithm	2-22
Failure Criterion	2-27
III. Analytical Model Preparation	3-1
Parameters and Ranges of Variation	3-1
Convergence Tests	3-3
IV. Results/Discussion	4-1
The Initial Snap Through	4-2
Comparison to Isotropic	4-6
Variation of the Parameters	4-15
Laminate Failure	4-32
V. Conclusions/Recommendations	5-1
Appendix A: Load/Displacement Data	A-1
Appendix B: Plots of Thickness Variance	B-1
Appendix C: Deformation Histories	C-1
Bibliography	R-1
Vita	V-1

List of Figures

Figure		Page
2-1	Cylindrical Shell Geometry	2-3
2-2	Fiber-Reinforced Lamina Definitions	2-4
2-3	SHELL 36 Degree of Freedom Element	2-18
2-4	Riks Method Solution Step	2-25
3-1	Study Parameters	3-2
3-2	Load vs w, Cross Ply Quarter Panel Test	3-5
3-3	Load vs w, Angle Ply Quarter Panel Test	3-5
3-4	Quarter Panel vs Full Panel End Profile	3-6
3-5	w vs Active DOF, 1 Radian Mesh Test	3-7
3-6	Load vs w, 1/2 Radian Mesh Test	3-8
3-7	w vs Active DOF, 1/4 Radian Mesh Test	3-9
3-8	Donnell vs Exact, 1 Radian $[0_6/90_6]_s$ Panel	3-10
3-9	Deformed Geometry, Laminated, Donnell Element	3-11
3-10	Deformed Geometry, Laminated, Large D&R Element	3-11
3-11	Donnell vs Exact, 1 Radian Isotropic Panel	3-13
3-12	Deformed Geometry, Isotropic, Donnell Element	3-14
3-13	Deformed Geometry, Isotropic, Large D&R Element	3-14
4-1	Laminate Definitions	4-7
4-2	Response Normalized to Bending Stiffness	4-10
4-3	w at Peak Load vs Shallowness, Hinged $[0/90]_s$	4-22
4-4	Transverse Shear Strain vs Shallowness	4-24
4-5	w at Peak Load vs Thickness, Hinged $[0/90]_s$	4-29
4-6	Transverse Shear Strain vs Thickness	4-31
A-1	Load vs Displacement, 8 Ply 1/4 Radian Shell	A-2

A-2 Load vs Displacement, 24 Ply 1/4 Radian Shell A-3

A-3 Load vs Displacement, 48 Ply 1/4 Radian Shell A-4

A-4 Load vs Displacement, 96 Ply 1/4 Radian Shell A-5

A-5 Load vs Displacement, 8 Ply 1/2 Radian Shell A-6

A-6 Load vs Displacement, 24 Ply 1/2 Radian Shell A-7

A-7 Load vs Displacement, 48 Ply 1/2 Radian Shell A-8

A-8 Load vs Displacement, 96 Ply 1/2 Radian Shell A-9

A-9 Load vs Displacement, 8 Ply 1 Radian Shell A-10

A-10 Load vs Displacement, 24 Ply 1 Radian Shell A-11

A-11 Load vs Displacement, 48 Ply 1 Radian Shell A-12

A-12 Load vs Displacement, 96 Ply 1 Radian Shell A-13

B-1 Effect of Thickness, Clamped $[0/\mp 45/90]_s$ 1/4 Rad ... B-2

B-2 Effect of Thickness, Hinged $[0/\mp 45/90]_s$ 1/4 Rad B-3

B-3 Effect of Thickness, Clamped $[0/90]_s$ 1/2 Rad B-4

B-4 Effect of Thickness, Hinged $[0/90]_s$ 1/2 Rad B-5

B-5 Effect of Thickness, Clamped $[0/\mp 45/90]_s$ 1 Rad B-6

B-6 Effect of Thickness, Hinged $[0/90]_s$ 1 Rad B-7

C-1 Contours, $[0_{24}/90_{24}]_s$ Clamped 1/2 Radian Shell C-2

C-2 Contours, $[0_{24}/90_{24}]_s$ Hinged 1/2 Radian Shell C-3

C-3 Contours, $[0_{12}/\mp 45_{12}/90_{12}]_s$ Hinged 1/2 Rad Shell C-4

C-4 Contours, $[0_6/90_6]_s$ Clamped 1 Radian Shell C-5

C-5 Contours, $[0_6/90_6]_s$ Hinged 1 Radian Shell C-6

C-6 Contours, $[0_3/\mp 45_3/90_3]_s$ Clamped 1 Radian Shell C-7

C-7 Contours, $[0_3/\mp 45_3/90_3]_s$ Hinged 1/2 Radian Shell C-8

List of Tables

Table		Page
2-1	Contracted Notation	2-4
4-1	[0/90]s Stiffness Parameters	4-8
4-2	[0/∓45/90]s Stiffness Parameters	4-9
4-3	Shell Material Effect on Transverse Shear	4-11
4-4	Boundary Effect on Transverse Shear	4-18
4-5	Thickness/Central Rise Parameter	4-20
4-6	Shallowness Effect on Transverse Shear	4-23
4-7	Thickness Effect on Transverse Shear	4-30

List of Symbols

A, D, F	linear and two higher order stiffness matrices
a, b	isoparametric element half dimensions in ξ, η directions (Chapter 2)
b	half chord length of open cylindrical shell (Chapters 3, 4, 5)
C_{ij}	unreduced constitutive matrix term
δ	open shell central rise over chordline
E	Young's (elastic) modulus
ε, ε°	strain, strain of middle surface
$\mathfrak{E}$, $\mathfrak{E}^{\circ}$	vector of ε, ε° strain terms
G	shear modulus
$\mathcal{H}$	Hermetian shape function
h	shell thickness
h_i	general coordinate system scale factors
K, N_1, N_2	constant, first and higher order stiffness matrices
K_T	tangent stiffness matrix
N, Q	linear, quadratic Lagrangian shape functions
P	applied load (vector)
Q_{ij}	lamina reduced stiffness matrix element
$\bar{Q}_{ij}$	transfomed reduced lamina stiffness
q	nodal displacement vector
R	radius of curvature
S	ply ultimate shear stress in plane of fibers
Δs	increment along equilibrium path for Riks solver
T	transformation matrix
U	strain energy

u	longitudinal (x-axis) displacement
V	work done by external forces
v	circumferential (s-axis) displacement
u°, v°, w	displacement of datum surface
w	transverse (z-axis) displacement
X_T, X_C	ply ultimate tensile, compressive stress along fiber axis
Y_T, Y_C	ply ultimate tensile, compressive stress 90° to fiber axis
θ	opening angle of cylindrical panel arc
ϕ	angle of ply fibers to shell x-axis
ψ_i	shear deformation of shell normal about i axis at middle surface
$\varkappa_{ij}$	out-of-plane strain terms
$\mathcal{K}$	matrix of out-of-plane strain terms $\varkappa_{ij}$
Π_p	potential energy
ξ, η	isoparametric x, s coordinates
υ	Poisson's ratio
σ	stress
Ω	shell middle surface designator
λ_i	load fraction for solution step i

Abstract

The static response of a circular cylindrical open shell (curved panel) constructed of an orthotropic graphite/epoxy laminate is numerically investigated. The shell is subjected to an inward point load, centered on and normal to the shell surface, which maintains its original orientation through deformation (i.e. dead load). The shell displacement response is seen to vary widely with shell geometry and boundary conditions, not only in magnitude of deformation but also in the nature and progression of the collapse under critical load.

The finite element analysis is conducted with a quasi-two dimensional thin shell element which incorporates parabolic transverse shear stress through the thickness. The element can be formulated with either large displacement/ rotation kinematics or the simpler Donnell relations.

To enable tracking through critical load and displacement points and investigation of the post-critical regime, a solution algorithm other than the popular Newton-Raphson technique with displacement control or load control is required. The algorithm employed here uses a modified Riks/Wempner technique. It allows continuous tracing of the load - deflection response through critical load and critical displacement points. Step size is automatically scaled to follow the solution path closely in the areas of large load or displacement changes which surround critical points.

Several parameters are independently varied in order to isolate their affect on structural response. Two symmetric ply layups are considered, [0/90]s and [0/-45/+45/90]s, in addition to an isotropic panel. Shell thickness ranges from 0.040 inch (8 ply) to 0.480 inch (96 ply). Shallowness is altered by varying the arc length of the panel. Values of (height)/(half chord) range from 0.063 to 0.255. The panel is constrained only along the straight edges; both hinged and clamped conditions are examined. Common to all cases is panel length and radius of curvature, and ply material properties.

To assess the imprecision of the Donnell theory when undergoing large displacements and rotations, several cases are solved with both formulations. Errors are seen to be negligible on the load up portion of the analysis, but the Donnell solution becomes appreciably stiffer during collapse when rotation of the shell middle surface exceeds 15 degrees.

FINITE ELEMENT INVESTIGATION OF A COMPOSITE CYLINDRICAL SHELL UNDER TRANSVERSE LOAD WITH THROUGH THICKNESS SHEAR AND SNAPPING

I. INTRODUCTION

Laminated composites offer numerous benefits over metals as structural materials. The composite's high strength to weight ratio and damage tolerance are especially valuable in aerospace applications. Despite the benefits, however, composites have been slow to gain acceptance in the design and construction of primary load carrying structures. A key cause of this reluctance is that the analytical and experimental investigations of the behavior of laminated composites under the wide range of load and environmental conditions to which structural members are subject is less than comprehensive. Another important consideration is that while laminated composites are physically well suited for thin shell applications, structurally optimizing a shell leaves it susceptible to buckling and collapse, and especially sensitive to transverse loads. The purpose of this research is to investigate numerically the static structural response of a laminated graphite/epoxy composite cylindrical shell (curved panel) subjected to a transverse normal point load.

Analytical Method

The computer program SHELL was used exclusively in this research. It was developed by Dennis (9) in order to incorporate the effects of through thickness shear stress when analyzing isotropic or laminated plates and cylindrical shells. While ignoring these particular stresses yields acceptable accuracy when analyzing thin isotropic structures, laminated material of like thickness may respond quite differently due to the coupling of extensional, bending and shear strains arising from ply angular orientation. Including transverse shear in design analyses will allow greater exploitation of composite's benefits through increased precision.

The most general type of analysis would incorporate both material and geometric nonlinearity. In structural applications, materials are normally restricted to the linear elastic region, so material linearity has been assumed in this work. This implies that any fiber or ply breakage during large transverse displacements and rotations is ignored. Geometric nonlinearity is unavoidable in the analysis of a three-dimensional curved structure, though.

SHELL offers two strain-displacement formulation options for the cylindrical shell finite element. The exact equations relating displacement to strain for a curved layered panel are quite complex and create a cumbersome computer program, but they are available. If the transverse displacement is small compared to the shell thickness, but large compared to the in-plane deformations, several terms in the strain - displacement equations can be neglected, resulting in a less complex solution set. For flat plates, such a simplification yields

the von Karman plate equations; for cylindrical shells, the corresponding relations are the Donnell equations. These constitute the other solution method option available in SHELL.

In either solution option, a parabolic distribution of transverse shear strain is included in the formulation via the displacement equations. Love theory and its offshoots (17) effectively ignore transverse shear effects.

The computational efficiency afforded by Donnell's simplifications is attractive, so several comparisons of early runs were made between the Donnell solution and the large displacement/rotation formulation solution. As shown in Chapter 3, the Donnell simplifications did not appreciably degrade accuracy until the shell collapsed, developing large deformations and rotations. These findings were supported by Hoff (14) who found those terms discarded by Donnell to be negligible for this geometry as long as displacements are small.

To summarize, the class of problems studied in this work is one of large displacements and rotations but small strains (so that linear elastic material behavior is retained). The Donnell - based analysis is used when possible (small rotations, as determined in Chapter 3). Through thickness shear effects are incorporated.

Previous Work

Engineering analysis of general shell structures dates back not more than a century. Although Simmonds (35) notes that A. E. Love in 1920 published a set of equations for circular cylindrical thin shell midsurface displacement, credit is usually given to W. Flügge for first

presenting the relations in a 1932 paper, "Die Stabilität der Kreiszylinderschale" (Ingenieur-Archiv, 3, pp. 463-506).

Simplification and specialization of Flügge's equations to the simpler cylindrical shell relations was accomplished in the following year by L. H. Donnell (11). He determined (both analytically and experimentally) that circumferentially trigonometric deformations with small wavelengths allow one to discard several terms in the curvature and twist equations. The complexity of the resulting expressions are on the order of the von Karman plate equations, making them tractable for engineering analysis. The primary restriction is that the transverse deformation must have a small circumferential wavelength compared to the cylinder radius, or accuracy suffers. The implication of this is that rotations of the midsurface must be small for accurate results, as is noted in the results in Chapter 3.

Several attempts have been made to improve on the accuracy and utility of the Donnell equations without increasing complexity too much. Morely (19), Knowles and Reissner (18) and others offered improvements of the same order of accuracy by retaining various terms neglected by Donnell. Some increase in applicability is gained, but, as Koiter points out, any attempt to improve upon the *order* of accuracy of Donnell's relations is doomed to failure since the order is set when the Love approximations are first applied. Thus a truly higher order theory must include features ignored in Love shell theory; namely, the effect of the transverse normal and shear stresses (17).

Sanders (32) nearly does this in his development of a first-order thin shell theory. His assumption that transverse shear strains are

negligible enables him to solve for the corresponding transverse shear stress resultants, partially incorporating transverse effects. One significant improvement over the theories based on Love's approximation is that by considering rotation of the shell normal, but neglecting rotations about this normal, Sanders' relations allow for small strain-free rigid body motion, which had long been an accepted inconsistency in Love's theory. Sanders offers his theory in both general form and reduced form for the circular cylindrical case; Simmonds (35) offers an alternate formulation of the theory, in which the governing equations are reduced to a single fourth order partial differential equation for the transverse normal displacement.

A variety of analytical solutions for first order isotropic shallow cylindrical shell theory have been published. Flügge and Elling (12) solved the case of normal surface loads. Their deformed geometry is mirrored by the results in this research. Chernyshev (5) also solved this case, and noted that the response was dominated by the bending terms of the governing equations (demonstrated in Chapter 4). Jahanshahi (15), Sanders (33) and Sanders and Simmonds (34) have all provided solutions to the shallow isotropic shell subject to various transverse loadings.

Isotropic cylindrical shell finite element analysis has been widely done. Most applicable to the present research is the work done by Sabir and Lock (31), which employed a solution algorithm capable of tracing post-buckling behavior by incrementing either load or displacement as required to avoid nnumerical singularity at critical points. Features of snapping, and thickness effects are shown. Sabir

and Lock used a two dimensional 20 DOF curved rectangular element in their analysis; Bergan et.al. compared very closely using a mesh of flat triangular elements (3). Ahmad, Irons and Zienkiewicz (1) developed a generally curved 20 DOF brick element which allowed for rotation of the normal to the shell surface. It could suffer from shear locking as thickness decreases, though, and hence neccessitated use of a shear correction factor.

First-order theory has recently been extended to laminated material. Chung and Widera's 1972 equations (6) reduce to those of Donnell when isotropy is enforced; the applicability of the laminated theory has the same restrictions on magnitude of deformations as Donnell. Chang and Kutlu (4) in 1989 used first-order finite element modeling in developing a progressive delamination/ply failure model for line loaded cylinders. Moser and Schmid (20), also in 1989, used a 20 DOF Ahmad-type element to analyze point loaded cylinders made of [±45] and [90/0/90] laminates. One conclusion was that the cross ply was stiffer than the angle ply shell; this is also discussed in Chapter 4.

All of the effort reported on up to this point was based on Love's first approximation, which is an acceptable simplification in the case of a thin elastic isotropic shell. The development of a higher order theory incorporating transverse effects was driven by the need to accurately analyze laminated composite shells with their relatively more severe transverse stresses. Comparable higher order theories incorporating first-order transverse effects have been presented for laminated shells by Reddy and Liu (25) and Dennis (9,10). This theory allows for fully nonlinear in-plane strains, but only linear transverse

shear strain - displacement relations. The acceptability of a linear transverse strain field in a nonlinear theory is explained by noting that transverse effects are small compared to the in-plane, so the even smaller higher-order terms of the already small transverse terms are negligible (9). With this theory, displacements due to shear stresses vary linearly through each ply thickness and are continuous from ply to ply in the laminate. Reddy also offers solutions to select cases of layup and geometry, primarily cross ply spherical shells (24).

Higher order (than linear) transverse shear effects have also been studied recently. Palazotto and Witt (22) maintained continuity of displacement and slope of the midsurface normal at ply boundaries. A trilinear element was formulated and shown to accurately model thick plate bending displacements and stresses. This triangular element could be readily applied to a general shell analysis. Hinrichsen and Palazotto (13) formulated a flat rectangular element which maintains continuity of the curvature of the deformed normal as well, by applying a cubic spline interpolation through the thickness. As expected, it also is very accurate for thick plates. Application to thin plates, however, surfaced problems. The authors explain that the solution does not converge to the elasticity solution for a thin plate since transverse shear strain does not disappear as thickness decreases, but transverse normal strain does (it is neglected from the outset) (21). This imbalance of transverse effects was felt to be the source of inaccuracy for thin plate. Application of either of the theories discussed in these papers to a general thin shell element is possible.

Analytical solutions of higher order theories is limited to very few ply layups (select symmetric and antisymmetric cross ply laminates), and load configurations. Ren (26,27) has obtained several interesting results for a semi-infinite cylindrical shell. He showed that for the case of cylindrical bending, the Donnell theory underpredicts displacement. For values of R/h greater than 20, though, the Donnell solution for transverse displacement is close and of constant bias with respect to R/h. No explanation is offered for the bias, but the increased bending stiffness is likely due to the missing rotational terms in the Donnell formulation. A second finding which illustrates conventional wisdom is the significant effect of ply stacking sequence. The magnitude of bending displacement for a $[90_4/0_4]$ was several times that of a $[90_2/0_4/90_2]$, although total thickness and ply count were equal. These results, however, are not easily generalized to the wide variety of problems which engineers encounter. Hence, numerical solution is the preferred approach for higher order composite analysis, due to the unmanageable mathematical complexity involved in the ply orientations and geometries of a real world structure.

The solution of geometrically nonlinear problems by the finite element method requires recalculation of the structure's stiffness matrix as it changes during deformation. The Newton-Raphson iteration method is widely used for such computations. Once the structure has reached a peak load, though, it has essentially zero stiffness, and inverting the stiffness matrix as required for load-controlled Newton-Raphson iteration to converge to the equilibrium solution is

impossible. Sabir and Lock (31) and others circumvented this difficulty by reformulating the equilibrium equations to step by displacement rather than load when a peak load was encountered, and using the usual load incrementing method to step through areas of zero or reversing incremental displacement. A robust solution algorithm without the need to swap between methods was developed by Riks (28,29) and Wempner (39), and applied to isotropic geometrically nonlinear structural problems by Crisfield (8). In it, a selected arc length of the equilibrium path is incremented rather than load or displacement. Since step size does not decrease to zero due to convergence to a peak load or peak displacement point as the former methods do, this technique steps past such singular areas and allows uninterrupted tracing of the equilibrium path (23). Tsai and Palazotto (38) have successfully applied this solution algorithm to the problem of snapping through of composite shell structures; a version of the code developed in that research is used in the present work.

Current Work

The subject of this research is the static response to a transverse point load of a class of laminated cylindrical shells. The layups studied here are a symmetric cross ply $[0/90]_s$ and a symmetric quasi-isotropic $[0/-45/45/90]_s$ laminate. No experiment or comparable numerical study could be found with which to compare results; hence, trends and general conclusions will be compared with conclusions in some of the studies referenced above. The computers used were a VAX 11/785 using the VMS operating system and an Elxsi 6400 running Unix.

II. Theory

In order to understand the theoretical basis for the data presented later, the details of the finite element formulation are now presented. The development of the relations governing cylindrical shell stress, strain and displacement is first presented. Employment of these equations in the finite element method is then shown, followed by the details of the 36 DOF element used for this work, and the solution algorithm employed in solving the static load case. A laminate failure criteria is also discussed, since very high load levels are achieved in this study. The end product of this section will be the finite element formulation for a laminated cylindrical shell incorporating a parabolic distribution of shear stress through the thickness.

Bathe and Ho (2) stated the following set of criteria for a desirable shell element:

1.) No spurious zero-energy modes should exist, so that reliable results can always be expected. No numerical fudge factors should be necessary, either.

2.) The element should be applicable to general shell structures, including those with beam stiffeners, cutouts, intersections, etc.

3.) The element should be cost-effective for linear as well as nonlinear static and dynamic analysis. This implies that the degrees of freedom is held to a minimum. It should allow

analysis of large displacement and large rotation problems, and materially nonlinear situations.

Criterion 1 is achieved in this formulation. The code has not been developed beyond the research stage, so application to other than plate and cylindrical shell cases modeled with rectangular elements is not yet possible. However, the underlying theory by which transverse shear is incorporated is not restricted geometrically, so criterion 2 is somewhat met. Material linearity is assumed in the formulation of the element, so criterion 3 is only partially fulfilled. The incorporation of through thickness shear effects in a shell structure, while maintaining a two dimensional analysis, well satisfies the first part of this criterion, however.

The following development applies specifically to cylindrical geometry. Dennis (9) presents the general case of a doubly curved shell.

Geometry and Assumptions

The curvilinear orthogonal coordinate system and nomenclature used in this formulation of the laminated cylindrical shell is shown in Figure 2-1. The shell has a radius of R, with a central angle θ. The x-axis is linear and oriented longitudinally, the s-axis follows the circumference, and the z-axis is everywhere normal to the shell middle surface, positive toward the center of curvature. The surface formed by the x and s axes lies in the center of the thickness of the panel, so the thickness coordinate is negative on the outer surface and positive on the inner surface. Displacements along the x, s and z axes

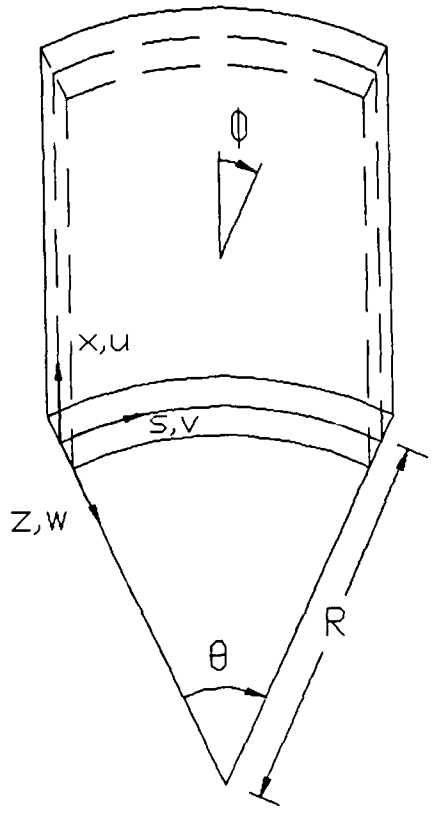

Figure 2-1. Cylindrical Shell Geometry

are u, v and w respectively. In the early vectorial development, the coordinate θ is used instead of s for simplicity; s is used when specializing to the cylindrical geometry. Since the structure analysedhere is an open shell, the angle θ is also useful for describing shallowness. The angle ϕ specifies the orientation of fibers of each ply in a laminate construction. Total thickness is denoted by h. Subscripts denoting stress and strain orientation are explained in Table 2-1 and Figure 2-2.

Constitutive Development

This research is limited to material response in the most simple linear regime, but complexity arises due to the directional response of

Table 2-1. Contracted Notation

stress		strain		cylindrical coordinates
explicit	contracted	explicit	contracted	
σ_{11}	σ_1	ε_{11}	ε_1	x → 1
σ_{22}	σ_2	ε_{22}	ε_2	s → 2
σ_{33}	σ_3	ε_{33}	ε_3	z → 3
σ_{23}	σ_4	$2\varepsilon_{23}$	ε_4	shear: s-z → 4
σ_{13}	σ_5	$2\varepsilon_{13}$	ε_5	x-z → 5
σ_{12}	σ_6	$2\varepsilon_{12}$	ε_6	x-s → 6

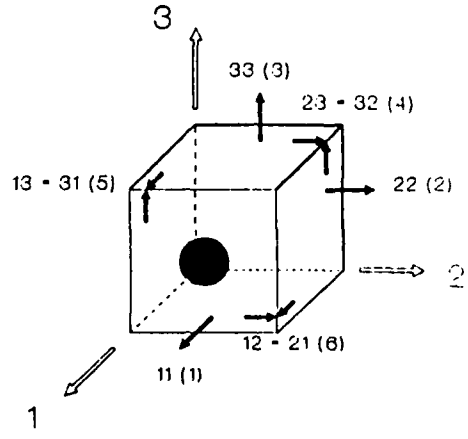

Figure 2-2. Fiber Reinforced Lamina Definitions

the oriented plies in the laminate. In this section the constitutive relations between stress and strain for a laminate of arbitrarily oriented transversely isotropic plies will be developed. The fundamental departure from the isotropic relations is the summation over the lamina thickness of the directional constitutive equation for each ply, arriving at the total laminate's effective stress-strain

relation. This section follows from the very readable references by Jones (16) and Dennis (9).

From basic strength of material relations, for isotropic material, stress σ and strain ε are related as

$$\sigma = E\varepsilon \tag{2-1}$$

with E being Young's modulus. For a general anisotropic material, Young's modulus can differ with different load orientations so this equation expands to

$$\begin{Bmatrix} \sigma_1 \\ \sigma_2 \\ \sigma_3 \\ \sigma_4 \\ \sigma_5 \\ \sigma_6 \end{Bmatrix} = \begin{bmatrix} C_{11} & C_{12} & C_{13} & C_{14} & C_{15} & C_{16} \\ C_{21} & C_{22} & C_{23} & C_{24} & C_{25} & C_{26} \\ C_{31} & C_{32} & C_{33} & C_{34} & C_{35} & C_{36} \\ C_{41} & C_{42} & C_{43} & C_{44} & C_{45} & C_{46} \\ C_{51} & C_{52} & C_{53} & C_{54} & C_{55} & C_{56} \\ C_{61} & C_{62} & C_{63} & C_{64} & C_{65} & C_{66} \end{bmatrix} \begin{Bmatrix} \varepsilon_1 \\ \varepsilon_2 \\ \varepsilon_3 \\ \varepsilon_4 \\ \varepsilon_5 \\ \varepsilon_6 \end{Bmatrix} \tag{2-2}$$

where C_{ij} is the stiffness matrix of 36 terms defining the stress - strain relationship for loading in the i-direction. When the area of study is restricted to the energy conservative elastic regime, the matrix is symmetric; i.e. $C_{12} = C_{21}$ and so forth, resulting in 21 independent terms. In the case of directional fiber-reinforced composite media, as pictured in Figure 2-2, the three mutually orthogonal planes of symmetry decouple shear strains from normal stresses and vice versa, and shear stresses and strains from each

other. This defines an orthotropic material, which has only nine independent stiffnesses:

$$\begin{Bmatrix} \sigma_1 \\ \sigma_2 \\ \sigma_3 \\ \sigma_4 \\ \sigma_5 \\ \sigma_6 \end{Bmatrix} = \begin{bmatrix} C_{11} & C_{12} & C_{13} & 0 & 0 & 0 \\ C_{12} & C_{22} & C_{23} & 0 & 0 & 0 \\ C_{13} & C_{23} & C_{33} & 0 & 0 & 0 \\ 0 & 0 & 0 & C_{44} & 0 & 0 \\ 0 & 0 & 0 & 0 & C_{55} & 0 \\ 0 & 0 & 0 & 0 & 0 & C_{66} \end{bmatrix} \begin{Bmatrix} \varepsilon_1 \\ \varepsilon_2 \\ \varepsilon_3 \\ \varepsilon_4 \\ \varepsilon_5 \\ \varepsilon_6 \end{Bmatrix} \qquad (2\text{-}3)$$

Further, such a material responds equally to any direction of load in the plane perpendicular to the fiber longitudinal axis (the 2-3 plane in Figure 2-2), so the 2 and 3 subscripts on C are interchangeable. This behavior is termed transverse isotropy, and it further reduces the number of independent stiffness terms to seven. Thus the stiffness terms are, in the more familiar terms of engineering constants E (Young's modulus) and υ (Poisson's ratio),

$$C_{11} = E_1 \frac{1-\upsilon_{23}^2}{\Delta}$$

$$C_{22} = C_{33} = E_2 \frac{1-\upsilon_{12}\upsilon_{21}}{\Delta}$$

$$C_{12} = C_{13} = E_1 \frac{1 + \upsilon_{23}}{\Delta}$$

$$C_{23} = E_2 \frac{\upsilon_{23} + \upsilon_{12}\upsilon_{21}}{\Delta} \qquad (2\text{-}4)$$

$$C_{44} = G_{23}$$

$$C_{55} = G_{31}$$

$$C_{66} = G_{12}$$

where $\Delta = 1 - 2\upsilon_{12}\upsilon_{21} - \upsilon_{23}^2 - 2\upsilon_{12}\upsilon_{21}\upsilon_{23}$, E_1 is Young's modulus for loads along the 1 axis, G_{12} is the shear modulus in the 1-2 plane, and υ_{12} denotes the ratio of strains $\varepsilon_2/\varepsilon_1$ for stress applied in the 1 direction.

Due to the thinness of the plies of the laminate, the assumption of plane stress ($\sigma_3 = \sigma_4 = \sigma_5 = 0$) is usually made at this point. However, in this development, nonzero through thickness shear stress is allowed, so a modified state of plane stress is assumed, in which only $\sigma_3 = 0$. Solving for ε_3 in Eq (2-3) after applying this assumption yields

$$\varepsilon_3 = -\frac{C_{13}}{C_{33}}\varepsilon_1 - \frac{C_{23}}{C_{33}}\varepsilon_2 \qquad (2\text{-}5)$$

Applying the modified plane stress assumption to Eq (2-3) and using the relation of Eq (2-5) to eliminate ε_3 produces the lamina constitutive relation

$$\begin{Bmatrix}\sigma_1\\ \sigma_2\\ \sigma_6\\ \sigma_4\\ \sigma_5\end{Bmatrix} = \begin{bmatrix}Q_{11} & Q_{12} & 0 & 0 & 0 & 0\\ Q_{12} & Q_{22} & 0 & 0 & 0 & 0\\ 0 & 0 & Q_{66} & 0 & 0 & 0\\ 0 & 0 & 0 & Q_{44} & 0 & 0\\ 0 & 0 & 0 & 0 & Q_{55} & 0\end{bmatrix} \begin{Bmatrix}\varepsilon_1\\ \varepsilon_2\\ \varepsilon_6\\ \varepsilon_4\\ \varepsilon_5\end{Bmatrix} \qquad (2\text{-}6)$$

where the Q_{ij} are reduced stiffness coefficients related to the C's by

$$Q_{ij} = C_{ij} - \frac{C_{i3}C_{j3}}{C_{33}} \qquad (2\text{-}7)$$

(The unusual renumbering in Eq (2-6) groups together the 1, 2 and 6 terms, since subsequent formulation will differ for these inplane terms and the transverse 4 and 5 terms.) In terms of the engineering coefficients again,

$$Q_{11} = \frac{E_1}{\omega} \qquad Q_{22} = \frac{E_2}{\omega} \qquad Q_{12} = \frac{\upsilon_{21} E_2}{\omega} \tag{2-8}$$

$$Q_{66} = G_{12} \qquad Q_{44} = G_{23} \qquad Q_{55} = G_{13}$$

where $\omega = 1 - \upsilon_{12}\upsilon_{21}$.

Finally, in order to analyze a stack of plies, they must all be referenced to a global axis system and their effects summed:

$$\left\{\sigma_i\right\}_k = \left[\ T\ \right] \left[\ Q_{ij}\ \right]_k \left[\ T\ \right]^T \left\{\varepsilon_i\right\}_k \tag{2-9}$$

where

$$\left[\ T\ \right] = \begin{bmatrix} c^2 & s^2 & -2cs \\ s^2 & c^2 & 2cs \\ cs & -cs & c^2 - s^2 \end{bmatrix} \quad \text{for} \quad \begin{bmatrix} Q_{11} & Q_{12} & 0 \\ Q_{12} & Q_{22} & 0 \\ 0 & 0 & Q_{66} \end{bmatrix}$$

$$\left[\ T\ \right] = \begin{bmatrix} c & -s \\ s & c \end{bmatrix} \quad \text{for} \quad \begin{bmatrix} Q_{44} & 0 \\ 0 & Q_{55} \end{bmatrix}$$

and $c = \cos(\phi)$, $s = \sin(\phi)$. With this transformation the constitutive relations are

$$\left\{\sigma_i\right\}_k = \left[\bar{Q}_{ij}\right]_k \left\{\epsilon_i\right\}_k \qquad (2\text{-}10)$$

with the transformed reduced stiffnesses

$$\bar{Q}_{11} = Q_{11}\cos^4\phi + 2(Q_{12} + 2Q_{66})\sin^2\phi\cos^2\phi + Q_{22}\sin^4$$

$$\bar{Q}_{12} = (Q_{11} + Q_{22} - 4Q_{66})\sin^2\phi\cos^2\phi + Q_{12}(\sin^4\phi + \cos^4\phi)$$

$$\bar{Q}_{22} = Q_{11}\sin^4\phi + 2(Q_{12} + 2Q_{66})\sin^2\phi\cos^2\phi + Q_{22}\cos^4$$

$$\bar{Q}_{16} = (Q_{11} - Q_{12} - 2Q_{66})\sin\phi\cos^3\phi + (Q_{12} - Q_{22} + 2Q_{66})\sin^3\phi\cos\phi$$

$$\bar{Q}_{26} = (Q_{11} - Q_{12} - 2Q_{66})\sin^3\phi\cos\phi + (Q_{12} - Q_{22} + 2Q_{66})\sin\phi\cos^3\phi$$

$$\bar{Q}_{66} = (Q_{11} + Q_{22} - 2Q_{12} - 2Q_{66})\sin^2\phi\cos^2\phi + Q_{66}(\sin^4\phi + \cos^4\phi)$$

$$\bar{Q}_{44} = Q_{44}\cos^2\phi + Q_{55}\sin^2\phi$$

$$\bar{Q}_{45} = (Q_{44} - Q_{55})\cos\phi\sin\phi$$

$$\bar{Q}_{55} = Q_{55}\cos^2\phi + Q_{44}\sin^2\phi \qquad (2\text{-}11)$$

Kinematic Development

The geometric nonlinearity arising from the panel's curvature is incorporated by the strain - displacement relations. It is also here that the through thickness shear effects are incorporated into the analysis. This development follows Dennis (9) who authored the computer code which employs these relations; Reddy and Liu (25) also published a similar higher order theory.

The incorporation of transverse shear is accomplished by assuming a modified state of plane stress for the lamina in which $\sigma_3 = 0$ (and hence $\epsilon_3 = 0$) but σ_4 and σ_5 are allowed to be small nonzero values.

These transverse shear stresses are assumed to go to zero on the top and bottom surfaces of each ply, and the associated strains will vary parabolically through the ply thickness.

To proceed, keeping just the linear (first order) displacement terms for the transverse shear strains ε_4 and ε_5, we see that (30)

$$\varepsilon_4 = \frac{1}{h_2}\left(u_{3',2} + h_2 u_{2',3} - u_2 h_{2',3}\right)$$
$$\varepsilon_5 = \frac{1}{h_1}\left(u_{3',1} + h_1 u_{1',3} - u_1 h_{1',3}\right) \qquad (2\text{-}12)$$

where the h_i are the coordinate system scale factors; for the cylindrical geometry used in this work, $h_1 = 1$ and $h_2 = 1 - z/R$.

The displacement equations in the thickness variable z which permit the incorporation of the desired through thickness feature are

$$u(x,\theta,z) = u^\circ + z\psi_1 + z^2\phi_1 + z^3\gamma_1 + z^4\theta_1$$
$$v(x,\theta,z) = v^\circ\left(1 - \frac{z}{R}\right) + z\psi_2 + z^2\phi_2 + z^3\gamma_2 + z^4\theta_2 \qquad (2\text{-}13)$$
$$w(x,\theta) = w$$

where u°, v°, w, ψ_i, ϕ_i, γ_i and θ_i are functions of the coordinates x and θ. The displacements u° and v° are of the shell middle surface; transverse displacement w is the same throughout the thickness since transverse normal strain is assumed negligible. The term ψ_i is a rotation of the surface normal in the i plane. Summing the ψ_i with the shear rotation of the normal to the shell due to transverse shear stress (denoted β_i), yields the slope of the elastic curve $w_{,i}$. The

terms $\emptyset_i$, γ_i and Θ_i are to be solved for by applying the assumption that transverse shear stresses σ_4 and σ_5 are zero on the shell surfaces. Substituting the equations for v and w into Eq (2-12) for ε_4 yields

$$\varepsilon_4 = \frac{1}{1-z/R}\left[w_{,2} + (1-z/R)\left(-\frac{v^\circ}{R} + \psi_2 + 2z\emptyset_2 + 3z^2\gamma_2 + 4z^3\Theta_2\right)\right.$$
$$\left. + \frac{1}{R}\left\{v^\circ\left(1 - \frac{z}{R}\right) + z\psi_2 + z^2\emptyset_2 + z^3\gamma_2 + z^4\Theta_2\right\}\right] \qquad (2\text{-}14)$$

For zero transverse shear stress at the surfaces, the associated strain will also be zero. If one enforces this condition by substituting $\pm h/2$ (h being thickness) for z in Eq (2-14), setting both resulting expressions to zero and hence equal to each other, and then solving for the unknown variables, the following is produced:

$$\emptyset_2 = 0 \qquad \Theta_2 = \frac{\gamma_2}{2R}$$
$$\left[1 - \frac{h^2}{8R^2}\right]\gamma_2 = \frac{-4}{3h^2}\left(\psi_2 + w_{,2}\right) \qquad (2\text{-}15)$$

It should be noted that an h/R value of 1/5 (quite high for practical aerospace shell geometries) allows neglect of the h/R term in the left side of Eq (2-15). By replacing $\emptyset_2$, Θ_2 and γ_2 in Eq (2-14) with the results in Eq (2-25), the transverse shear strain ε_4 in terms of transverse displacement w and rotation ψ_2 becomes:

$$\varepsilon_4 = \frac{1}{1-z/R}\,(w_{,2} + \psi_2)\left(1 - \frac{4z^2}{h^2} + \frac{8z^3}{3h^2R}\right) \qquad (2\text{-}16a)$$

(Note again that there are 1/R terms to be neglected.) A similar analysis with ε_5 (simpler, since $h_1 = 1$) provides

$$\varepsilon_5 = (w_{,1} + \psi_1)\left(1 - \frac{4z^2}{h^2}\right) \qquad (2\text{-}16b)$$

Replacing $\emptyset_i$, θ_i and γ_i in Eq (2-13) with the expressions found in Eq (2-15) yields the displacement equations:

$$\begin{aligned} u(x,\theta,z) &= u^\circ + z\psi_1 - \frac{4}{3h^2}\,z^3\left(\psi_1 + w_{,1}\right) \\ v(x,\theta,z) &= v^\circ\left(1 - \frac{z}{R}\right) + z\psi_2 - \frac{4}{3h^2}\,z^3\left(\psi_2 + w_{,2}\right) \\ w(x,\theta) &= w \end{aligned} \qquad (2\text{-}17)$$

At this point one can note that this formulation provides seven degrees of freedom: u, v, w, $w_{,1}$, $w_{,2}$, ψ_1 and ψ_2.

Now that we have displacement equations which incorporate a parabolic through thickness shear stress distribution, the in-plane kinematic equations are derived for the shell middle surface. The fully general strain displacement relations are quite extensive; the theoretical development incorporating them can be found in Dennis' large displacement/rotation general shell development. For brevity here, Donnell's assumptions for thin cylindrical shell analysis (11)

will be applied immediately. For example, the circumferential strain ε_2 for a cylindrical geometry is

$$\varepsilon_2 = \frac{v_{,2}}{1-z/R} - \frac{w}{R(1-z/R)} + \frac{1}{2}\left(v_{,2} - \frac{w}{R}\right)^2 + \frac{1}{2}\left(w_{,2} - \frac{v}{R}\right)^2 + \frac{1}{2}\, u_{,2}^2 \qquad (2\text{-}18)$$

Applying Donnell's assumptions, the shell is considered thin such that the z/R terms in the denominators can be neglected; the inplane strains $v_{,2}$ and $u_{,2}$ are small so that higher order (than linear) terms are negligible; the transverse displacement w is small compared to the radius of curvature so that higher order w/R terms can be neglected; and the inplane displacement v is so small that v/R is negligible. A physical description of such deformation is that the transverse displacement w varies periodically and rapidly along the circumferential direction with a small wavelength compared to R. The remaining terms yield the Donnell relation:

$$\varepsilon_2 = v_{,2} - \frac{w}{R} + \frac{1}{2}\, w_{,2}^2 \qquad (2\text{-}19)$$

If one neglects similar terms in the exact formulation for the other inplane strain ε_1 and shear strain ε_6, the following set of Donnell kinematic relations for a cylindrical shell is produced:

$$\begin{aligned} \varepsilon_1 &= u_{,1} + \frac{1}{2}\, w_{,1}^2 \\ \varepsilon_2 &= v_{,2} - \frac{w}{R} + \frac{1}{2}\, w_{,2}^2 \\ \varepsilon_6 &= u_{,2} + v_{,1} + w_{,1} w_{,2} \end{aligned} \qquad (2\text{-}20)$$

Substituting the displacement Eqs (2-17) into Eq (2-20) gives, for any position through the shell thickness,

$$\varepsilon_1 = u^{\circ}_{,1} + z\psi_{1',1} + z^3 k(w_{,11} + \psi_{1',1}) + \frac{1}{2} w^2_{,1}$$

$$\varepsilon_2 = v^{\circ}_{,2} - \frac{w}{R} + z\left(\frac{-v^{\circ}_{,2}}{R} + \psi_{2',2}\right) + z^3 k(w_{,22} + \psi_{2',2}) + \frac{1}{2} w^2_{,2}$$

$$\varepsilon_6 = u^{\circ}_{,2} + v^{\circ}_{,1} + z\left(\psi_{1',2} + \psi_{2',1} - \frac{v^{\circ}_{,2}}{R}\right) \qquad (2\text{-}21)$$

$$+ z^3 k(2w_{,12} + \psi_{1',2} + \psi_{2',1}) + w_{,1} w_{,2}$$

where $k = -4/3h^2$. The following equivalent representation of the strains separates the midplane terms from the out-of-plane terms (denoted by $\varkappa_{ij}$) and is conducive to the matrix operations of the potential energy formulation in the next section:

$$\varepsilon_1 = \varepsilon^{\circ}_1 + z^p \varkappa_{1p} \; ; \qquad \varepsilon^{\circ}_1 = u_{,1} + \frac{1}{2} w^2_{,1}$$

$$\varkappa_{11} = \psi_{1',1}$$

$$\varkappa_{13} = k(w_{,11} + \psi_{1',1})$$

$$\varkappa_{1p}(p = 2,4,5,6,7) = 0$$

$$\varepsilon_2 = \varepsilon^{\circ}_2 + z^p \varkappa_{2p} \; ; \qquad \varepsilon^{\circ}_2 = v_{,2} - \frac{w}{R} + \frac{1}{2} w^2_{,2}$$

$$\varkappa_{21} = \psi_{2',2} - \frac{v_{,2}}{R}$$

$$\varkappa_{23} = k(w_{,22} + \psi_{2',2})$$

$$\varkappa_{2p}(p = 2,4,5,6,7) = 0$$

$$\varepsilon_6 = \varepsilon_6^\circ + z^p \varkappa_{6p} \; ; \qquad \varepsilon_6^\circ = u_{,2} + v_{,1} + w_{,1} w_{,2}$$

$$\varkappa_{61} = \psi_{1,2} + \psi_{2,1} - \frac{v_{,1}}{R}$$

$$\varkappa_{63} = k(2w_{,12} + \psi_{1,2} + \psi_{2,1})$$

$$\varkappa_{6p}(p = 2,4,5,6,7) = 0$$

$$\varepsilon_4 = \varepsilon_4^\circ + z^p \varkappa_{4p} \; ; \qquad \varepsilon_4^\circ = w_{,2} + \psi_2$$

$$\varkappa_{42} = 3k(w_{,2} + \psi_2)$$

$$\varkappa_{4p}(p = 1,3,4,5,6,7) = 0$$

$$\varepsilon_5 = \varepsilon_5^\circ + z^p \varkappa_{5p} \; ; \qquad \varepsilon_5^\circ = w_{,1} + \psi_1$$

$$\varkappa_{52} = 3k(w_{,1} + \psi_1) \qquad (2\text{-}22)$$

$$\varkappa_{5p}(p = 1,3,4,5,6,7) = 0$$

This allows assembly of the strain displacement equations into a matrix format:

$$\begin{Bmatrix} \varepsilon_1 \\ \varepsilon_2 \\ \varepsilon_6 \end{Bmatrix} = \begin{Bmatrix} \varepsilon_1^\circ \\ \varepsilon_2^\circ \\ \varepsilon_6^\circ \end{Bmatrix} + \begin{bmatrix} \varkappa_{11} & \varkappa_{13} \\ \varkappa_{21} & \varkappa_{23} \\ \varkappa_{61} & \varkappa_{63} \end{bmatrix} \begin{Bmatrix} z \\ z^3 \end{Bmatrix}$$

$$\begin{Bmatrix} \varepsilon_4 \\ \varepsilon_5 \end{Bmatrix} = \begin{Bmatrix} \varepsilon_4^\circ \\ \varepsilon_5^\circ \end{Bmatrix} + \begin{bmatrix} \varkappa_{42} \\ \varkappa_{52} \end{bmatrix} z^2 \qquad (2\text{-}23)$$

In a general expression,

$$\{\mathfrak{E}\} = \{\mathfrak{E}^\circ\} + [\mathfrak{K}]\{\mathfrak{Z}\} \qquad (2\text{-}24)$$

It is worth noting that these kinematics avoid the common pitfall of shear locking, wherein the model becomes artificially stiff as the shell thickness is decreased. This is a problem with finite element formulations which incorporate constant or linearly distributed shear strain through the thickness, and it neccessitates the use of a correction factor. However, examination of the compatibility relations associated with the strain displacement equations developed in this section shows that the terms associated with transverse shear drop out as thickness is reduced to zero. (9)

Once again, note that the kinematics developed in this section is specifically for the cylindrical geometry with the Donnell simplifications applied. The computer analyses done in this work used both the Donnell and the LD/R formulations; the latter is detailed in Dennis (9).

Potential Energy

The shell potential energy is the sum of the internal strain energy and the work done by external forces:

$$\Pi_p = U + V \tag{2-25}$$

where the internal strain energy is given by

$$U = \int_{\Omega}\int_{h} \frac{1}{2}\left([\bar{Q}]\{\varepsilon\}\right)^T \{\varepsilon\}\, dz\, d\Omega \tag{2-26}$$

where Ω represents the shell middle surface. The internal strain

energy U is composed of in plane and normal terms (set U_1), and transverse shear terms (set U_2). Expanding the expression for U by inserting Eq (2-22) through (2-24) into Eq (2-26) gives

$$U_1 = \frac{1}{2}\int_\Omega\int_h \Big[\bar{Q}_{11}(\varepsilon_1^\circ + z^p\varkappa_{1p})^2 + \bar{Q}_{22}(\varepsilon_2^\circ + z^p\varkappa_{2p})^2 + 2\bar{Q}_{12}(\varepsilon_1^\circ + z^p\varkappa_{1p})(\varepsilon_2^\circ + z^r\varkappa_{2r}) + \bar{Q}_{66}(\varepsilon_6^\circ + z^p\varkappa_{6p})^2 + 2\bar{Q}_{16}(\varepsilon_1^\circ + z^p\varkappa_{1p})(\varepsilon_6^\circ + z^r\varkappa_{6r}) + 2\bar{Q}_{26}(\varepsilon_2^\circ + z^p\varkappa_{2p})(\varepsilon_6^\circ + z^r\varkappa_{6r})\Big]\, dz\, d\Omega \tag{2-27}$$

$$U_2 = \frac{1}{2}\int_\Omega\int_h \Big[\bar{Q}_{44}(\varepsilon_4^\circ + z^2\varkappa_{42})^2 + \bar{Q}_{55}(\varepsilon_5^\circ + z^2\varkappa_{52})^2 + 2\bar{Q}_{45}(\varepsilon_4^\circ + z^2\varkappa_{42})(\varepsilon_5^\circ + z^2\varkappa_{52})\Big]\, dz\, d\Omega$$

where p,r = 1,2,...,7. Integrating the z over ± h/2 yields the equation for strain energy as a function of the middle surface only, which is the desired formulation for this shell problem. A further simplification performed in the coding of the SHELL program is one of symmetry in ply layup. This results in the cancellation of elasticity arrays which are multiplied by odd powers of the transverse coordinate z. Rearranging yields, for the Donnell application, the final forms of

$$U_1 = \frac{1}{2}\int_\Omega \{\varepsilon^\circ\}^T[A]\{\varepsilon^\circ\}\, d\Omega \qquad (1,2,6)$$

$$U_2 = \frac{1}{2}\int_\Omega \Big(\{\varepsilon^\circ\}^T[A]\{\varepsilon^\circ\} + 2\{\varepsilon^\circ\}^T[D][\varkappa] + [\varkappa]^T[F][\varkappa]\Big)\, d\Omega \qquad (4,5) \tag{2-28}$$

where stiffness matrices $\{[A, D, F]\} = \int_h [\bar{Q}]\{1, z^2, z^4\}dz$.

The 36 DOF Element

In this section the relationship between the continuum diplacements and the discrete nodal displacements for the shell element used in this research (pictured in Figure 2-3) is defined. The seven degrees of freedom at each corner node were found in the previous sections to be u, v, w, $w_{,1}$, $w_{,2}$, ψ_1 and ψ_2. Thus, C^0 continuity is required of all but the $w_{,i}$ slope terms, which require C^1 continuity. Simple Lagrangian shape (interpolating) functions will be used for the displacement DOF, then, and more complex Hermetian functions used only where necessary.

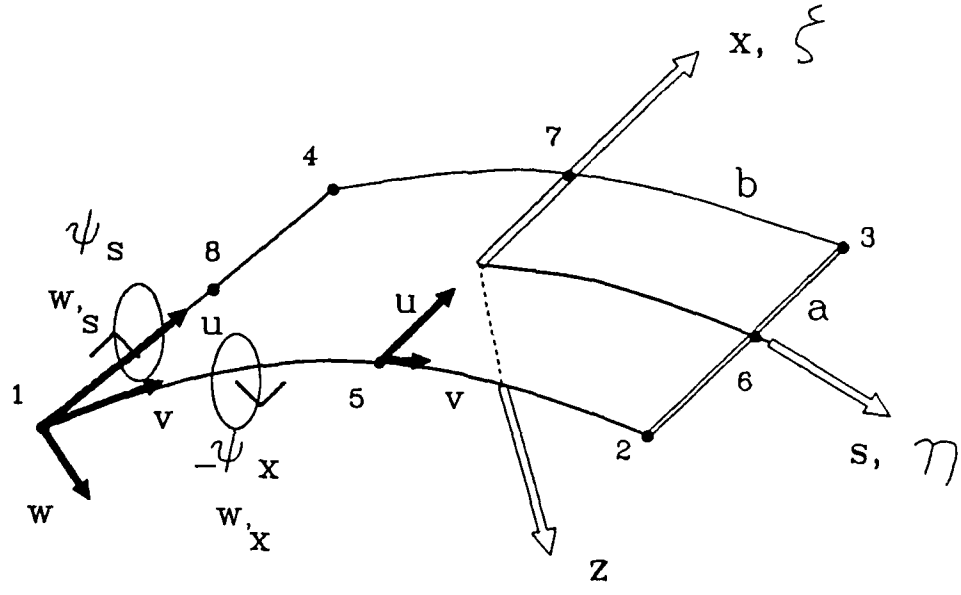

Figure 2-3. SHELL 36 Degree of Freedom Element

The assumed transverse displacement equation for the cylindrical shell element is

$$w(x,s) = a_1 + a_2x + a_3s + a_4x^2 + a_5xs + a_6s^2 + a_7x^3 + a_8x^2s + a_9xs^2 + a_{10}s^3 + a_{11}x^3s + a_{12}xs^3 \qquad (2\text{-}29)$$

This rectangular element may be isoparametrically scaled and oriented such that the longitudinal coordinate $x \rightarrow \xi$, circumferential coordinate $s \rightarrow \eta$, and the side lengths are scaled by

$$\xi = \frac{x}{a} \qquad \eta = \frac{s}{b} \qquad (2\text{-}30)$$

where a and b are the scaled element half dimensions in the ξ and η directions, respectively. Now the element transverse displacement equation can be written as:

$$w(x,s) = \begin{bmatrix} \mathcal{H}_1 & \mathcal{H}_2 & \mathcal{H}_3 & \mathcal{H}_4 \end{bmatrix} \begin{Bmatrix} q_1 \\ q_2 \\ q_3 \\ q_4 \end{Bmatrix} \qquad (2\text{-}31)$$

where $\{q\}_k^T = \{w \quad w_{,1} \quad w_{,2}\}$ for the kth corner node, and $\mathcal{H}$ are Hermetian shape functions (7):

$$\mathcal{N}_k^T = \begin{Bmatrix} \mathcal{N}_{k1} \\ \mathcal{N}_{k2} \\ \mathcal{N}_{k3} \end{Bmatrix} = \begin{Bmatrix} \frac{1}{8}(1+\xi_k\xi)(1+\eta_k\eta)(2+\xi_k\xi+\eta_k\eta-\xi^2-\eta^2) \\ \frac{a}{8}\xi_k(1+\xi_k\xi)^2(\xi_k\xi-1)(1+\eta_k\eta) \\ \frac{b}{8}\eta_k(1+\xi_k\xi)(\eta_k\eta-1)(1+\eta_k\eta)^2 \end{Bmatrix} \tag{2-32}$$

The formulation for DOFs u, v, and ψ_i is a simpler Lagrangian form, and the midside nodes 5 - 8 are also now included:

$$\begin{Bmatrix} u \\ v \\ \psi_1 \\ \psi_2 \end{Bmatrix} = \left[\begin{array}{cccc:c:cccc:c:c} \mathcal{Q}_1 & 0 & 0 & 0 & & \mathcal{Q}_4 & 0 & 0 & 0 & \mathcal{Q}_5 & & \mathcal{Q}_8 \\ 0 & \mathcal{Q}_1 & 0 & 0 & & 0 & \mathcal{Q}_4 & 0 & 0 & 0 & & 0 \\ 0 & 0 & N_1 & 0 & \cdots & 0 & 0 & N_4 & 0 & 0 & \cdots & 0 \\ 0 & 0 & 0 & N_1 & & 0 & 0 & 0 & N_4 & 0 & & 0 \end{array}\right] \begin{Bmatrix} q_1 \\ \vdots \\ q_4 \\ q_5 \\ \vdots \\ q_8 \end{Bmatrix} \tag{2-33}$$

where $\{q\}_k^T = \{u\ v\ \psi_1\ \psi_2\}$ for nodes 1 through 4 and $\{u\ v\}$ for nodes 5 through 8, and N and $\mathcal{Q}$ are linear and quadratic (respectively) Lagrangian shape functions (7):

$$N_k = \frac{1}{4}(1+\xi_k\xi)(1+\eta_k\eta)$$

$$\mathcal{Q}_k = \frac{1}{4}(1+\xi_k\xi)(1+\eta_k\eta)(\xi_k\xi+\eta_k\eta-1),\ k = 1,2,3,4$$

$$\mathcal{Q}_k = \frac{1}{2}(1-\xi^2)(1+\eta_k\eta),\ k = 6,8 \tag{2-34}$$

$$\mathcal{Q}_k = \frac{1}{2}(1-\eta^2)(1+\xi_k\xi),\ k = 5,7$$

The overall equation defining the isoparametric discretization of continuum displacements into nodal displacements is obtained by merging the above relationships:

$$\underset{(7x1)}{\{u\}} = \underset{(7x36)}{[N]} \underset{(36x1)}{\{q\}} \qquad (2\text{-}35)$$

Finite Element Formulation

The solution of the static finite element problem involves finding the equilibrium state between applied load and structural response. This state can be determined by finding where the system potential energy is stationary, i.e. where its variation is zero. Recall Eq (2-25):

$$\Pi_p = U + V \qquad (2\text{-}25)$$

where now internal strain energy can be represented by

$$U = \frac{1}{2} q^T \left[K + \frac{N_1}{2} + \frac{N_2}{3} \right] q = \frac{1}{2} q^T \bar{K} q \qquad (2\text{-}36)$$

where q = column array of nodal displacements, K = constant stiffness terms, N_1 = stiffness terms linear in displacement, and N_2 = stiffness terms quadratic in displacement. The external work can be represented as

$$V = - q^T \lambda P \qquad (2\text{-}37)$$

where P is a column array of applied nodal loads and λ is a multiplier whose utility will be seen in the section on the solution algorithm. Equilibrium is defined as the state at which internal strain energy and external work balance; potential energy is at a relative minimum here.

This point can be found by substituting Eqs (2-36) and (2-37) into Eq (2-25) and taking the first variation:

$$\delta\Pi_p = \delta q^T \left[\bar{K}\, q - \lambda P\right] = 0 \qquad (2\text{-}38)$$

Since displacements δq are nonzero for all but the trivial solution, the bracketed expression must be zero for equilibrium. It is a function (we'll call it g) of q and λ:

$$\bar{K}\, q - \lambda P = 0 = g(q,\lambda) \qquad (2\text{-}39)$$

Since $\bar{K}$ varies with load and displacement, a numerical iterative solution is used to solve Equation (2-39) incorporating the Newton-Raphson method as discussed next.

Solution Algorithm

The technique advanced by Riks (28,29) and Wempner (39) and demonstrated by Crisfield (8) of incrementing a desired arc length along the load-displacement curve, while solving iteratively via the Newton-Raphson method, is the solution technique used in this work. The modified Riks-Wempner algorithm, added to the SHELL program by Tsai and Palazotto (38), allows for tracing of the load-displacement response through both load reversing (snap through) and displacement reversing (snap back) critical points, so the most complex behavior can be continuously followed.

The essence of the Riks/Wempner method is that neither load P nor displacement q is independently controlled; rather, a selected "arc" length Δs (actually the chord, as will be seen) of the load - displacement curve is incremented. The equilibrium condition is found which satisfies the relation:

$$\Delta q_{i+1} \cdot \Delta q_{i+1} + \Delta\lambda_{i+1}^2 P \cdot P = \Delta s^2 \qquad (2\text{-}40)$$

where Δq_{i+1} is the incremental displacement for step $i+1$, and $\Delta\lambda_{i+1}$ is the fraction of load P applied at step $i+1$. The effect of the constraint equation (2-40) is that each subsequent step solution is searched for on an arc of radius Δs from the current solution. The initial value for the quantity $\Delta\lambda$ is specified with the problem input data; values of this parameter of 0.1 to 0.5 worked well in this work.

To apply the Newton-Raphson method, the first variation of equation (2-39) is taken and applied at steps i:

$$K_T \delta q_i = \delta\lambda_i P - g(q_i, \lambda_i) \qquad (2\text{-}41)$$

where

$$\delta q_i = \delta q_{i1} + \delta\lambda_i \delta q_{i2} \qquad (2\text{-}41a)$$

$$\delta q_{i1} = -K_T^{-1} g(q_i, \lambda_i) \quad \text{(out-of-balance term)} \qquad (2\text{-}41b)$$

$$\delta q_{i2} = K_T^{-1} P \quad \text{(linear term)} \qquad (2\text{-}41c)$$

and

$$K_T = \left[K + N_1 + N_2 \right] \qquad (2\text{-}41d)$$

In the following brief description of the operation of the algorithm on load step n, i denotes an iteration at step n along the solution path, and Figure 2-4 depicts the quantities discussed.

a.) The tangent stiffness matrix K_T at the current deformed geometry is determined.

b.) The linear incremental displacement δq_{i2} is computed (Eq 2-41c).

c.) (First iteration) Compute $\Delta q_1 = \Delta\lambda_1 \delta q_{i2}$, with $\Delta\lambda_1 = \Delta\lambda_{n-1}$, or a user - defined value if $n = 1$ (first increment). The parameter $\Delta\lambda$ indicates the fraction of total load to be applied at the first increment. A value of 0.25 for the first increment worked well for cases which displayed near linear response initially; complex nonlinear load up was better followed with a smaller initial step of 0.1.

d.) The constraint equation (2-40) is solved for Δs. The load term is often ignored in this relation, since the the load and displacement values typically differ by many orders of magnitude, which can cause numerical difficulty. Convergence to a solution is not hindered by ignoring load at this step.

e.) K_T is updated at $q = q_n + \Delta q_i$.

f.) The out-of-balance displacement δq_{i1} is computed (Eq 2-41b).

g.) Equations (2-41a) in (2-40) are solved for $\delta\lambda_i$, which will have two roots $\delta\lambda_{i1}$ and $\delta\lambda_{i2}$ due to the quadratic feature.

h.) $\delta\lambda_i$ is selected from $\delta\lambda_{i1}$ and $\delta\lambda_{i2}$, by criteria detailed in Crisfield (8), to ensure that the solution path does not return to equilibrium points previously found.

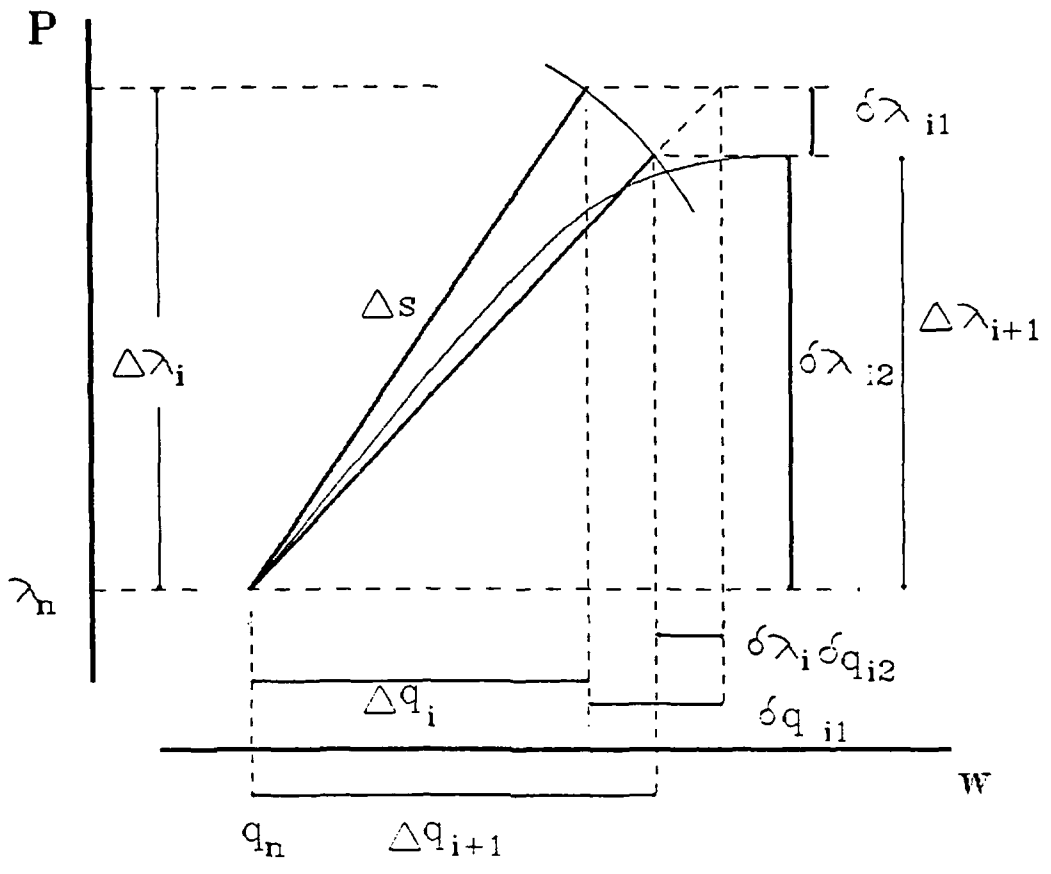

Figure 2-4. Riks Method Solution Step

i.) Displacement increment $\Delta q_{i+1} = \Delta q_i + \delta q_i$ and load factor increment $\Delta\lambda_{i+1} = \Delta\lambda_i + \delta\lambda_i$ are updated.

j.) When Δq_i and $\Delta\lambda_i$ computed at successive iterations (steps e-i) differ by less than a selected convergence tolerance (0.1% for simple paths; as low as 0.0001% required for tightly curved paths), the step n solution has been found:

$$\Delta q_i \rightarrow \Delta q_n$$
$$\Delta\lambda_i \rightarrow \Delta\lambda_n \qquad (2\text{-}42)$$

At the completion of each step, cumulative displacement and load factor are computed:

$$q_n = q_{n-1} + \Delta q_n$$
$$\lambda_n = \lambda_{n-1} + \Delta \lambda_n \qquad (2\text{-}43)$$

This technique can follow an equilibrium path which progresses in any direction, by solving for negative incremental displacement or load, or both. This allows one to automatically solve for even the most convoluted nonlinear equilibrium curve, without concern over the singularities at critical load or displacement points.

The efficiency of the algorithm is improved by scaling the step (n+1)'s target Δs length by the ratio of a user-selected desired number of iterations (set to 4 iterations for this work) to the number of iterations to converge at step n. Thus, in near-linear parts of the load-displacement curve, wide spacing of solution points is allowed; when the curve rounds corners (around limit points) the method has to iterate more to converge and hence Δs is reduced until the curve straightens out again.

The inability to solve for equilibrium at a limit load point is circumvented due to the nature of the stepping method. The technique shoots a tangent from the current equilibrium point, then searches an arc about the tip for the next solution point, so the exact limit load point is almost always skipped over. Auxiliary equations can be programmed to enable determination of the critical point (28).

Failure Criterion

The Tsai-Wu failure criterion, being tensor based, can incorporate transverse shear effects. However, since in-plane stresses are much larger than the transverse stresses, the two-dimensional theory will give a valid indication as to the material limit load. Since the stiffness of the panel would be altered after ply failure, and the SHELL program does not allow this, the analysis would ideally be terminated at this point. However, early in the research it was noted that the ply failures occurred almost at the onset of loading, due to the high stress gradient near the point of application. In practice, the load would have to be distributed over a finite area to prevent punch through. Therefore, stresses were not considered any closer to the load point than the thickness dimension, to allow for distribution through the thickness (and through at least two layers of elements in the model).

Of the several laminate failure criteria available (16), the Tsai-Wu is desirable because it accounts for the interaction of the tensile, compressive and shear stresses developed along the load path and off axis. It is, however, more complex and less intuitive than, say, a maximum stress criterion, which simply looks for stresses which exceed material limits. According to Tsai-Wu, first ply failure occurs when the following inequality is violated:

$$F_1\sigma_1 + F_2\sigma_2 + F_{11}\sigma_1^2 + F_{22}\sigma_2^2 + F_{66}\sigma_6^2 + F_{12}\sigma_1\sigma_2 < 1 \qquad (2\text{-}44)$$

where

$$F_1 = \frac{1}{X_T} + \frac{1}{X_C}$$

$$F_2 = \frac{1}{Y_T} + \frac{1}{Y_C}$$

$$F_{11} = -\frac{1}{X_T X_C}$$

$$F_{22} = -\frac{1}{Y_T Y_C}$$

$$F_{66} = \frac{1}{S^2}$$

$$F_{12} = -\left(X_T X_C Y_T Y_C\right)^{-1/2} \quad (37)$$

and X_T is ultimate tensile stress in the principal direction of the ply, Y_C is ultimate compressive stress in a direction perpendicular to the fibers in the ply, and S is ultimate shear stress. In searching for ply failure, the stresses computed at each ply's elemental Gauss points are first transformed to align with the ply principal direction. Then Equation (2-44) is computed and checked for failure.

III. ANALYTICAL MODEL PREPARATION

The geometric and material parameters studied are presented in this chapter. A discussion of the model preparation and validation effort is then offered.

Parameters and Ranges of Variation

Material. The analysis is performed on laminates constructed of high strength/low modulus Hercules AS4-3501-6 graphite/epoxy with the following ply physical properties and dimensions (36,9):

ply thickness= 0.005 inch

$E_1 = 18.844 \times 10^6$ psi

$E_2 = E_3 = 1.468 \times 10^6$ psi

$G_{12} = G_{13} = 0.91 \times 10^6$ psi

$G_{23} = 0.45 \times 10^6$

$\upsilon_{12} = 0.28$

$\upsilon_{21} = \upsilon_{31} = 0.0218$

$\sigma_{ult-T} = 285.6$ ksi (0°) / 9.12 ksi (90°)

$\sigma_{ult-C} = 141.7$ ksi (0°) / 37.2 ksi (90°)

$\tau_{ult} = 11.1$ ksi

Panel Geometry. Common to all of the models is a radius of curvature of 12 inches and a length of 18 inches. All combinations of the following parameters are studied:

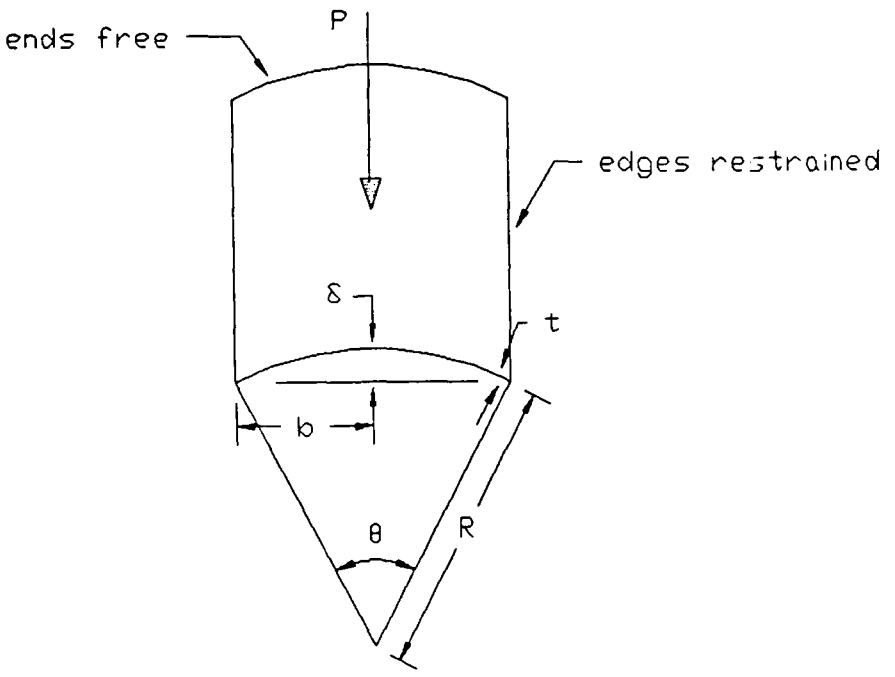

Figure 3-1. Study Parameters

1.) ply layup:

(a.) $[0/90]_s$ cross ply

(b.) $[0/-45/+45/90]_s$ quasi-isotropic

2.) boundary conditions (straight edges only - curved ends always free):

(a.) simple (hinged), $u = v = w = w_{,x} = \psi_x = 0$

(b.) clamped, $u = v = w = w_{,x} = w_{,s} = \psi_x = \psi_s = 0$

3.) R/h (radius of curvature/thickness):

(a.) 300 → h = 0.04 inch → 8 plies

(b.) 100 → h = 0.12 inch → 24 plies

(c.) 50 → h = 0.24 inch → 48 plies

(d.) 25 → h = 0.48 inch → 96 plies

4.) θ (opening angle at center of curvature):

(a.) 1 radian → $\delta/b = 0.255$ (nonshallow)

(b.) 1/2 radian → $\delta/b = 0.126$ (borderline)

(c.) 1/4 radian → $\delta/b = 0.063$ (shallow)

A total of 12 geometries of each layup were analyzed at each of the boundary conditions. The parameter δ/b noted with respect to θ is called the "shallowness parameter," and is a non-angular measure of the ratio of central rise to span.

Load. The applied load is a centered point load, acting normal to the panel surface at the onset. As the panel deforms, the load maintains its original orientation; thus it can be likened to a dead weight. Due to symmetry of the deformed panel being enforced by quarter panel modeling (see below), this will result in the load being maintained normal to the local panel surface.

Convergence Tests

Since no experimental work against which to compare results was found, and all of the analytical solutions were either for isotropic panels or for different layups than the ones analyzed here, considerable effort went into verifying convergence of the model solution. Tests were run to assess the validity of quarter panel modeling for this geometry, to determine the degree of mesh refinement required at the load application point for each of the panel widths, to determine whether the Donnell simplifications would yield accurate results, and to determine the distance away from the load point that

stress values could be used for ply failure determination. These tests are now summarized.

Quarter Panel Modeling. The different arc lengths of inner and outer plies in any curved laminated composite will set up asymmetric inplane shear stresses about the laminate middle surface. The error due to assuming symmetry about the x- and s- planes of the distortion due to the significant in-plane shear stresses present in the angle-ply layup was assessed. A hinged, θ = 1 radian, R/h = 100 shell was modeled with a uniform 12x8 mesh of 1.5 inch x 1.5 inch elements, and also as a quarter shell by symmetry, with a 6x4 element mesh.

Cross-Ply Panel. Comparison of full- and quarter-panel model load versus displacement performance shows exact agreement (Figure 3-2).

Angle-Ply Panel. Comparison of full- and quarter-panel model runs indicate less than 5% variation in displacement at corresponding loads (Figure 3-3). The panel end profile, however, indicates that the angle-ply laminate develops a twist (Figure 3-4). Thus, mirroring the solution for one side of the model to the missing parts will result in a falsely symmetric depiction of the deformed shape, but the load versus displacement data will be acceptable.

Mesh Refinement: Due to problem solution run times, using a uniform mesh of elements fine enough to converge to a solution was not possible. In the following series of runs, an accurate nonuniform mesh for each size panel was determined by assessing the variation of the solution by increasingly fine meshes. The models ranged from a uniform mesh of 1.5 x 1.5 inch elements to graduated meshes with elements as

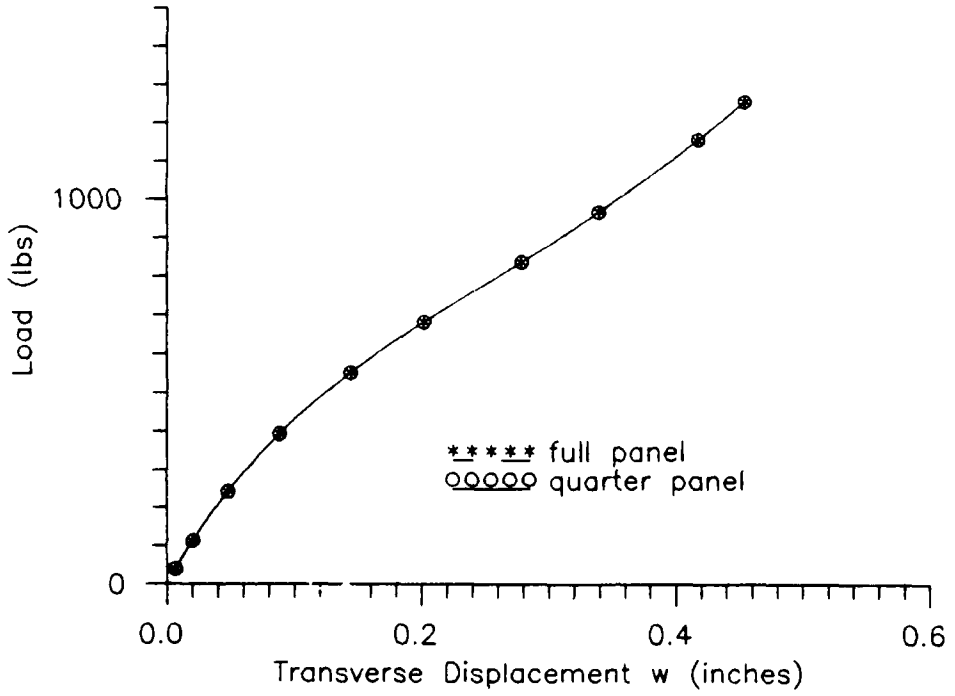

Figure 3-2. Load vs w, Cross Ply Quarter Panel Test

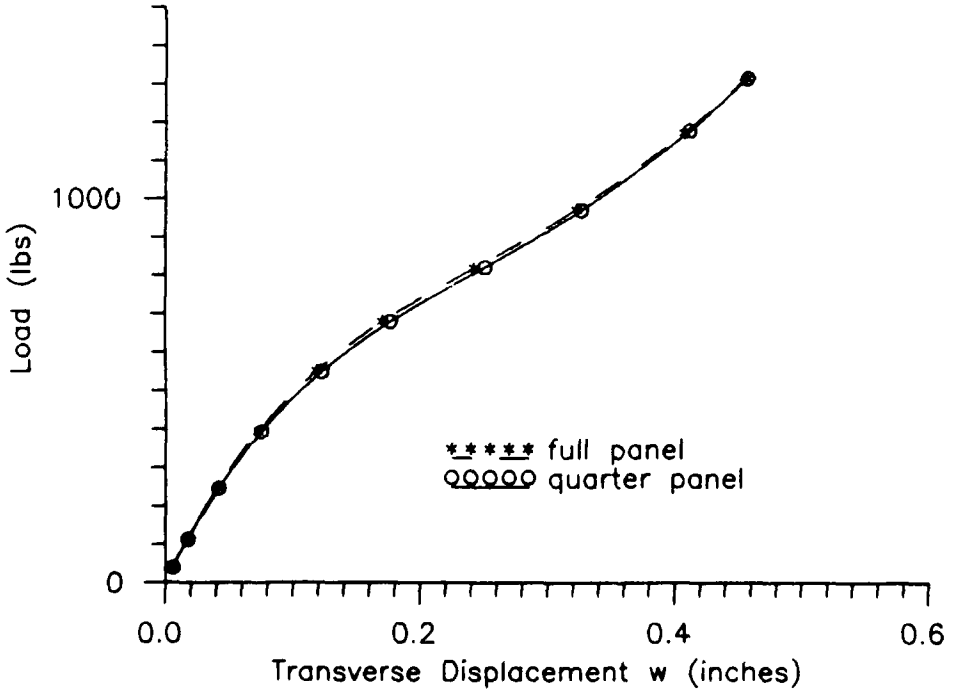

Figure 3-3. Load vs w, Angle Ply Quarter Panel Test

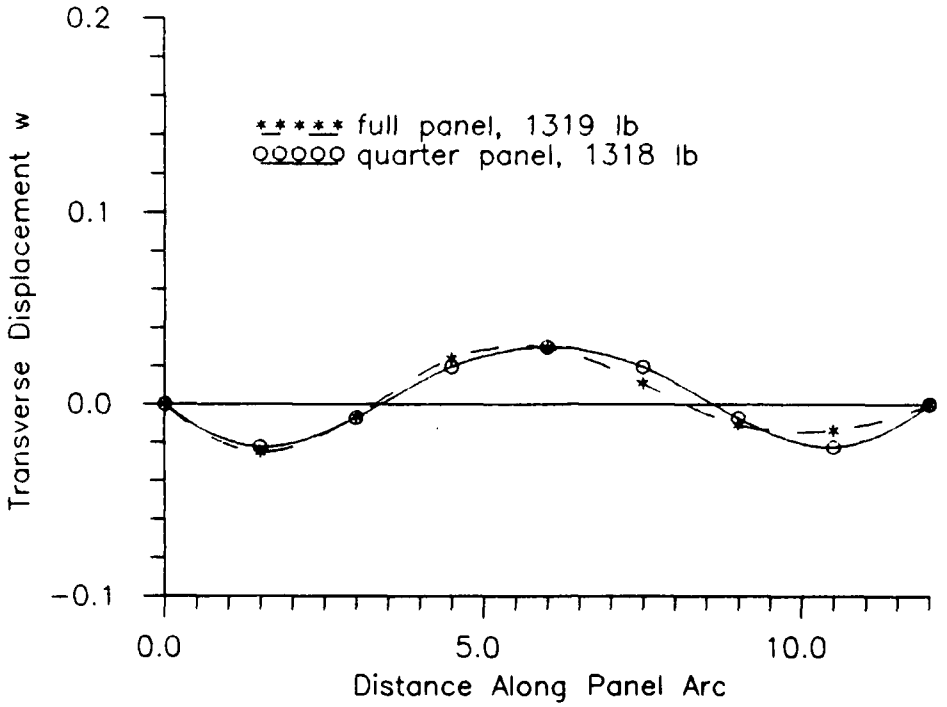

Figure 3-4. Quarter Panel vs Full Panel End Profile

small as 0.125 x 0.125 inch. Element aspect ratios (AR) ranged from 1 to 8, with AR = 1 maintained for at least two layers around the load point. The highest element density was concentrated in the circumferential direction since this is the direction of highest stress variance as the load is transferred from the shell center to the restrained edges.

Wide Panel: (θ = 1 radian, Figure 3-5) Convergence was achieved with a 1146 DOF, 11 x 8 element mesh. This model has an element range of 0.5 x 0.5 inch to 1.0 x 1.0 inch, with AR = 1 to 2.

Medium Panel: (θ = 1/2 radian, Figure 3-6) Convergence was achieved with a 961 DOF, 12 x 6 mesh. This model has an element size range of 0.375 x 0.375 inch to 1.0 x 0.75 inch, with AR = 1 to 2.7.

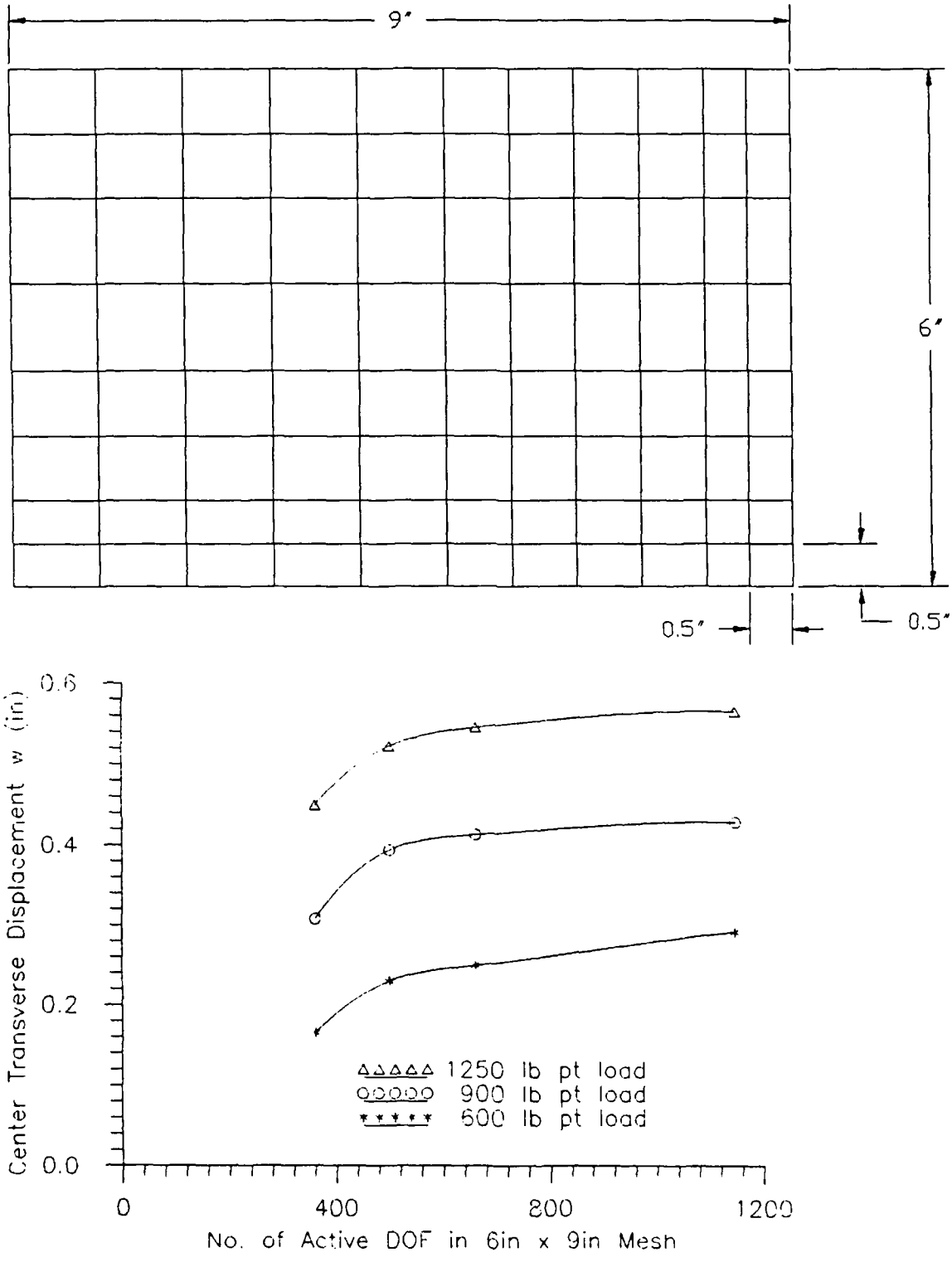

Figure 3-5. W vs Active DOF, 1 Radian Mesh Test

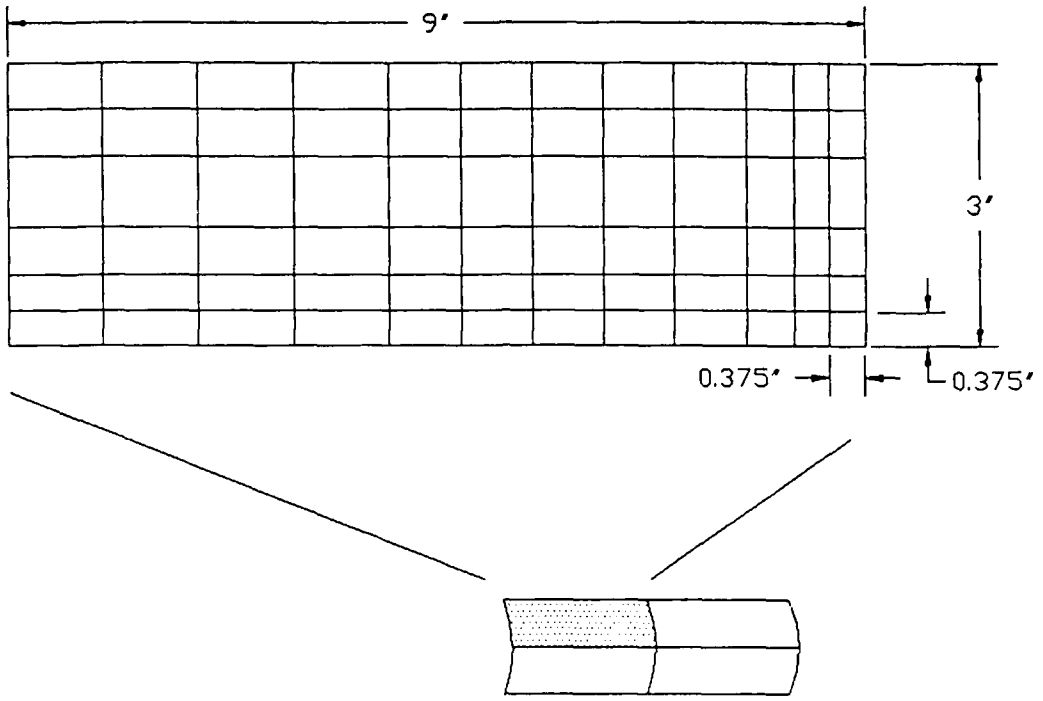

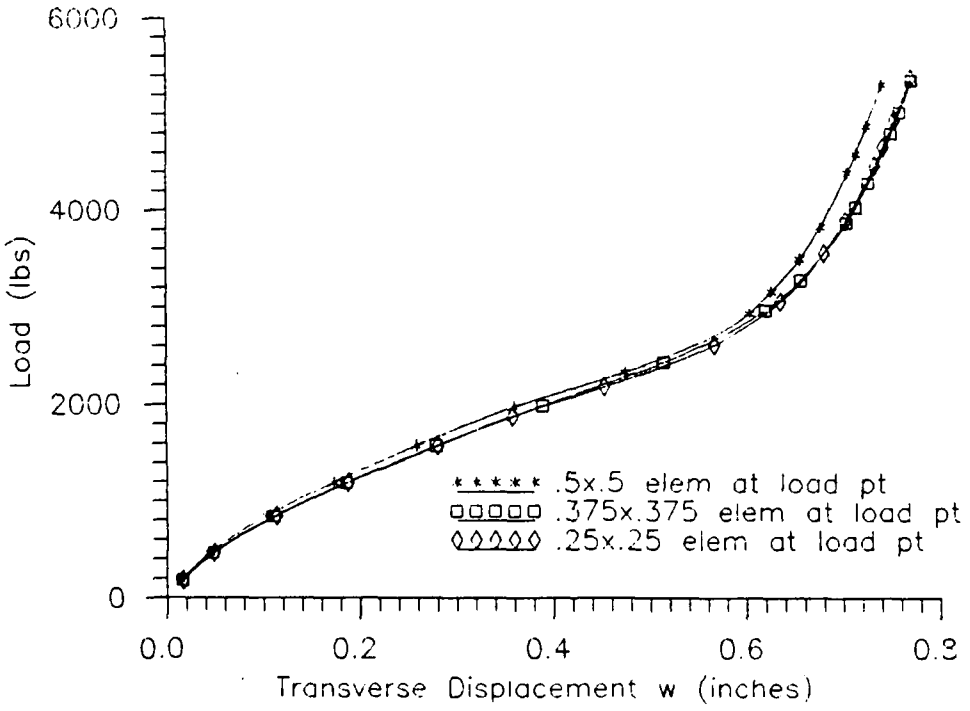

Figure 3-6. Load vs w, 1/2 Radian Mesh Test

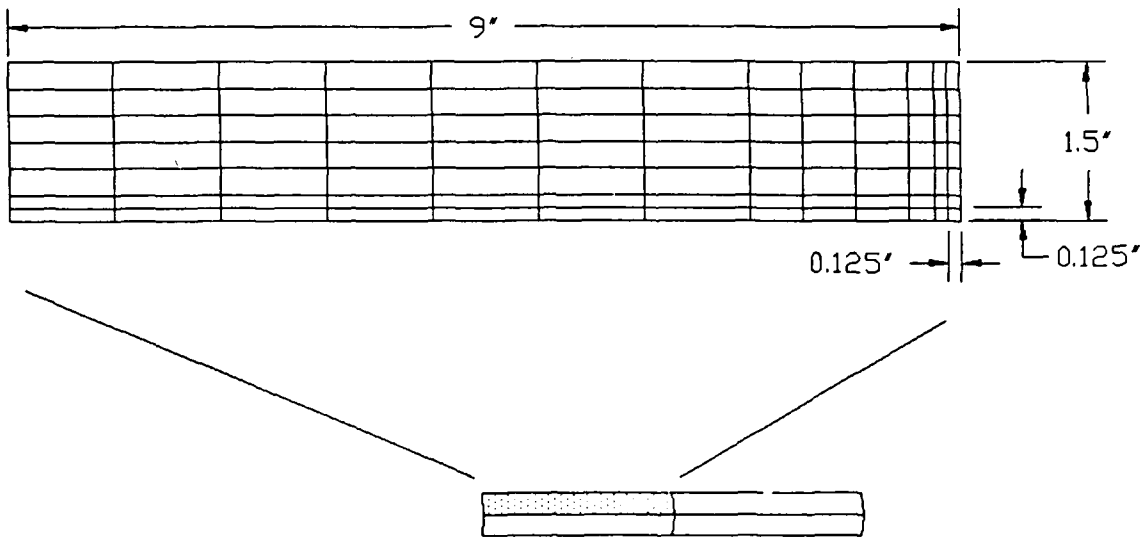

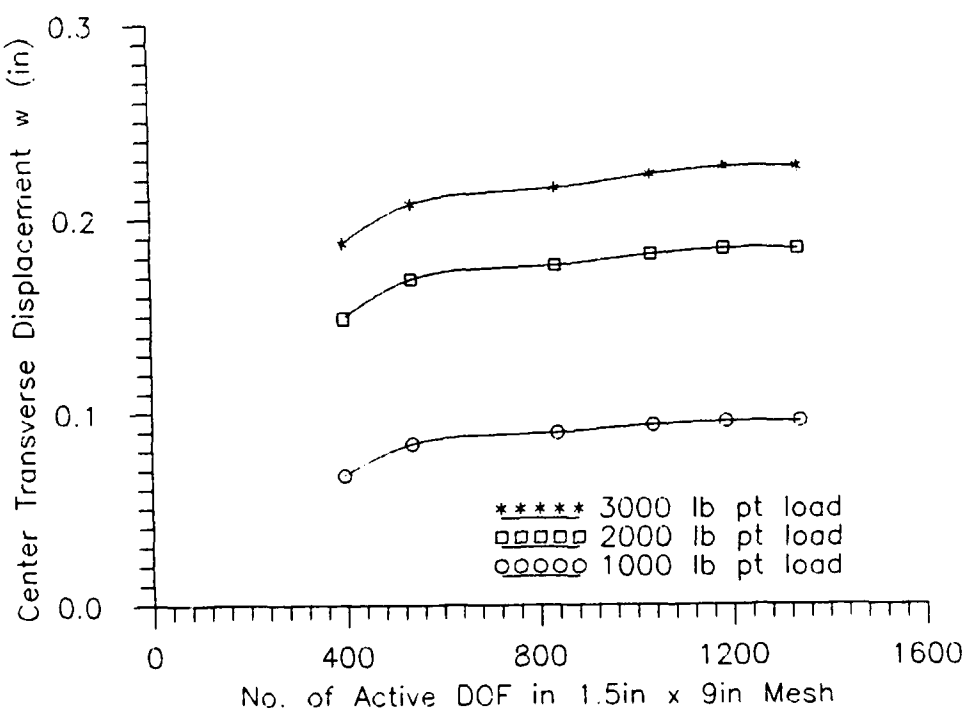

Figure 3-7. W vs Active DOF, 1/4 Radian Mesh Test

Narrow Panel: (θ = 1/4 radian, Figure 3-7) Convergence was achieved with a 1188 DOF, 13 x 7 element mesh. This model has an element size range of 0.125 x 0.125 inch to 0.25 x 1.0 inch, with AR = 1, to 8 (longitudinally) or 2 (circumferentially).

Donnell versus Large Deformation/Rotation Solution. Comparison of solutions of the same model with the Donnell-based element versus the large displacement/rotation (large d&r) element indicate imperceptible difference on the loading up portion of the load - displacement curve (Figure 3-8). The curves deviate after the maximum load, when the shell is collapsing to a locally inverted shape and transverse displacements far exceed the magnitude of the shell thickness. The rotation of the middle surface of the shell, the elastic curve, was between 15 and 20 degrees when solution divergence occurred just after

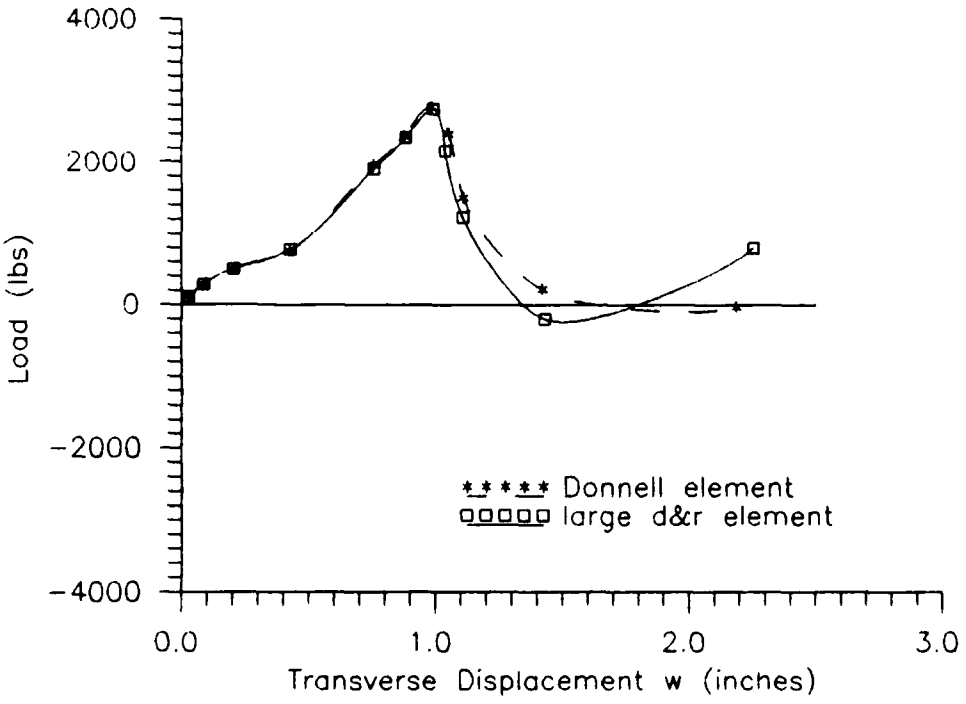

Figure 3-8. Donnell vs Exact, 1 Radian [0 /90] Panel

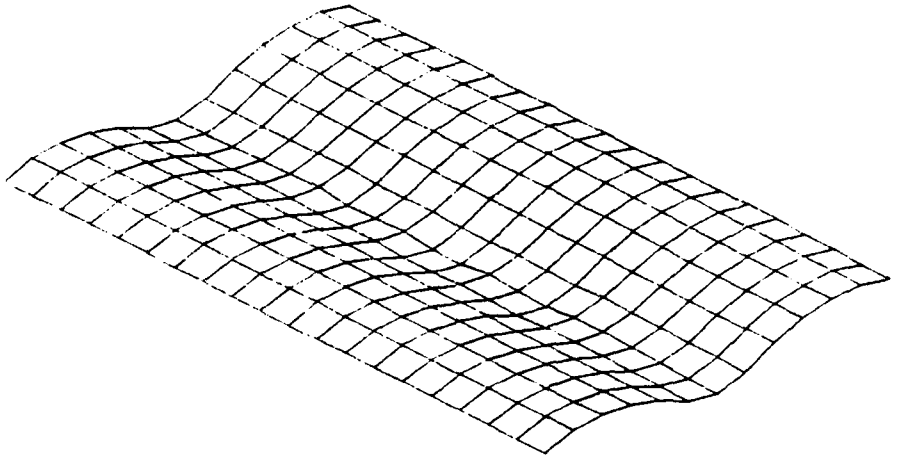

Figure 3-9. Deformed Geometry, Laminated, Donnell Element

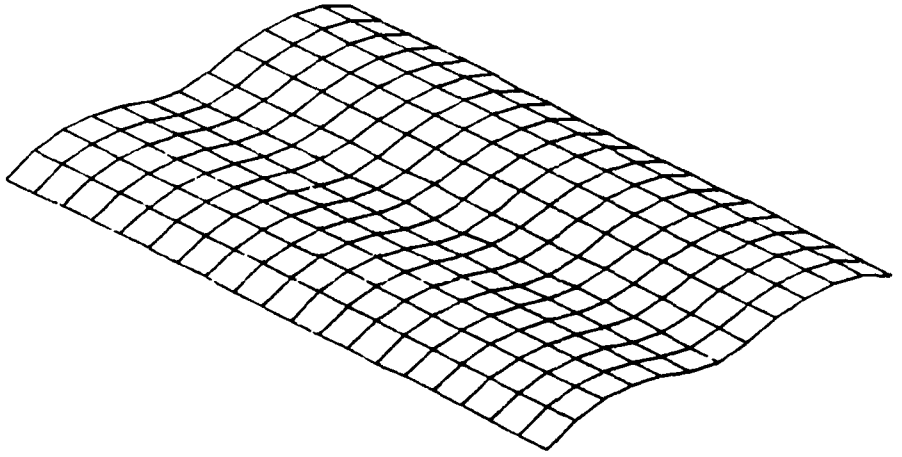

Figure 3-10. Deformed Geometry, Laminated, Large D&R Element

peak load for the three cases compared. Since the only difference between the two solutions is the element formulation, the source of the difference was suspected to be the Donnell simplifications. Neither small displacement relative to thickness, nor large wavelength relative to radius of curvature, can be assumed here, as assumed by Donnell (11). The Donnell solution, which ignores the higher order rotational terms, was stiffer than the large displacement/rotation solution after collapse.

Comparison of the deformed geometry after snapping as predicted by the Donnell formulation (Figure 3-9) and the exact formulation (Figure 3-10) shows agreement in the general nature of the deformation, even though the load-displacement solutions have diverged.

To examine this divergence further, an isotropic panel of the same thickness was analyzed, to eliminate any effect of interply stresses. Aluminum, with average physical properties of $E = 10.3 \times 10^6$ psi, $\upsilon = 0.33$, and $G = 3.85 \times 10^6$ psi was selected for comparison. The load-displacement curves (Figure 3-11) and the displaced geometries (Figures 3-12, 3-13) indicate it responds generally like the laminated panel, with the same solution divergence after peak load. Maximum rotation at the peak is 21 degrees. Thus, the Donnell simplifications, and not interply effects, seem to be the cause of the solution divergence at large displacement and rotation. A full comparison of isotropic versus laminated composite performance is in the next chapter.

This set of tests led to the selection of different elements for various models. The computationally efficient Donnell-based element

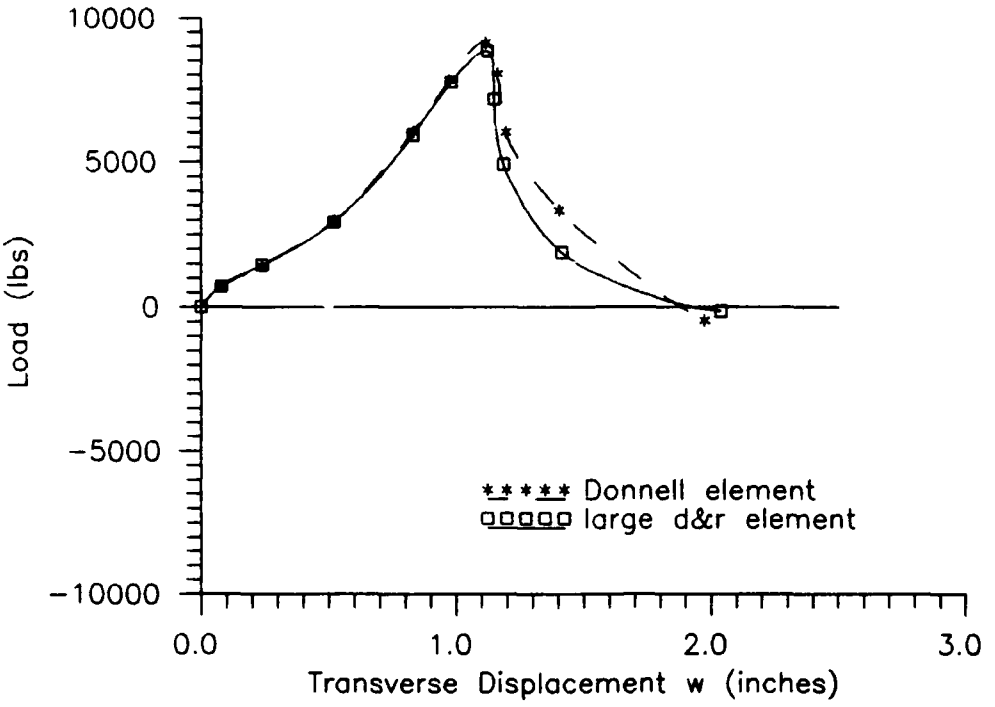

Figure 3-11. Donnell vs Exact, 1 Radian Isotropic Panel

was used only for the cases which undergo small rotations (less than 15 degrees measured at the elastic curve). The shallow (θ = 1/4 radian) shells fall into this category, regardless of boundary conditions, thickness or ply layup. The large displacement/rotation element was used for the remaining analyses due to the large rotations experienced as the center of the arc is driven down relative to the upward slope of the restrained edges.

Stress Computation. Since displacement features were of most interest in this work, ply failure was not rigorously determined. It was used only to gauge when to terminate load incrementing in the shallow clamped cases since they snapped weakly (if at all). However, due to the mathematical singularity of stress at the point of application in this finite element model, computed stresses near that

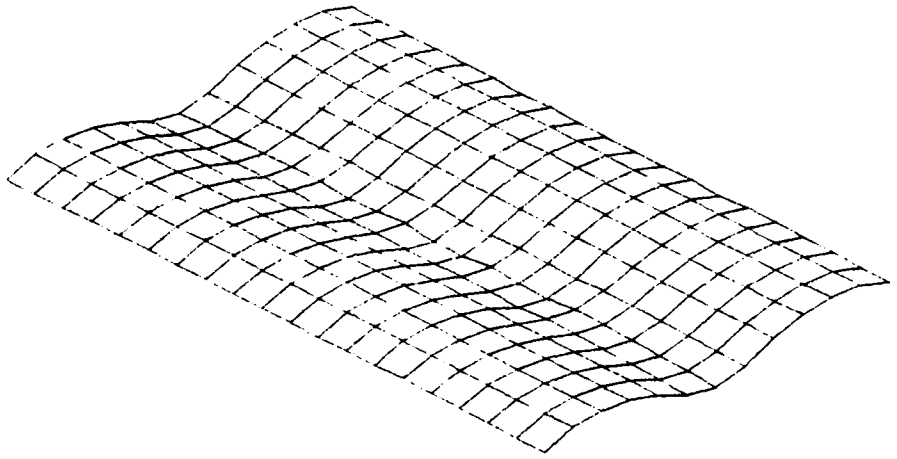

Figure 3-12. Deformed Geometry, Isotropic, Donnell Element

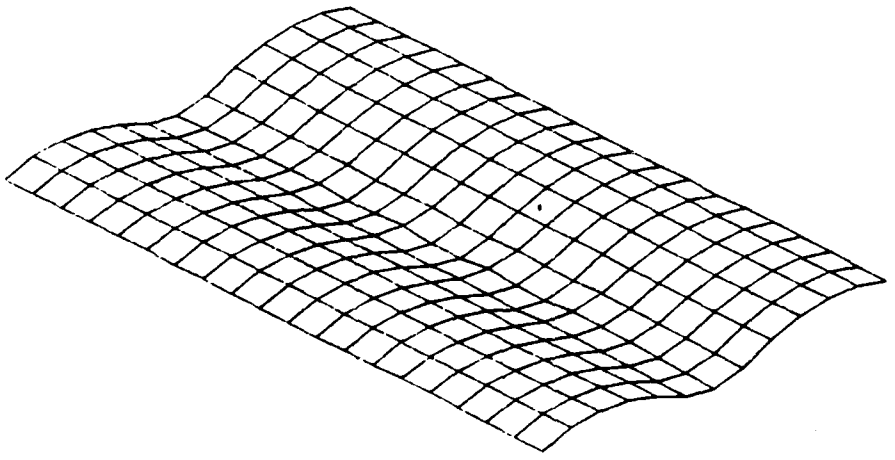

Figure 3-13. Deformed Geometry, Isotropic, Large D&R Element

point falsely predicted very early ply failure. A stress study sought to determine where more accurate stresses could be obtained.

The distribution of shear stress in a pre-snapped loaded shell was plotted. The stress values at the laminate middle surface were seen to vary widely and change sign until after two layers of elements away from the load point. Thus, stresses for ply failure determination were obtained from the third layer and beyond.

Summary. Quarter panel modeling by symmetry was used in all cases in this work. The graded mesh selected for each geometry was fine in the vicinity of the load application point, and was denser in the circumferential direction than longitudinally. There are at least six elements between the load and the boundary in each model. The shallow (θ = 1/4 rad) configuration was solved with the Donnell-based element due to the small rotations experienced. The deeper configurations were modeled with the large displacement/rotation element, with the goal of each run to proceed through snap and reassumption of load.

IV. Results/Discussion

In this chapter the effect of changing ostensibly one parameter at a time is investigated. It is not truly possible to vary certain geometric parameters independently with a cylindrical shell. The primary violator of this attempt to isolate the variances is the shallowness parameter (δ/b). The key determinants of load capacity controlled by shallowness are the angle at which the ends of the middle surface curve meet the chord (the same angle as the opening angle θ), the radius of curvature - to - thickness ratio R/h and the span. Either R or θ can be changed independently to adjust shallowness, but each adjustment will affect the other dimensions differently. For this study R is held fixed and only θ is varied, so the effect of shallowness is combined with the effect of varying the inplane distance from the load point to the restrained edges. In addition, another important geometric feature which is affected is the aspect ratio, a plate parameter that has meaning here when defined as (longitudinal length)/(arc length). By holding the longitudinal dimension constant while varying θ, the aspect ratios in this study range from 6 for the shallow shell to 1.5 for the nonshallow shell. The load path to the free ends is longer compared to the path to the restrained edges for larger aspect ratio. Thus, changing shallowness also changes the load path in two directions, which will affect the shell's static response. However, the effects of these other variables often becomes apparent in the following data presentations.

Generalization of the results pertaining to shallowness to a closed or deeper shell would require redefinition of the shallowness parameter δ/b. Since the deflection under a transverse point load of this class of shells always entails simply three half sine waves in the circumferential direction, b is a valid parameter to characterize the circumferential dimension of the deformation. In a closed or deeper shell, however, more half sine waves could form. In such a case, the arc segment over which each half sine wave forms is the proper dimension for characterizing shallowness.

The Initial Snap Through

This section addresses in qualitative terms the phenomenon of snap through observed with this shell. In later sections dealing with geometric and material effects the post-critical behavior will be correlated to specific parameters.

Snap through is a dynamic process for which analytical prediction and physical reality have yet to be fully reconciled. In a dead load situation as is considered in this study, the problem shifts from a purely static one to a dynamic one once the load peaks and begins to drop off. The equilibrium path obtained beyond the critical point may only be of interest inasmuch as it enables the analyst to determine the displaced configuration at which the structure can resume the applied load. Even then, the true state may differ from the predicted static state due to the inertia developed during the dynamics of the snap through.

Since this study considers only the static equilibrium states, the focus of interest will be on the load response leading up to the critical load point. Beyond that, the discussions of "snapping" are concerned with equilibrium states which may or may not occur as the shell dynamically seeks another configuration at which it can resume supporting the critical load. It must be stressed that the equilibrium curves presented do not reflect any dynamic response nor do they reflect material failure or other such nonlinearity. The response is purely geometry dependent, and represents various equilibrium energy states.

For the equilibrium curves which do eventually return to (and surpass) the critical load value, the shell will be assumed to have snapped and be supporting the load again. It is acknowledged that this is an oversimplification due to neglect of the dynamic nature of the response.

In this study the shell is seen to collapse in two distinct ways. The term "local" collapse or snap will be used to denote inversion of a circumferential section of the shell around the point of load application, while the free ends of the shell maintain their original downward concavity. "Full" collapse or snap is said to occur when the free ends also have turned under. The difference between local snap and full length snap can be readily seen in Figures C-2 and C-5. In either case, the load curve reaches zero slope as the snap initiates, with diminishing load capacity as the inversion progresses. Snap can be just barely critical (Figure C-3) or severe (Figure C-5), but if zero slope does not occur, the shell does not snap.

During a full-length collapse, the load-displacement curve becomes near-vertical in several of the cases, exhibiting load change with no displacement of the load point. Figure C-5 illustrates the shell response during this unloading phase. At peak load, the shell has stored strain energy due to the transverse deflection of the central load point. Further displacement results in this stored energy developing moments which drive the free ends down to an inverted shape. If the shell is clamped or otherwise geometrically stable, it will recover after the ends collapse, and resume the load (Figure A-11, clamped cases). A geometrically unstable shell, though, has an increasingly negative equilibrium path (Figure A-11, hinged cases), possibly indicating total geometric failure.

Whether a shell will snap locally or fully is determined by a combination of its stiffness (thickness, ply orientation) and geometric parameters (shallowness, aspect ratio). With either type of snap, the deformation progression starts the same. The deformation histories in Figures C-2 and C-5 illustrate this progression. In both, the center of the shell under the load point is seen to initially invert, or "dimple;" in the thinner and deeper shells an inflection point in the curve becomes apparent at the onset of dimpling (Figure C-6). After this initial dimpling, the inverted area "grows" circumferentially and longitudinally as the load is increased. Critical load is reached when the dimple has reached an edge. In local snapping, the dimple reaches the constrained edges before the free ends, and only a central section of the shell inverts as the load drops off (Figure C-2). In a full snap case, the dimple travels more longitudinally than

circumferentially, and the load capacity drops off as the free ends invert (Figure C-5).

The type of snap to which a shell is susceptible would be of interest to designers looking for some degree of failsafety. Full snaps are generally more severe, and often result in negative load values. Negative loads mean that in order to maintain the shell at such a deformed state of equilibrium the center load would have to be pulling up. Local snap, on the other hand, was never seen to result in negative loads over the range of parameters tested. When both local and full snap points are reached nearly simultaneously, the equilibrium path is complex and twisting, as seen by the partial trace shown in Figure C-7. (Experimentally, such a load-deformation response may not be realizable, as this may be just a numerical artifact.)

An interesting feature which is included in this finite element is the deformation of the shell normal due to transverse shear stress. The linear transverse shear strain-displacement approximation in this code results in the transverse shear stress showing up as a rotation of the shell normal separate from the rotation due to bending of the shell middle surface. These two rotations combine to yield the total rotation (strain) of the shell normal. The proportion of strain which is due to transverse shear effects will be noted in the comparisons in the remainder of this chapter, in an effort to determine the importance of including such effects in the analysis of transversely loaded shell structures.

Comparison to Isotropic

To allow comparison of laminated shell load - displacement performance to an isotropic shell of equal thickness, the response data was normalized. In his analysis of isotropic shells, Chernyshev (5) determined that the response of such a transversely loaded shell is dominated by bending features, so normalization was based on the bending stiffness parameter. Shell thickness with both materials was identical (0.12 inch, corresponding to a 24 ply laminate) to allow for the generation of comparable through thickness shear stresses. The normalization, for comparison with shells of identical thickness and geometry but different material, is:

$$\text{Laminated:}\quad \bar{w} = \frac{wD_{22}}{P} \qquad \bar{P} = P/D_{22} \qquad \text{Isotropic:}\quad \bar{w} = \frac{wD}{P} \qquad \bar{P} = P/D \qquad (4\text{-}1)$$

where

barred values are normalized

$$D = \frac{Eh^3}{12(1-\upsilon^2)} = 1664 \text{ lb-in (0.12 in thick Al)}$$

$$D_{22} = \sum\left(\bar{Q}_{22}\right)_k \left(h_k \bar{z}_k^2 + \frac{h_k^3}{12}\right), \quad k = 1,2,\ldots,n \text{ plies}$$

Figure 4-1 defines the geometry for determining the laminated bending stiffness parameter D_{22}. Tables 4-1 and 4-2 list this and the rest of the inplane and bending stiffnesses of all of the laminates. (The graphite/epoxy lamina, and aluminum, material properties are given in Chapter 3.) Although these normalized values are not fully nondimensionalized ($\bar{w}$ and $\bar{P}$ have units of in^2 and in^{-1}), they allow for valid comparison between identically dimensioned shells.

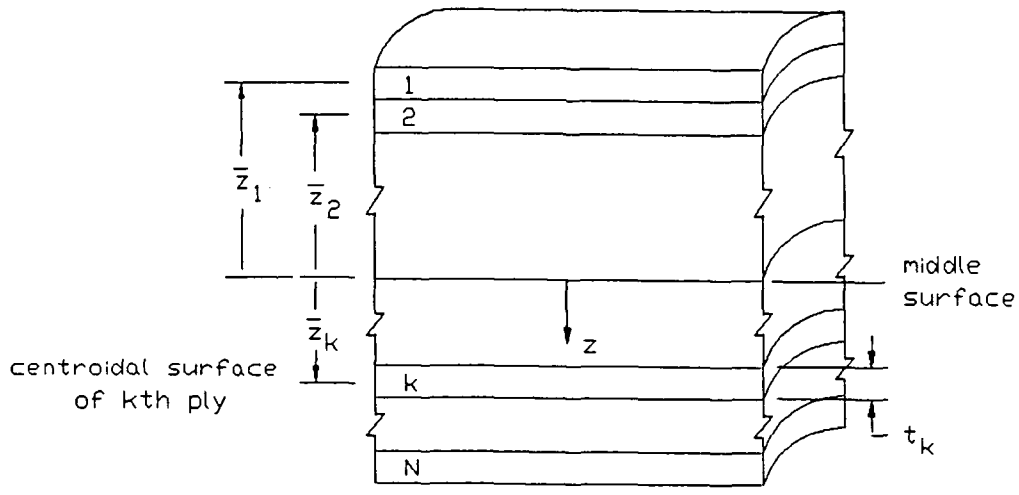

Figure 4-1. Laminate Definitions

Figure 4-2 shows that the isotropic and the laminated shells deflect very similarly overall with respect to bending stiffness in the circumferential direction. There is a point of inflection upon load up on only the laminated curves however, which corresponds to the load at which the area around the load point dimples in. Prior to dimpling, the load is supported through the membrane by inplane compression. The composite shells are relatively stiffer at this point; the cross ply and angle ply layups deflect only 76% and 60% of the value of $\bar{w}$ for the isotropic shell at the same $\bar{P}$. After dimpling, when significant bending develops, the deformation is proportional to the bending stiffness as with the isotropic shell. This illustrates the importance of designing a thin shell composite structure to take advantage of its superiority of membrane over bending stiffness.

Observing the transverse shear strain in each of the shells allows evaluation of the relative importance of including this feature in the

Table 4-1. $[0/90]_s$ Stiffness Parameters

	Plies, Thickness (inches):			
	8, 0.04	24, 0.12	48, 0.24	96, 0.48
Extensional terms (lb/in):				
A_{11} ($x10^6$)	0.4087	1.226	2.452	4.905
A_{22} ($x10^6$)	0.4087	1.226	2.452	4.905
A_{12} ($x10^3$)	16.543	49.628	99.256	198.512
A_{12}	0	0	0	0
A_{16}	0	0	0	0
A_{66} ($x10^3$)	36.4	109.2	218.4	436.8
Coupling terms:				
B_{ij} all are zero due to symmetry				
Bending terms (lb-in):				
D_{11}	89.4637	2415.52	19324.2	154593.
D_{22}	19.5325	527.378	4219.03	33752.2
D_{12}	2.2057	59.5535	476.428	3811.42
D_{12}	0	0	0	0
D_{16}	0	0	0	0
D_{66}	4.8533	131.04	1048.32	8386.56

Table 4-2. $[0/\mp45/90]_s$ Stiffness Parameters

	Plies, Thickness (inches):			
	8, 0.04	24, 0.12	48, 0.24	96, 0.48
Extensional terms (lb/in):				
A_{11} ($x10^6$)	0.3289	.9867	1.9733	3.9467
A_{22} ($x10^{6)}$	0.3289	.9867	1.9733	3.9467
A_{12} ($x10^3$)	96.391	289.174	578.348	1156.70
A_{12}	0	0	0	0
A_{16}	0	0	0	0
A_{66} ($x10^3$)	116.248	348.744	697.488	1394.98
Coupling terms:				
B_{ij} all are zero due to symmetry				
Bending terms (lb-in):				
D_{11}	72.0721	1945.95	15567.6	124541.
D_{22}	19.6237	529.841	4238.73	33909.8
D_{12}	10.8560	293.111	2344.89	18759.1
D_{16}	-4.3707	-118.009	-944.071	-7552.57
D_{26}	-4.3707	-118.009	-944.071	-7552.57
D_{66}	13.5035	364.595	2916.76	23334.1

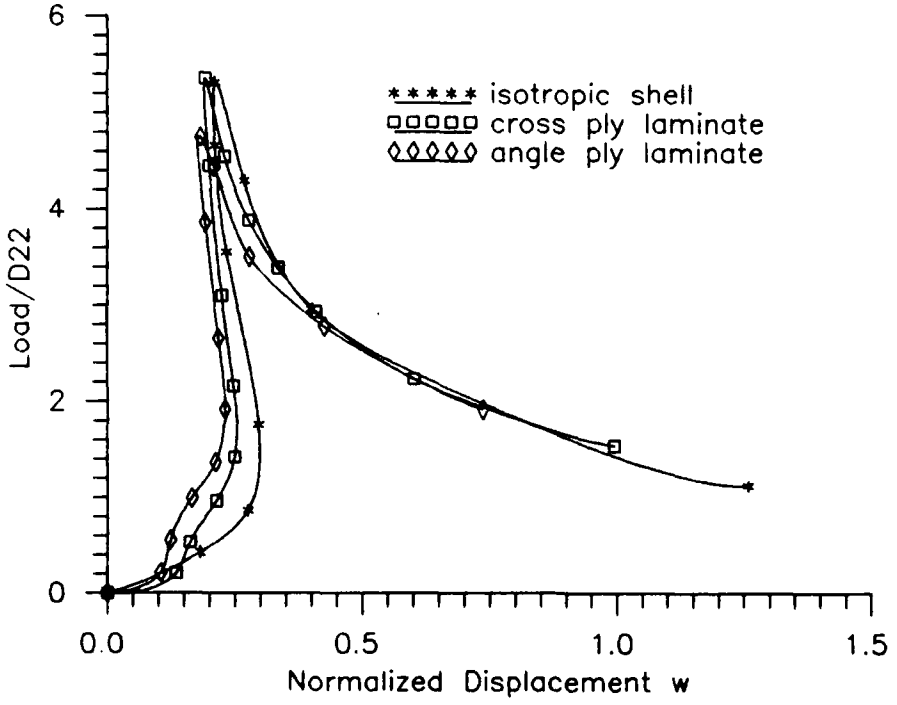

Figure 4-2. Response Normalized to Bending Stiffness

analysis of laminated and isotropic structures. Table 4-3 lists the maximum transverse shear strain developed circumferentially (β_s) in each type of shell at roughly equal load. The location of maximum β_s is given in terms of (x,s) coordinates, in inches, away from the centered load point. The magnitude of β_s relative to the rotation of the shell normal due to bending of the middle surface in the circumferential plane is also noted, as a percentage $\beta_s/w,_s \times 100$.

At low initial load, when the support mechanism is membrane compression, we see that all shells develop very little transverse shear strain. The β_s in the laminated shells are 1.5 to 1.6 times the

Table 4-3. Shell Material Effect on Transverse Shear

shell construction	applied load, lbs	location (x,s) in	β_s, rad	% of $w_{,s}$
Onset of loading; no bending yet:				
isotropic	512	0, 1	$.337 \times 10^{-3}$	1.2
$[0_6/90_6]_s$	611	0, 1	$.520 \times 10^{-3}$	0.4
$[0_3/\mp45_3/90_3]_s$	526	0, 1	$.530 \times 10^{-3}$	0.6
Dimple has formed around load point:				
isotropic	1146	0, 1	$.852 \times 10^{-3}$	1.1
$[0_6/90_6]_s$	960	0, 1	$.114 \times 10^{-2}$	0.7
$[0_3/\mp45_3/90_3]_s$	1015	0, 1	$.144 \times 10^{-2}$	1.7
Continuing to apply load:				
isotropic	1699	0, 1	$.125 \times 10^{-2}$	0.9
$[0_6/90_6]_s$	1415	0, 1	$.168 \times 10^{-2}$	0.9
$[0_3/\mp45_3/90_3]_s$	1407	0, 4.5	$.228 \times 10^{-2}$	39.6
Laminates reach peak load; isotropic is 29% of way to peak:				
isotropic	2550	0, 1	$.162 \times 10^{-2}$	1.0
$[0_6/90_6]_s$	2733	.5, 1	$.220 \times 10^{-2}$	0.9
$[0_3/\mp45_3/90_3]_s$	2514	0, 4.5	$.414 \times 10^{-2}$	7.9
Isotropic at peak load:				
	8762	0, 1	$.272 \times 10^{-2}$	1.0

value of β_s developed at comparable load in the isotropic shell, but because the isotropic shell has deflected less at this load, its β_s is larger compared to its $w_{,s}$.

After the area around the load point forms a dimple the cross ply shell is developing 1.3 times the transverse shear strain compared to the isotropic shell, but β_s maintains a proportion of 1% of $w_{,s}$, as does the isotropic shell. These relations stay fairly constant throughout the remainder of the load up of the isotropic and cross ply shells.

Significant differences appear when bending comes into play with the angle ply shell, though. After the center of the shell dimples, the β_s in the angle ply has grown to 1.7 times the isotropic β_s. By the time the angle ply shell has reached 56% of its peak load (the third load case in Table 4-3), the factor has grown to over 1.8. Also at this load, the transverse shear strain rotation is 40% as large as the slope of the elastic curve on the center arc at a point 2/3 of the way from the center to the constrained edge. This points out the nonnegligible effect of transverse shear strain on the structural response in the bending regime with angle ply laminated structures.

Continuing on to peak load with the angle ply shell, the transverse shear strain increases to a value of β_s which is 2.6 times that of the isotropic shell, and nearly 2 times that of the cross ply laminated shell, at comparable load. Now, though, transverse shear strain is back down to 8% compared to $w_{,s}$, since the middle surface slope has increased relatively more than β_s has grown over the same load increase.

The magnitude of the transverse shear strain corresponds to the relative magnitudes of inplane shear stiffness A_{66} and the transverse shear stiffnesses A_{44} and A_{55}. Since isotropic material exhibits identical material properties in all directions, these three terms are equal in the isotropic shell. Accordingly, Table 4-3 shows it to develop less transverse shear strain than either of the laminated shells. The values of A_{44} and A_{55} in the laminated shells are the same for both ply layups examined, at 81.6 x 10^3 lb/in. This is 75% of the value of A_{66} for the cross ply laminate (Table 4-1), and we see from Table 4-3 that it develops a bit more transverse shear strain than the isotropic shell. The transverse shear stiffness is only 23% of the value of A_{66} for the quasi-isotropic laminate (Table 4-2), though, and we see that it develops the greatest magnitude of transverse shear strain at all loads.

The relative load capacities of the two types of shells correspond roughly to the relative bending stiffnesses. The isotropic shell supports 3.13 and 3.51 times the load before collapse than do the cross and angle ply laminates respectively; the isotropic shell's bending stiffness D is 3.16 and 3.14 times the value of D_{22} for the cross and angle ply shells. This correlation is expected because the transverse response of this thin shell is primarily bending. The relative inferiority of laminates in bending compared to isotropic materials as seen here is the reason why designs which are optimized for thin composite materials place the composite members in membrane loading, which exploits the superior in-plane properties of thin composites. The laminate can also be rearranged to place plies which will best

support anticipated bending the furthest away from the neutral axis.

A popular technique of estimating laminate material properties is to compute effective engineering properties which are then used as if the material were orthotropic. In the load case studied here, where the dominant response is bending, use of these effective engineering values would lead to overprediction of strength, as will be shown next.

The effective Young's modulus in the circumferential direction, E_y, and Poisson's ratio ν_{xy}, are computed from the extensional stiffnesses:

$$E_y = \frac{A_{11}A_{22} - A_{12}^2}{h\,A_{11}} \qquad \nu_{xy} = \frac{A_{12}}{A_{22}} \tag{4-2}$$

Using the values for A_{ij} in Tables 4-1 and 4-2 to obtain E_y and ν_{xy}, and then computing the bending stiffness D as for an isotropic material in Equation 4-1, bending stiffnesses of 1471 lb-in for the $[0_6/90_6]_s$ and 1184 lb-in for the $[0_3/\mp45_3/90_3]_s$ are predicted. Considering that the bending stiffness is 1664 lb-in for the aluminum shell of equal thickness, this would lead to the mistaken conclusion that the laminated shell's peak load would be at least 70% of that for the isotropic shell. In fact, the laminates collapse at less than 1/3 the load at which the isotropic shell does. This illustrates that application of laminated effective engineering properties to configurations which undergo significant bending in support of a load is not advisable.

Variation of the Parameters

The next discussion covers the effect of independently varying each of the four parameters in this study. Rather than scatter the graphs throughout this chapter, they have been grouped into three appendices. Appendix A contains the load versus displacement curves for the 48 cases analyzed. Appendix B contains plots where load has been normalized to facilitate comparison of shells of the same geometry but different thicknesses. Appendix C shows graphically the progression of deformation for a sample of each type of load - displacement curve seen in this study.

Due to the way the Riks algorithm steps past critical load points, the critical load values for the highly peaked curves such as in Figures A-9 and A-10 are not as credible as the critical loads found on the curves with less slope change at the critical point. Therefore, no conclusions are drawn concerning the pre-collapse load capacity of the thin deep shells, which all display sharply peaked critical load points.

Effect of Ply Layup. Direct comparison of the two layups is possible using the plots in Appendix A. Not surprisingly, the angle ply laminate is stiffer in response to a transverse load. It deforms less at the same load and collapses earlier (and unloads less when it does) than a cross ply laminate of the same geometry. Figure A-8 give the best illustration of this.

The curves of the two layups do not diverge until significant bending has taken place. The only difference of any magnitude in the physical properties is the much higher shear (A_{66}), twisting (D_{66}) and

coupling (A_{12} and D_{12}) stiffnesses of the angle ply laminate (Tables 4-1, 4-2), plus the fact that the angle ply layup has nonzero twisting stiffnesses D_{16} and D_{26}. Because of these higher twisting and biaxial coupling properties, the angle ply better resists the twisting which accompanies the bending as the geometrically nonlinear shell undergoes three dimensional transverse deformation.

Neither orientation is independently superior with regards to load capacity. In Figure A-6, the angle ply shell is seen to reach critical load at 11% less deformation than the cross ply, at which point it is carrying 6% more load than the cross ply shell at collapse. In Figure A-5, though, the angle ply collapses at 15% less deformation, but this time at 2% less load than the cross ply. This graph also shows that while both layups exhibit critical load points, the cross ply collapses through critical displacement points as well. This highlights the effect of ply orientation on predominantly displacement behavior. No consistent pattern of effect on load capacity was seen with the two layups tested, though.

The transverse shear strain on load up generally is greater with the angle ply laminate than for the cross ply. A comparison of the 24 ply 1 radian hinged shell was presented in the previous section. How much greater depends on thickness and shallowness, from the thin shallow shells of either layup showing about equal β_s at peak load to the clamped 24 ply 1/4 radian shell showing 2.4 times more β_s in the quasi-isotropic layup than in the cross ply layup. The one exception to this observation is the 8 ply 1 radian shell, in which the cross ply

developed about 10% greater β_s throughout the equilibrium path, with either boundary condition studied.

In general, it can be said that the ply orientation affects the deformation prior to critical load such that a layup with comparable direct stiffnesses but higher shear and inplane coupling stiffnesses (due to the presence of angle plies) will collapse at less transverse displacement. Load capacity at collapse, which is more directly controlled by other geometric factors, may be higher or lower. The angle ply layup can generate more transverse shear stress which would tend to reduce its stiffness, but this effect is obscured by the increased shear and twisting stiffness of the angle plies.

Effect of Boundary Condition. Clamping prevents snapping of the shallow θ = 1/4 radian shell and the thicker 1/2 radian cases. For the 8 ply 1/2 radian shell and the 1 radian shells, clamping caused collapse to occur at less transverse displacement, although it supports more load than the hinged shell at corresponding displacement on the initial load up curve. In any case where geometric failure occurred (negative loads with no load recovery), clamping stabilized the response to a simple snap (Figures A-5, 11, 12). Clamping also eliminates the possibility of local snap, since no portion of the bound edge is allowed to rotate - a feature required for local snapping. Any snapping of a clamped shell is one of free end inversion and must occur after the dimple has traversed the longitudinal length.

The boundary condition's role in hastening the onset of collapse (when the clamped shell does collapse) can be understood from Figures C-4 and C-5. In the hinged case (Figure C-5), the load dimple travels

in two directions - longitudinal and circumferential. With the edges clamped (Figure C-4), the dimple cannot progress as far circumferentially due to the increased stiffness from the clamped edge, so all of the deformation is concentrated in the lengthwise direction. This results in the dimple consistently reaching the free ends at a lower value of central displacement compared to the hinged shell.

The maximum transverse shear strain rotation developed in the 8 angle ply shells at each boundary condition are noted in Table 4-4, along with the x and s distances from the center where this maximum occurs. The 1/2 and 1/4 radian clamped shells generate slightly greater transverse shear strain compared to bending rotation than do the hinged shells, due to localization of the deformation. The hinged boundary as applied in this study allows both midsurface rotation (bending) and rotation of the normal (transverse shear strain), in the

Table 4-4. Boundary Effect on Transverse Shear

boundary condition	applied load, lbs	location (x,s) in	β_s, rad	% of $w_{,s}$
$[0/\mp45/90]_s$, θ = 1/4 radian				
hinged	46	2, .5	$.667 \times 10^{-3}$	7.3
clamped	44	0, .25	$.122 \times 10^{-2}$	2.0
$[0/\mp45/90]_s$, θ = 1/2 radian				
hinged	148	0, 2	$.120 \times 10^{-2}$	1.0
clamped	150	0, 2	$.180 \times 10^{-2}$	1.9
$[0/\mp45/90]_c$, θ = 1 radian				
hinged	95	.5, 1	$.155 \times 10^{-2}$	0.9
clamped	113	0, 3.5	$.146 \times 10^{-2}$	1.5

circumferential direction, at the otherwise bound edges. Thus the rotations of the shell normal due to transverse shear strain can extend all the way to the hinged edge. The clamped boundary condition restricts to zero rotation of any kind of the shell normal along the bound edge, so the transverse shear strain rotations are restricted to lie between the center plane of symmetry and the clamped edges. This results in the transverse shear strains being concentrated over less of the shell, causing higher values locally for the clamped cases. The deep 1 radian shells did not follow this trend, but the cause for this may relate to the length of the load path to the constrained edges.

The effect of other parameters is highlighted with the hinged boundary condition. Clamping the edges stabilizes the shell since the bending loads are supported by a rigid boundary, leaving only the central ridge portion free to invert under load. Freeing up the edges to rotate means that the shell alone must resist the bending loads. Figures A-4, A-6 and A-8 are examples which show how the hinged curves emphasize layup differences. In upcoming sections examining thickness and shallowness, the variation in displacement at the onset of collapse is studied. The hinged cases are used for those studies both because they reach a critical load point more often and also because the effect of the other geometric variables is greater than when the boundary is clamped.

Effect of Shallowness. The effect of varying the opening angle θ ties together several parameters which directly affect the static response of the shell, as discussed in the opening paragraph of this chapter. Length of the load path to the restrained edges, "aspect

ratio" and central rise are key determinants of load capacity and displacement at collapse, and are all changed by varying θ. Realizing this, we are not able to conclusively attribute the trends discussed in this section to depth only. These conclusions are valid, then, for direct application only to a family of cylindrical shells which holds the same parameters (R, h and length) constant while varying only θ, unless otherwise stated.

The one parameter which appears to apply universally to all hinged shells is one that compares the thickness h to the central rise δ. The value of $(h/2)/\delta$ gives a qualitative indication of the severity of collapse. A value of this parameter of ≥ 1 means that some portion of the cross sectional thickness of the shell extends below the chordline of the arch over the entire span; the shell is either very shallow, very thick, or both. The values of this parameter for the range of geometries in this study are listed in Table 4-5.

Table 4-5. Thickness/Central Rise Parameter $(h/2)/\delta$

No. plies, h (inch)	Opening angle θ rad (central rise, inch): 1/4 (0.094)	1/2 (0.373)	1 (1.469)
8 (0.04)	0.214	0.054	0.014
24 (0.12)	0.641	0.161	0.041
48 (0.24)	1.282	0.322	0.082
96 (0.48)	2.564	0.643	0.163

No critical point is observed when $(h/2)/\delta > 1$; the shell just loads up without interruption. When $(h/2)/\delta < 1$, the shell exhibits a load peak and an increasingly sharp unloading as the parameter

decreases. A critical range exists between 0.054 - 0.163, where geometric failure as indicated by a near vertical negative curve occurs. At values of $(h/2)/\delta < 1$ but outside the range 0.054-0.163, the structure snaps through and reassumes the critical load in an inverted and stiffer state.

The relationship between shallowness and maximum displacement prior to collapse is observed by plotting (w at load peak)/(δ/b) versus (δ/b). Figure 4-3 shows this data for the twelve hinged $[0/90]_s$ cases, with a trend suggested by investigation of the post-unloading deformed contours. To the left of each curve peak, on the upslope, the shell inverts locally. To the right, on the down slope, full length inversion occurs. Since the 48 (R/h = 50) and 96 (R/h = 25) ply cases offer only 2 data points (the 1/4 radian shells of those thicknesses did not collapse), extrapolation of the trend to the thicker shells warrants further study.

A side effect of the selection of controlled variables in this study is that the "aspect ratios" of these shells correlate to their shallowness factors such that the horizontal axis in Figure 4-3 could just as well be "(longitudinal length)/(arc length)." Further study is required to isolate the true determinant of this trend.

A comparison of pre-collapse load capacity versus shallowness did not indicate any consistent relation, partly due to inaccuracy in using the fitted curve peak as the peak load. Riks acknowledged that peak values will be stepped past with this solution algorithm and thus are not accurate (28); he suggested employing auxiliary algorithms to determine critical load. The large step size used on the sharply

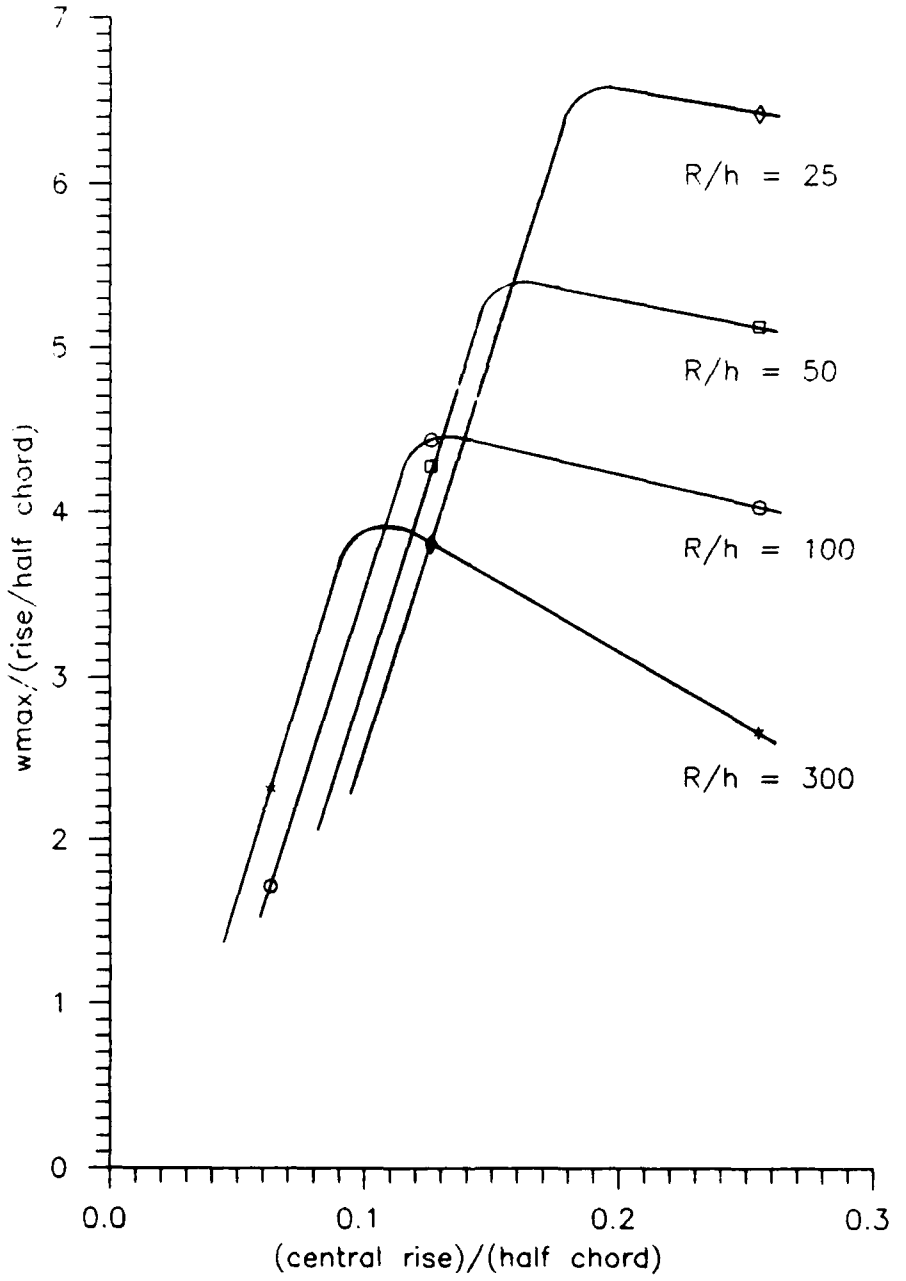

Figure 4-3. w at Peak Load vs Shallowness, Hinged [0/90]$_s$

peaked curves (Figure A-10, for example) prohibits even approximating the peak load in this study. Another effect clouding load comparison is that the shallowness parameter is a characteristic of the middle surface of a thin shell, which for thicker shells ignores the contribution to load support due to increased cross section.

The shallow shells develop higher transverse shear strain in comparison to the bending rotation of the elastic curve. Table 4-6 shows the maximum transverse shear strain rotation developed in a sample of the shells. The expected effect was for β_s to decrease as depth increase, but this trend only held when going from the 1/4 radian to the 1/2 radian shell. Then, the value of β_s is larger in the 1

Table 4-6. Shallowness Effect on Transverse Shear

opening angle θ (radians)	applied load, lbs	location (x,s) in	β_s, rad	% of $w_{,s}$
$[0_6/90_6]_s$, hinged				
1/4	825	.125, .25	$.407\times10^{-2}$	5.7
1/2	825	.75, .75	$.998\times10^{-3}$	1.2
1	960	0, 1	$.114\times10^{-2}$	0.7
$[0/\mp45/90]_s$, hinged				
1/4	65	2, .5	$.125\times10^{-2}$	5.4
1/2	63	0, 2	$.728\times10^{-3}$	1.6
1	62	.5, 1	$.124\times10^{-2}$	0.9
$[0/\mp45/90]_s$, clamped				
1/4	87	3, .75	$.212\times10^{-2}$	18.8
1/2	89	0, 2	$.107\times10^{-2}$	4.5
1	113	0, 3.5	$.146\times10^{-2}$	1.5

radian shell than in the 1/2 radian shell. However, since the 1 radian shell is much wider and bends more, the relative value of β_s in comparison to the slope $w,_s$ is less than the relative value for the shallower shell, so the trend is continued. This trend is clearly seen in Figure 4-4.

Shallowness is seen therefore to affect primarily the displacement at critical load. Varying θ while holding R, L and h constant produces a $(w_{peak})/(\delta/b)$ vs (δ/b) curve in which the peak corresponds to both maximum pre-collapse transverse displacement and the separation between local and full inversion. Increasing the shell thickness moves the curve peak up and right, which increases the maximum displacement prior

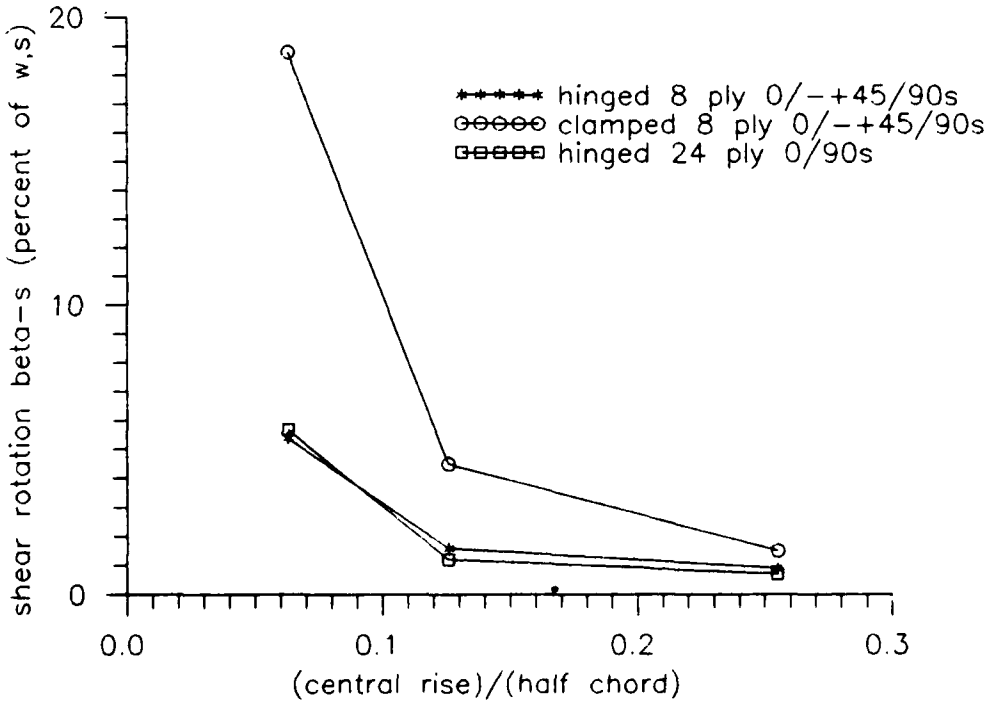

Figure 4-4. Transverse Shear Strain vs Shallowness

to the onset of full length inversion, as well as upping the shell depth at which the inversion goes full length. Note that the 24 ply (R/h = 100) 1/2 radian shell sits on the peak separating the two types of response. The deformed contour history in Figure C-7 indicates that the collapse of this geometry is a mixed mode of local and full inversion. Figure 4-3 indicates that this depth yields the maximum normalized pre-collapse displacement for the R/h = 100 shell. Finally, while the magnitude of transverse shear rotation may increase or decrease with increasing depth, the relative magnitude compared to the bending rotation decreases as depth increases.

Effect of Thickness. In order to compare plots of different thickness, the load data must be normalized. The comparison to isotropic done earlier in this chapter confirmed that in general, the response of this class of shells is dominated by the bending stiffness D_{22}. As indicated by the plots in Appendix B, though, such a normalization ignores the increased membrane capacity due to the increase in the cross section as h increases and depresses the bending-normalized load values for the thicker shells.

An attempt to determine a more accurate normalization factor was not conclusive. For this effort, the bending stiffness D_{22} and the membrane stiffness A_{11} were assumed to be the only significant contributions to the shell's load suppo t. Thus, the difference in the load ΔP supported at equal displacement for two shells of different thickness but otherwise identical geometry is a combined effect of the bending and membrane stiffness differences:

$$f_A \Delta P + f_D \Delta P = \Delta P \qquad (4\text{-}3)$$

where

f_A = proportion of load difference due to membrane stiffness, which scales as thickness h

f_D = proportion of load difference due to bending stiffness, which scales as thickness cubed h^3

Since these two effects are assumed to be the only determinants of load capacity, $f_A + f_D = 1$. To provide a second equation to allow for solution of these two unknowns, the loads supported by the two shells are compared to the relative stiffnesses:

$$\frac{\text{(load on shell x)}}{\text{(load on shell y)}}\Bigg|_{\text{same w}} = f_A\left(\frac{A_{11x}}{A_{11y}}\right) + f_D\left(\frac{D_{22x}}{D_{22y}}\right) \qquad (4\text{-}4)$$

By balancing the two equations ($f_A + f_D = 1$, and 4-4), one obtains an approximation of the relative contributions to the load capacity of the bending and membrane stiffnesses (assuming those are the only effects at work). The combined thickness scaling factor obtained is

$$h^{\left(f_A + 3f_D\right)} \qquad (4\text{-}5)$$

The combined scaling factor ranged from $h^{1.3}$ to h^2, depending on the magnitude of the thickness difference of the shells under comparison, as well as the degree of shallowness. Thus, the geometric

nonlinearity as well must be incorporated into such a scaling factor. The conclusion drawn with respect to load capacity is that the absolute pre-snap load is of course greater for the thicker shell, and the scaling is somewhere between h and h^3, depending on the shell geometry and the magnitude of the thickness change.

The plots in Appendix B, being normalized by h^3, have removed the effect of bending stiffness variation as thickness varies. Since transverse shear stress is a by-product of bending, its effects are also removed. Appendix B, then, highlights the transition of the shell from a thin membrane to a thick structure carrying an increasingly larger proportion of the load in bending and proportionally less in the membrane as thickness is increased.

The response effects of increasing the thickness of a shallow shell can be observed in Figure B-2. Compared to the 8 ply shell, the 24 ply shell reaches critical load at less displacement and unloads less when it does snap through. At 48 ply thickness, the shell does not snap but begins to respond like a plate.

Figure B-6 illustrates the thickness effect on a nonshallow shell. The deep (θ = 1 radian) thin (R/h = 300) shell peaks at the lowest transverse displacement, but the load capacity stays positive and the shell eventually surpasses the critical load in the snapped configuration. Increasing the thickness and stiffening the shell now has the effect of increasing the severity of the collapse, driving the curve into the negative load regime of geometric failure. Notice also that for a shell of this shallowness and thickness range the transverse displacement at critical load increases with thickness.

A combination of the effects discussed for the 1/4 and 1 radian shells above can be seen in Figure B-4, which pertains to the hinged 1/2 radian shell. The 8 ply shell collapses fully. Increasing the thickness to 24 plies both increases the displacement at critical load and complicates the equilibrium curve with loops and cutbacks. Increasing the thickness further to 48 plies settles out the response so that it snaps through and no longer goes negative, but the displacement at critical load has decreased. The 96 ply curve continues the trends seen with the 48 ply case.

Insight into this reversing trend can be gained by considering the type of deformation occurring in each case. Figure 4-5 is a plot of the displacement at which load peaks for each shell geometry, plotted against the thickness parameter R/h. An effect very similar to the one in Figure 4-3 is suggested when the type of inversion occuring with each geometry is noted. The data points which fall on an upsloped curve again correspond to shells which invert locally; those on a curve downslope correspond to full length-inverting shells (this includes the peak point on the 1/2 radian curve).

As before in the shallowness comparison, we see in Figure 4-5 that the 24 ply (R/h = 100) 1/2 radian shell sits at the critical point of the curve, indicating that the normalized transverse displacement of the 1/2 radian shell is maximized at this thickness. The observed trend suggests that the 1 radian shell would have to be thicker (R/h $<$ 25) to invert only locally, and that the 1/4 radian shell will not invert full length until it is thinner (R/h $>$ 300). Common sense tells us that these curves are shifted in the horizontal direction by the

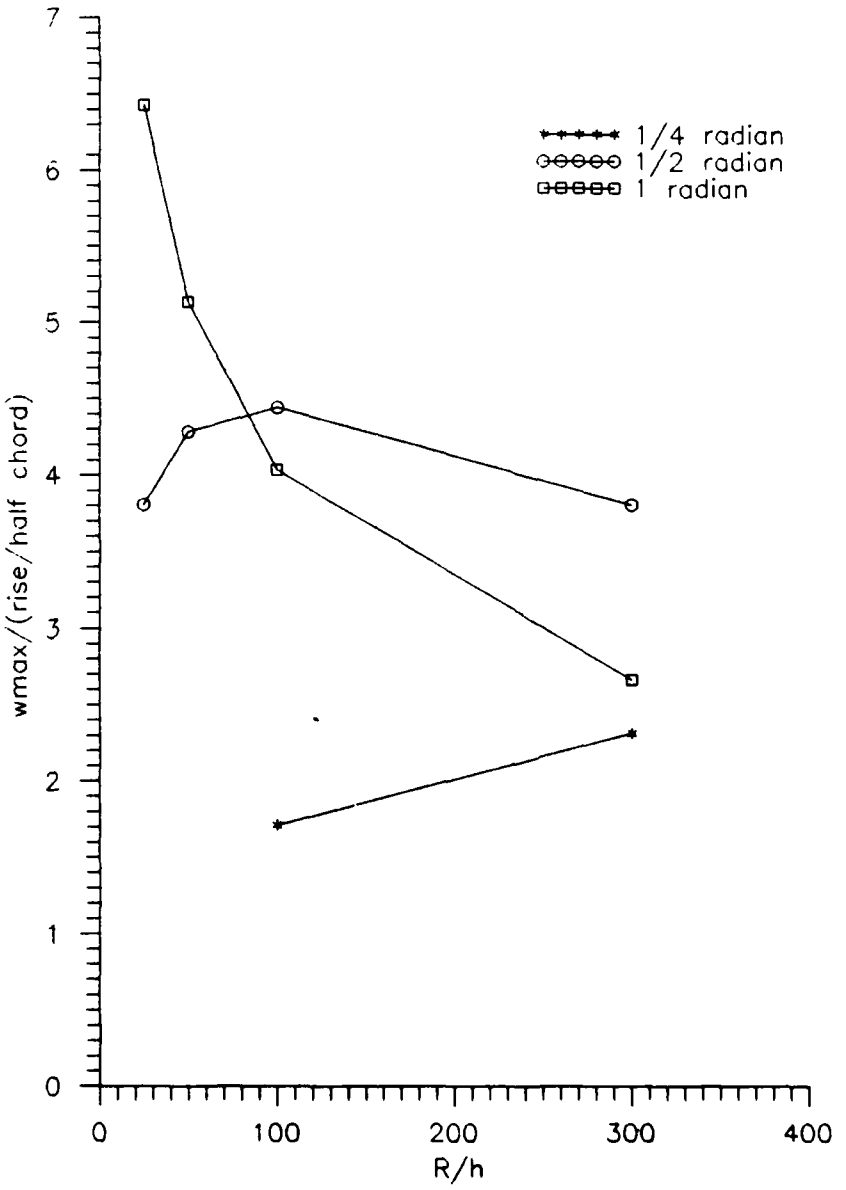

Figure 4-5. w at Peak Load vs Thickness, Hinged [0/90]$_s$

shell's "aspect ratio," though, so drawing such conclusions before studying the effect of that parameter would not be wise.

Rotation of the shell normal due to transverse shear stress increases with increasing thickness of the 1/4 radian angle ply shell (Table 4-7). Compared to the bending rotation $w_{,s}$, though, the relative transverse shear strain is minimized with the 24 ply laminate, and increases when thickness is reduced to 8 plies.

Table 4-7. Thickness Effect on Transverse Shear

shell thickness (#plies, inch)	displ w, in /load, lbs	location (x,s) in	β_s, rad	% of $w_{,s}$
$[0/\mp45/90]_s$, θ = 1/4 radian, clamped				
8, 0.04	.137/ 87	3, .75	$.212\times10^{-2}$	18.8
24, 0.12	.079/ 934	0, .25	$.911\times10^{-2}$	15.4
48, 0.24	.073/ 4893	0, .25	$.208\times10^{-1}$	38.1
96, 0.48	.091/27041	0, .25	$.540\times10^{-1}$	69.8
$[0/\mp45/90]_s$, θ = 1/4 radian, hinged				
8, 0.04	.120/ 77	3, .5	$.169\times10^{-2}$	13.4
24, 0.12	.111/ 846	0, .5	$.543\times10^{-2}$	6.6
48, 0.24	.086/ 3836	0, .25	$.172\times10^{-1}$	36.2
96, 0.48	.121/25056	0, .25	$.511\times10^{-1}$	63.5
$[0/90]_s$, θ = 1 radian, hinged				
8, 0.04	.437/ 54	0, 1	$.139\times10^{-2}$	1.0
24, 0.12	.460/ 960	0, 1	$.114\times10^{-2}$	0.7
48, 0.24	.469/ 6560	1, 1	$.262\times10^{-1}$	1.7
96, 0.48	.380/35863	.5, 1	$.115\times10^{-1}$	8.6

This dip in relative magnitude seen in all of the cases may correlate to the same geometric effect which causes the peaked curve of w_{Pmax} vs δ/b and thickness. The deep cross ply shell, though, develops the lowest absolute magnitude of transverse shear rotation in the 24 ply case. The cause of this unexpected result is unknown, but is not considered significant because the transverse effects in this pair of cross ply cases are less than 1% of the bending deformation.

The overall trend of the effect of thickness on transverse shear strain is depicted in Figure 4-6.

The effect due to thickness is therefore seen to be much like the effect due to shallowness in the area of maximum presnap displacement,

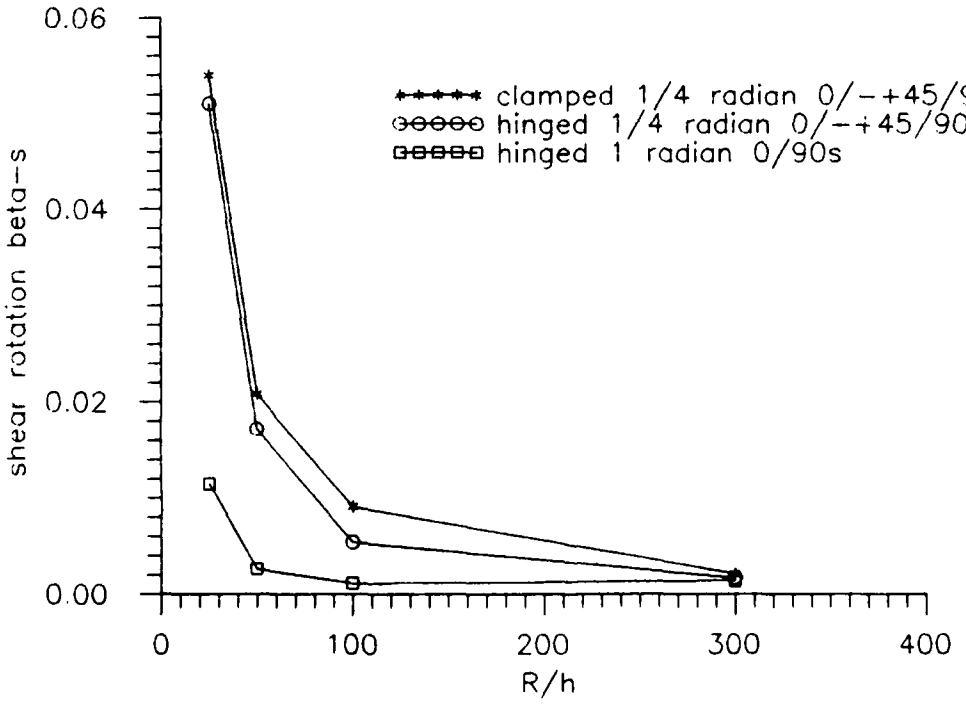

Figure 4-6. Transverse Shear Strain vs Thickness

where a given shell geometry will achieve maximum presnap transverse displacement at a state which separates snapping behaviors. When a shell snaps locally, increasing the thickness reduces the pre-snap deflection. When the shell snaps full length, increasing the thickness will result in more deformation prior to snap through. The load capacity scales as a factor of h somewhere between the inplane (h^3) and bending (h) stiffness effects, and is also affected by geometric variations. Transverse shear effects decrease with decreasing thickness, until a critical thinness is reached beyond which the transverse effects increase again.

Laminate Failure

It has been assumed that ply failure or delamination does not occur in solving for these equilibrium curves. Since this may not actually be the case, a study was done to determine when material failure would be predicted by the stresses developed in the deformed shell.

The two-dimensional Tsai-Wu failure criterion outlined in Chapter 3 predicts very early failure for this geometry and load configuration. The onset of ply failure corresponded with the initial dimpling of the shell, with the attendant large rotations. Extensive ply failure was predicted for rotations above 2.5 degrees. In the thicker shells, the laminate was seen to fail even before significant bending occurs, as a result of the compressive membrane stresses generated by the large applied load.

Attributing these ply failures solely to rotation is suspected to be inaccurate. Laminated panels have been observed under rotations at least as large as these, yet the panels did not fail in the gross manner predicted. The more likely cause for the failure is that such rotations in an edge-constrained shell result in deformations with small radius of curvature near the boundary, which is not taken into account when computing the magnitude of rotation of the shell middle surface.

The failure predicted when rotation has not become significant appears reasonable given the magnitude of the load applied to the thicker shells for which this occurs. For example, the 96 ply 1/2 radian shell is predicted to fail by the time the load reaches 10,000 lbs, at which time it will only have deformed 1.6 degrees in bending.

To study the effect of parametric variations on the snapping behavior in this thesis, such early material failures had to be ignored.

V. Conclusions/Recommendations

Conclusions

This study has pointed out several features of the response of laminated cylindrical shells to transverse loading, which bear consideration in the design and analysis of such structures:

1. Between the two layups investigated, the $[0/\mp45/90]_s$ was stiffer for this geometry and load configuration than the $[0/90]_s$. This conclusion cannot be generalized to say that angle ply laminates are preferred for transversely loaded cylindrical shells, though, because these results may have been very different if the $[0/\mp45/90]_s$ layup had been compared to a $[90/0]_s$, which places the cross plies further from the middle surface to better resist the bending of the shell.

2. Clamping the longitudinal boundary prevents the snapping of thicker and more shallow shells. When a thin or deep shell is clamped, the collapse occurs at less displacement, but displays a simpler equilibrium path to second load up than the hinged case. This may translate to a less violent snap through.

3. A shell with a ratio of thickness to depth $(h/2)/\delta$ greater than 1 does not appear to snap through or reach any critical points on its equilibrium curve.

4. The pre-collapse displacement of a hinged shell of given thickness, ply orientation, radius of curvature, and length, divided by

the shallowness factor (δ/b), will be maximized at some value of the shallowness factor. This peak value of shallowness divides the response regime between full length and localized collapse.

5. The pre-collapse displacement of a hinged shell of given shallowness, ply orientation, radius of curvature, and length, divided by the shallowness factor (δ/b), will be maximized at some thickness. This peak value of thickness, as with the shallowness in item 5, divides the response regime between full length and localized collapse.

6. Transverse shear is a significant effect in the response of a laminated shell to a transverse point load. While an isotropic shell analysis can ignore transverse shear stress, a laminated orthotropic shell develops nonnegligible transverse effects as bending occurs. The deformations of the normal to the middle surface of a composite shell can be of the same order of magnitude as the bending rotation of the shell middle surface, which surely qualifies as a significant effect.

7. The angle ply laminate was seen to develop more transverse shear strain than the cross ply laminate. Transverse effects were greater with increased thickness, reduced depth and more rigid boundary conditions. One exception to all of these trends is the deep thin 1 radian 8 ply shell, which developed more shear rotation compared to the 24 ply shell, developed more shear rotation in the cross ply layup, and developed more shear rotation with a hinged boundary.

8. The Donnell equations develop significant inaccuracy when rotations of the middle surface exceed 15 degrees.

While significant transverse shear stress and strain are developed in the laminated shells, it appears that the difference in response seen with the two layups tested here, and in the comparison with the isotropic shell, is more a result of the difference in shear stiffnesses. When the geometry of the shell is varied, the transverse shear strain is seen to vary also, but the nature of the response is more readily correlated to the geometric parameters than to the transverse shear. Thus one could conclude that transverse shear effects have less impact on structural response than geometric effects, but such a conclusion would be unsupported until comparison with an analysis which neglects transverse shear strain is performed.

Recommendations

These results were obtained by varying the parameters over very few values. The effect of thickness, having been investigated at four values, was the easiest for which to determine trends. The effect of ply layup and boundary condition, while only assuming two values each, were still quite readily determined due to the simplicity of their effect. That is, these effects are not complicated by the geometric nonlinearity of the structure, as are the thickness and the last parameter, shallowness.

The effect of shallowness requires further study, since it is inextricably tied to load path length and panel aspect ratio. Varying radius of curvature is one option for another study, as is varying opening angle and panel length together to fix aspect ratio. Each of

these tests, though, would introduce its own peculiarities due to the combination of parameters varied.

The location of the maximum transverse shear rotation was different with different ply orientation. If the transverse shear distribution is desired, contour plots of β_s would be of value.

Assessing the impact of transverse shear effects on the response of a shell could be accomplished by analyzing a similar set of shells with a finite element which neglects transverse shear strain.

Appendix A: Load/Displacement Data

The following pages contain the load versus center transverse displacement data for the 48 cases analyzed. Each plot applies to one thickness and opening angle θ, with four curves covering the two ply layups and two boundary conditions.

Not all of the curves progress through snap to second load up, although it is possible with this solution algorithm to trace the full equilibrium path. Several factors led to considering only the first load up and relief for the more convoluted curves:

1. In practical applications, a curved shell structure should be designed so as not to dynamically snap. The full length inversions seen at the onset of the severely snapping equilibrium curves (i.e., the θ = 1/2 radian, 24 ply hinged case) would therefore indicate structural failure, beyond which analysis is not too useful.
2. Once snap through begins, the problem becomes a dynamic one, and static analysis may lose its utility.
3. The computer time required to trace the full path is prohibitive with these meshes with 250-plus nodes. Each path increment step required an average of 50 minutes of CPU time for solution. Further, the actual path traversed to the snapped state may be very different than the mathematical one solved for numerically here.

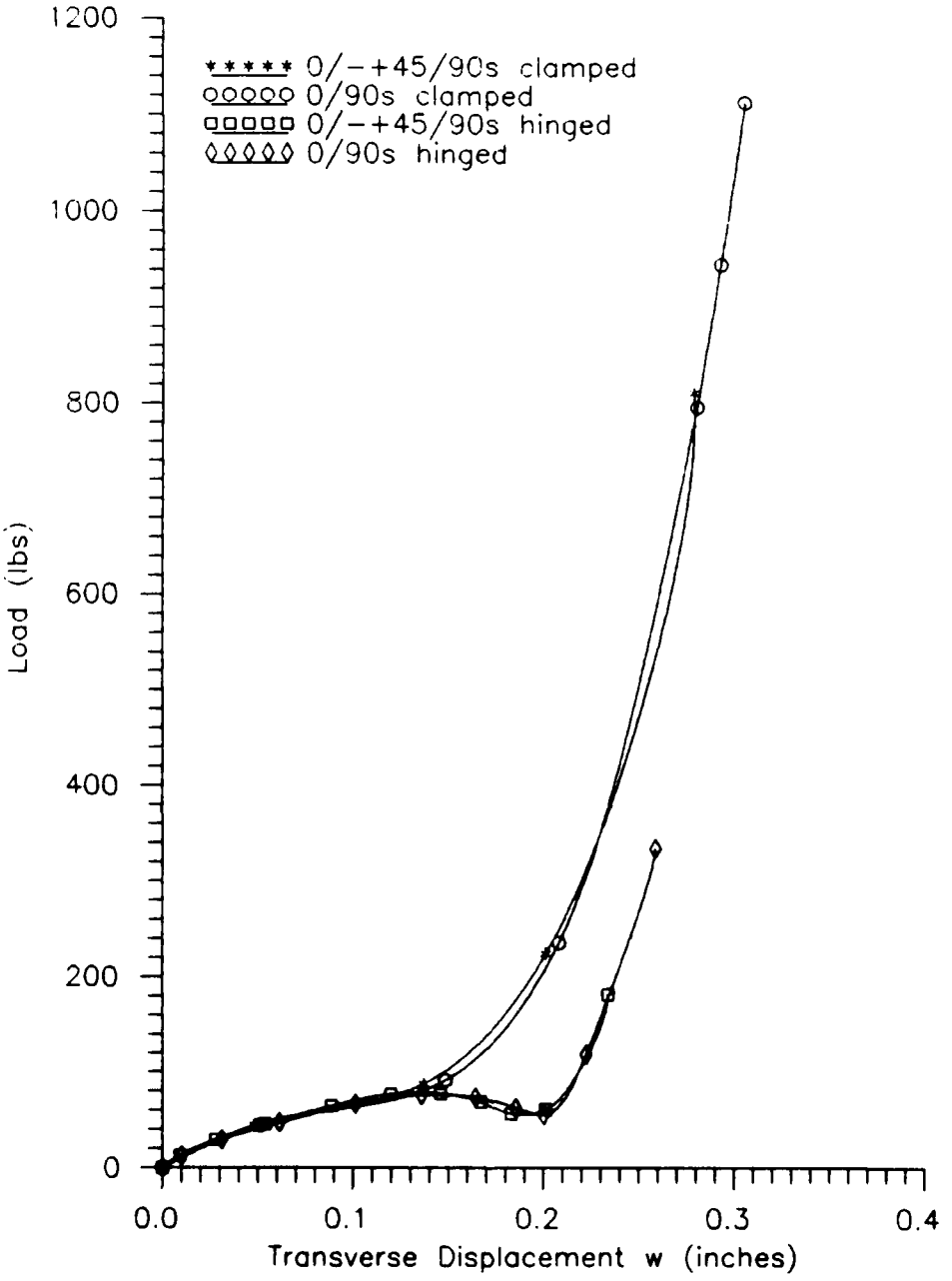

Figure A-1. Load vs Displacement, 8 Ply 1/4 Radian Shell

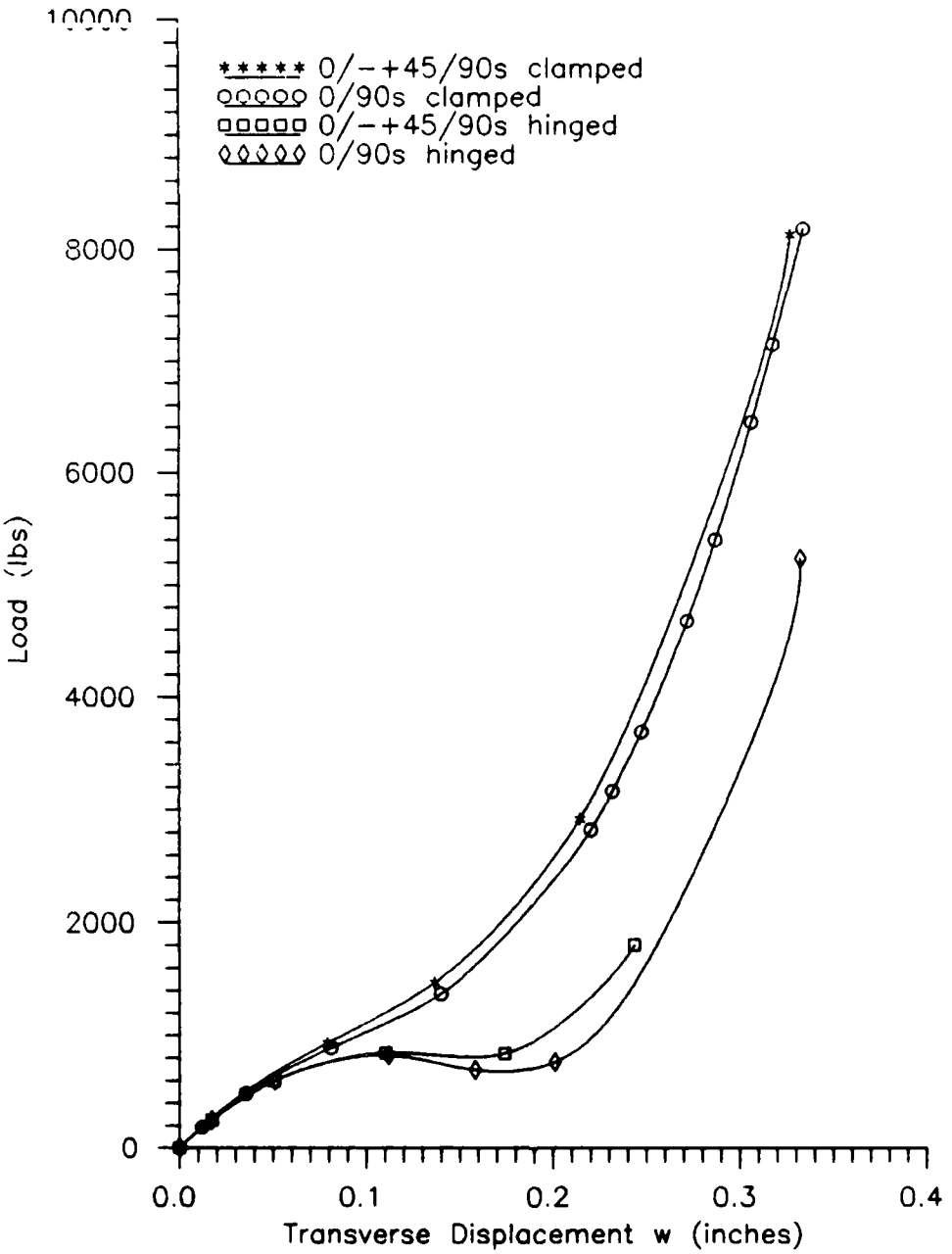

Figure A-2. Load vs Displacement, 24 Ply 1/4 Radian Shell

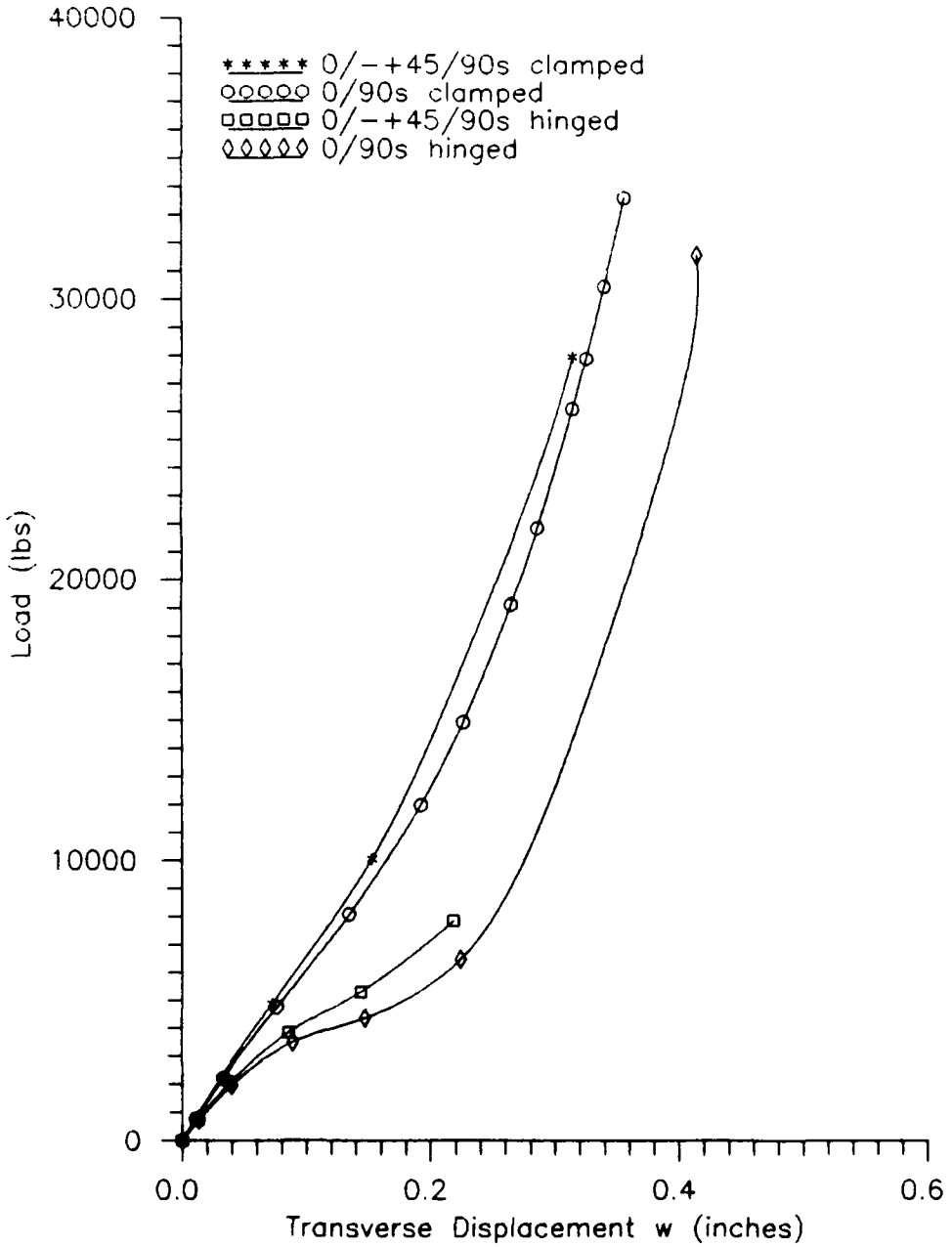

Figure A-3. Load vs Displacement, 48 Ply 1/4 Radian Shell

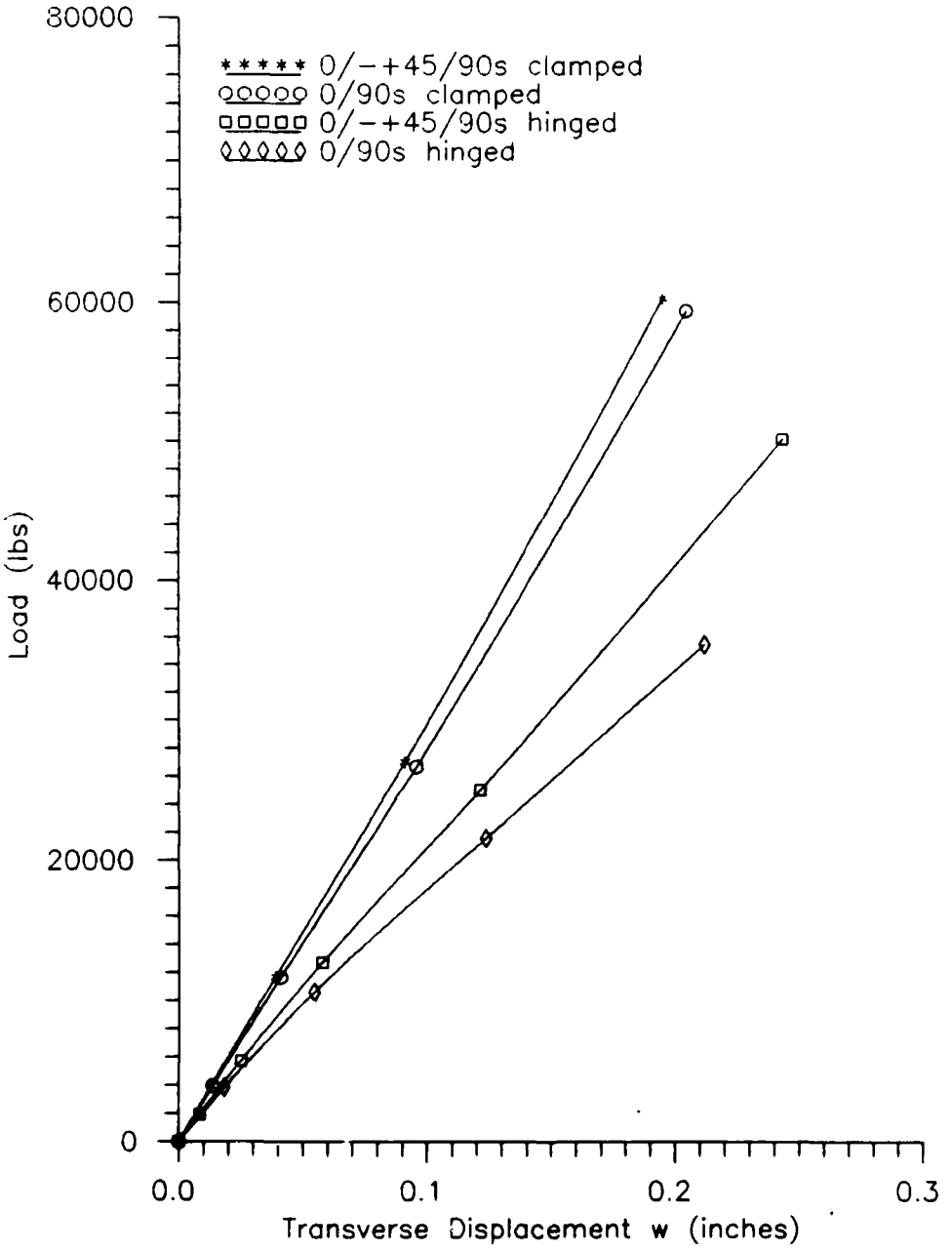

Figure A-4. Load vs Displacement, 96 Ply 1/4 Radian Shell

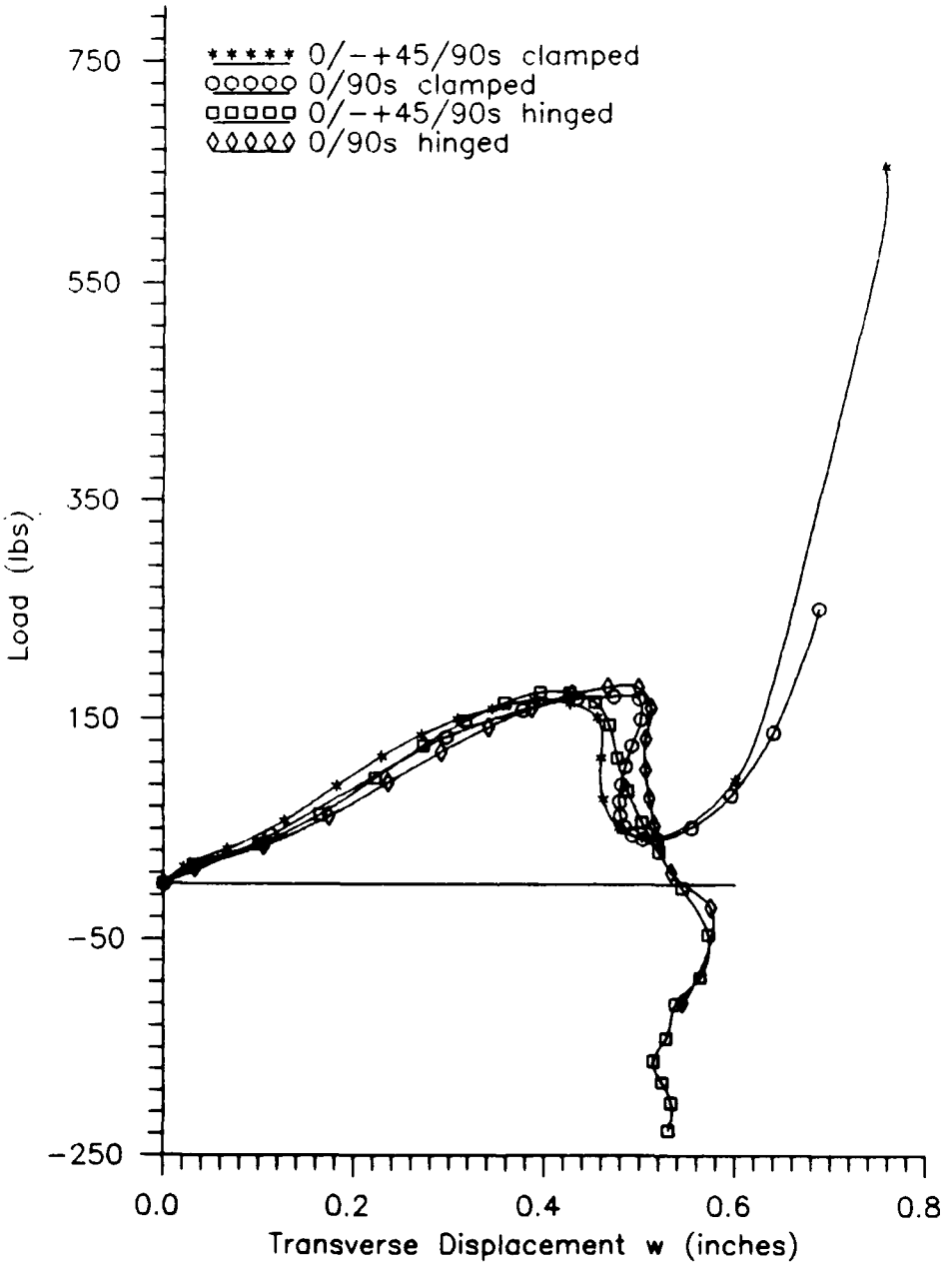

Figure A-5. Load vs Displacement, 8 Ply 1/2 Radian Shell

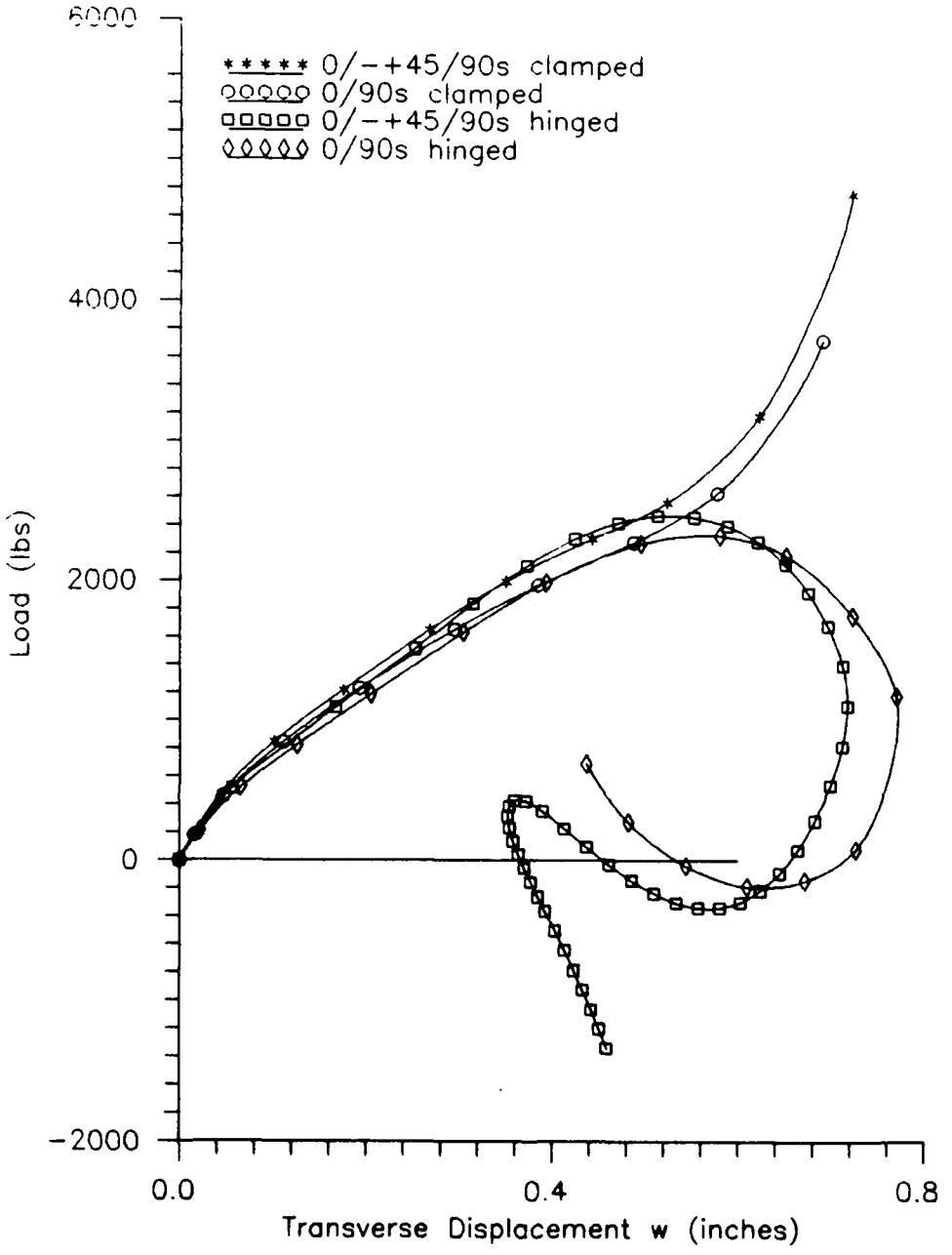

Figure A-6. Load vs Displacement, 24 Ply 1/2 Radian Shell

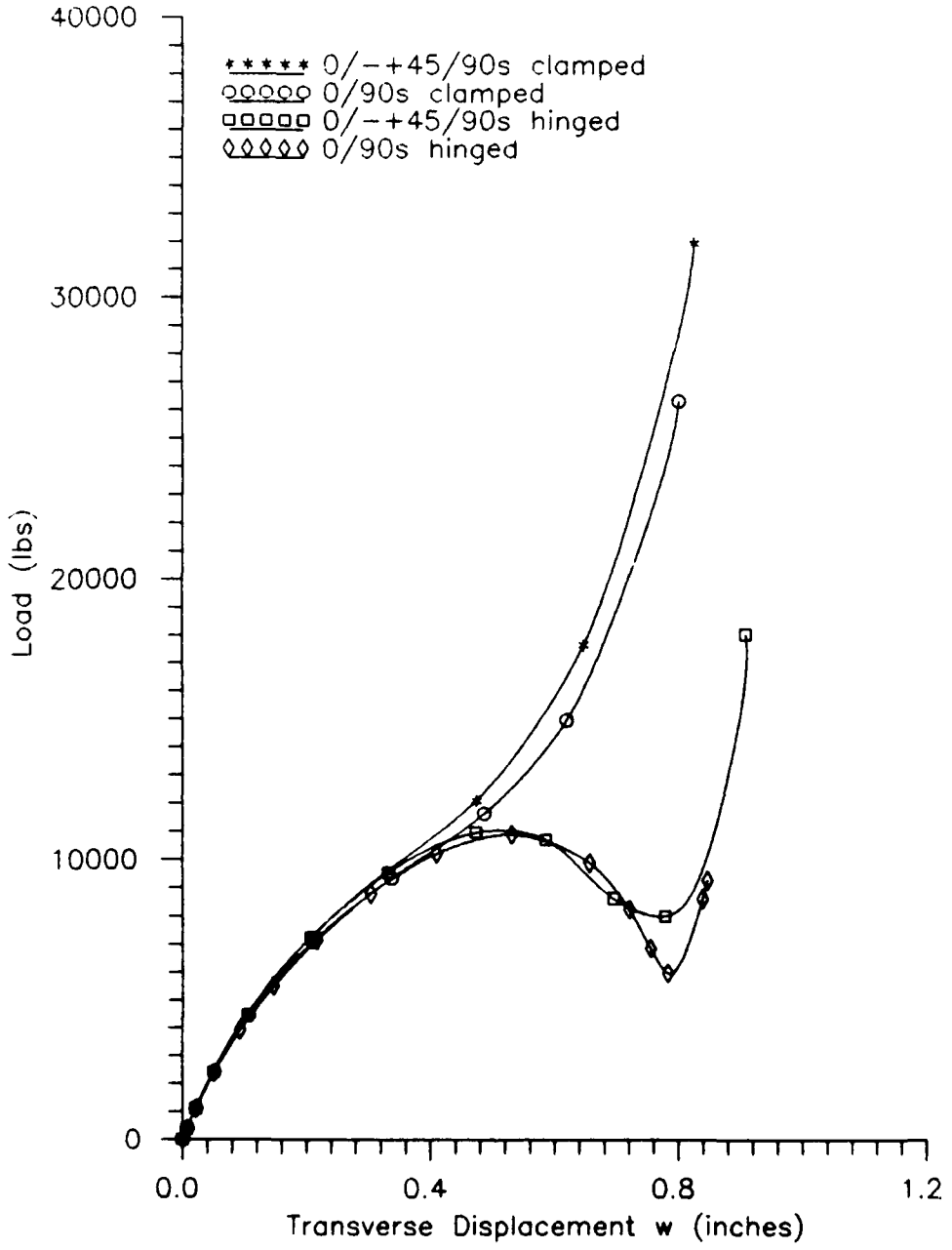

Figure A-7. Load vs Displacement, 48 Ply 1/2 Radian Shell

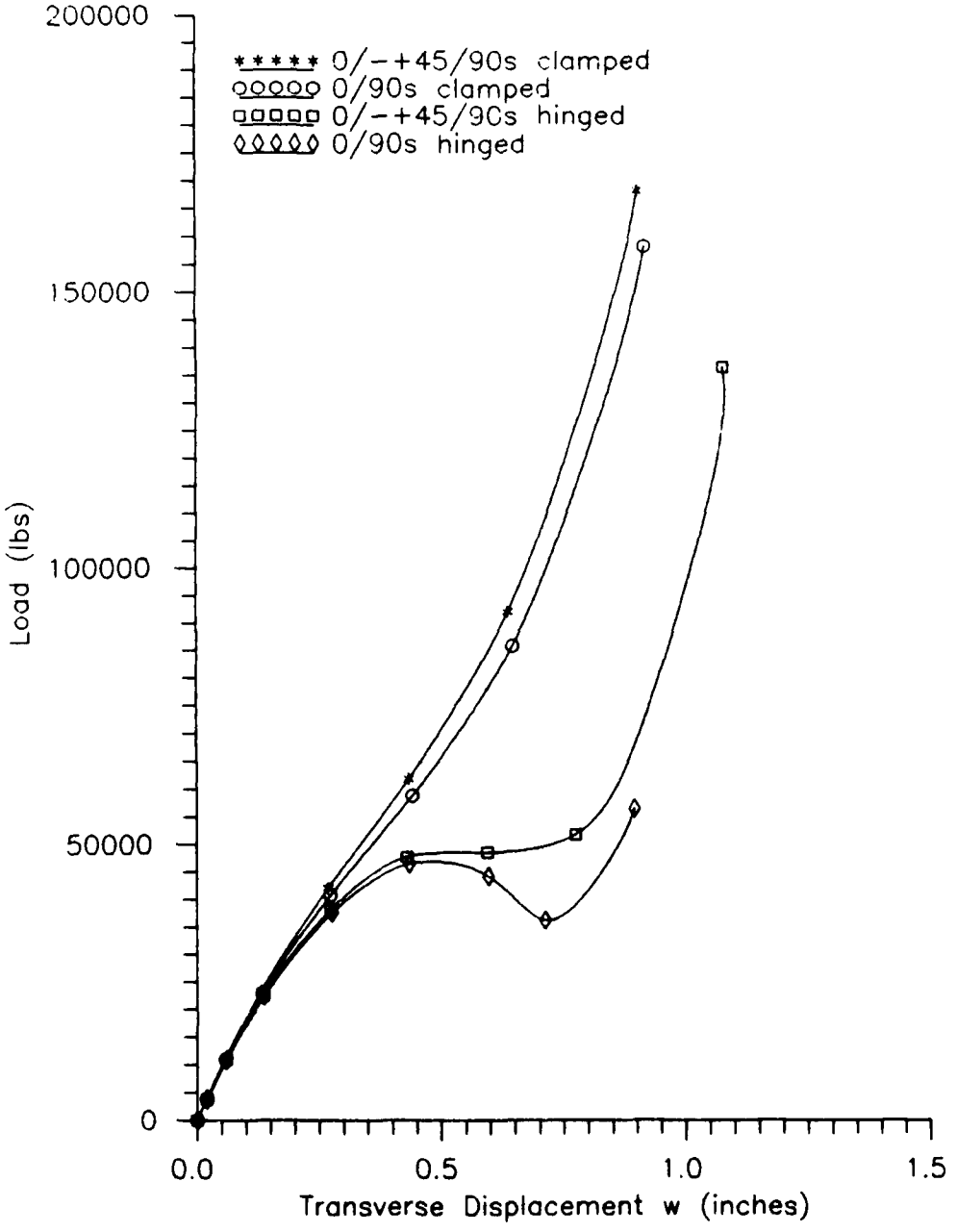

Figure A-8. Load vs Displacement, 96 Ply 1/2 Radian Shell

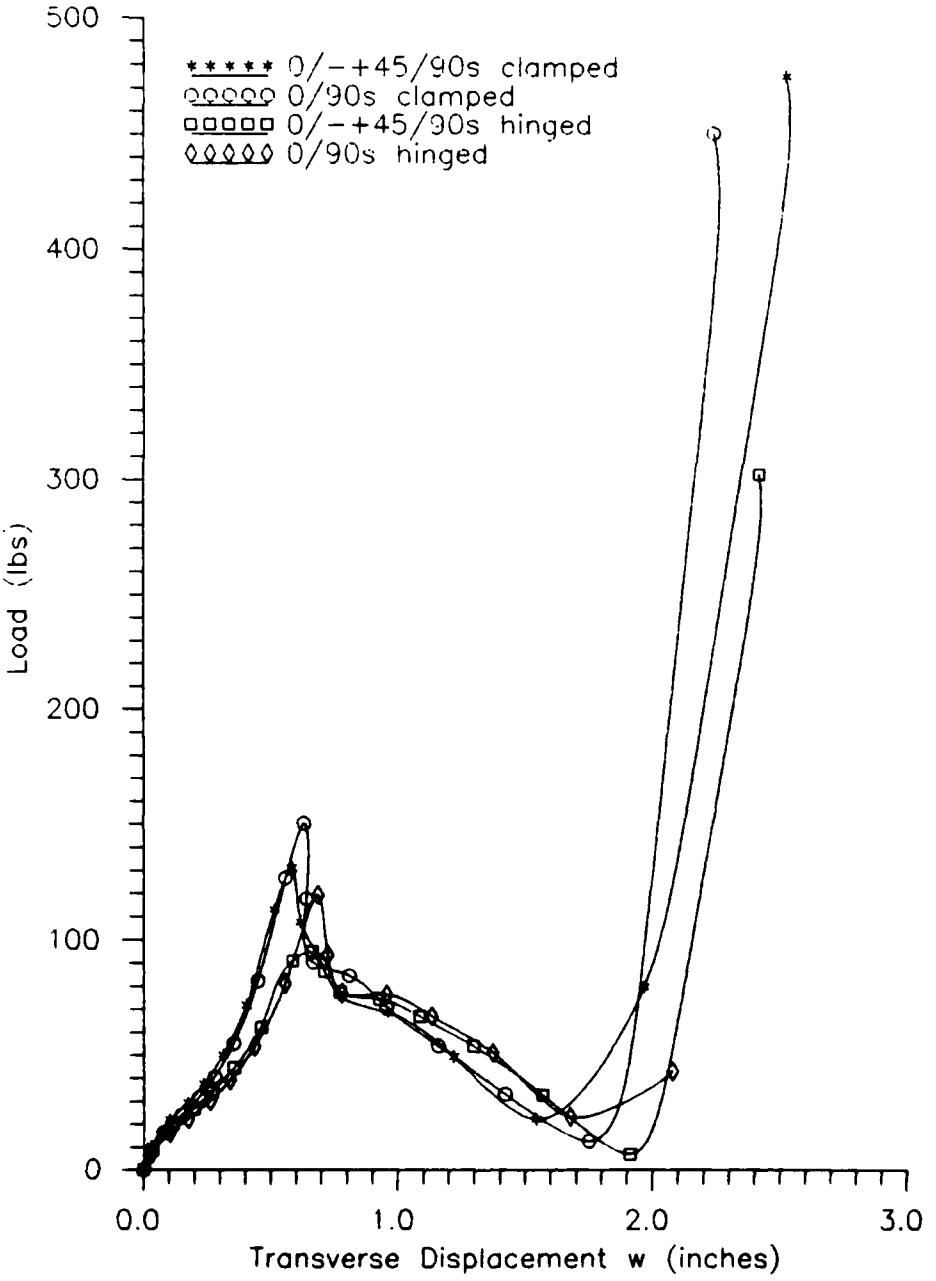

Figure A-9. Load vs Displacement, 8 Ply 1 Radian Shell

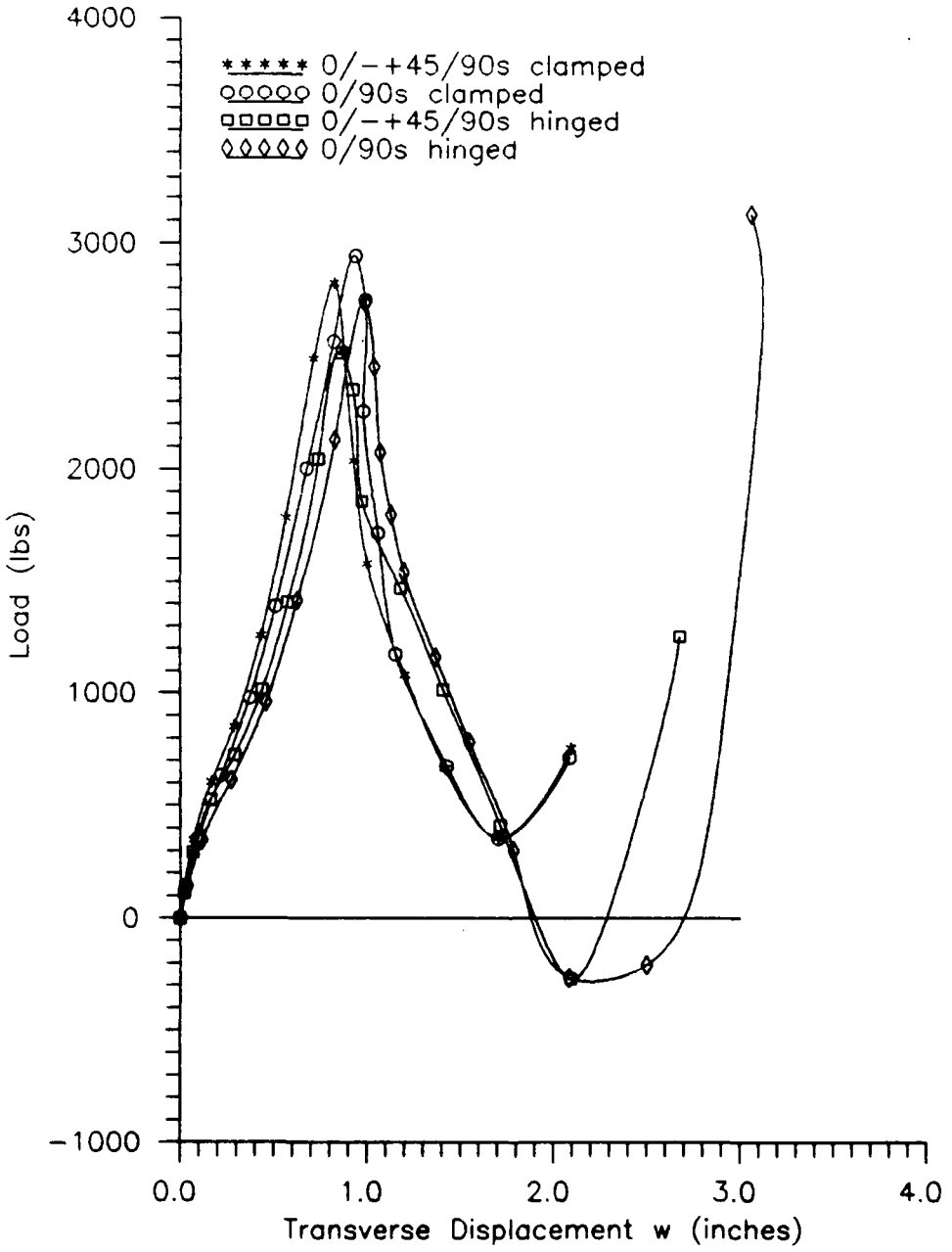

Figure A-10. Load vs Displacement, 24 Ply 1 Radian Shell

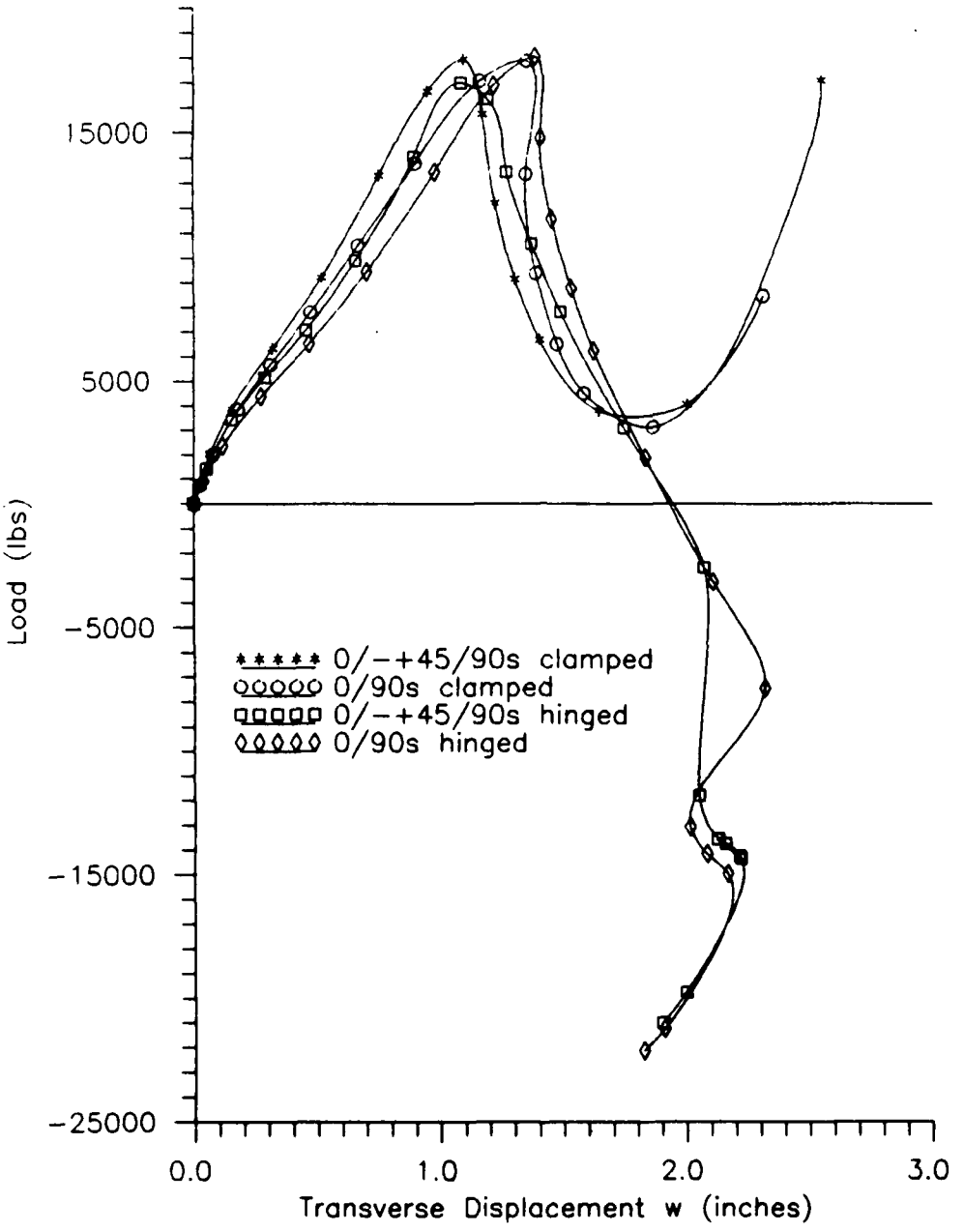

Figure A-11. Load vs Displacement, 48 Ply 1 Radian Shell

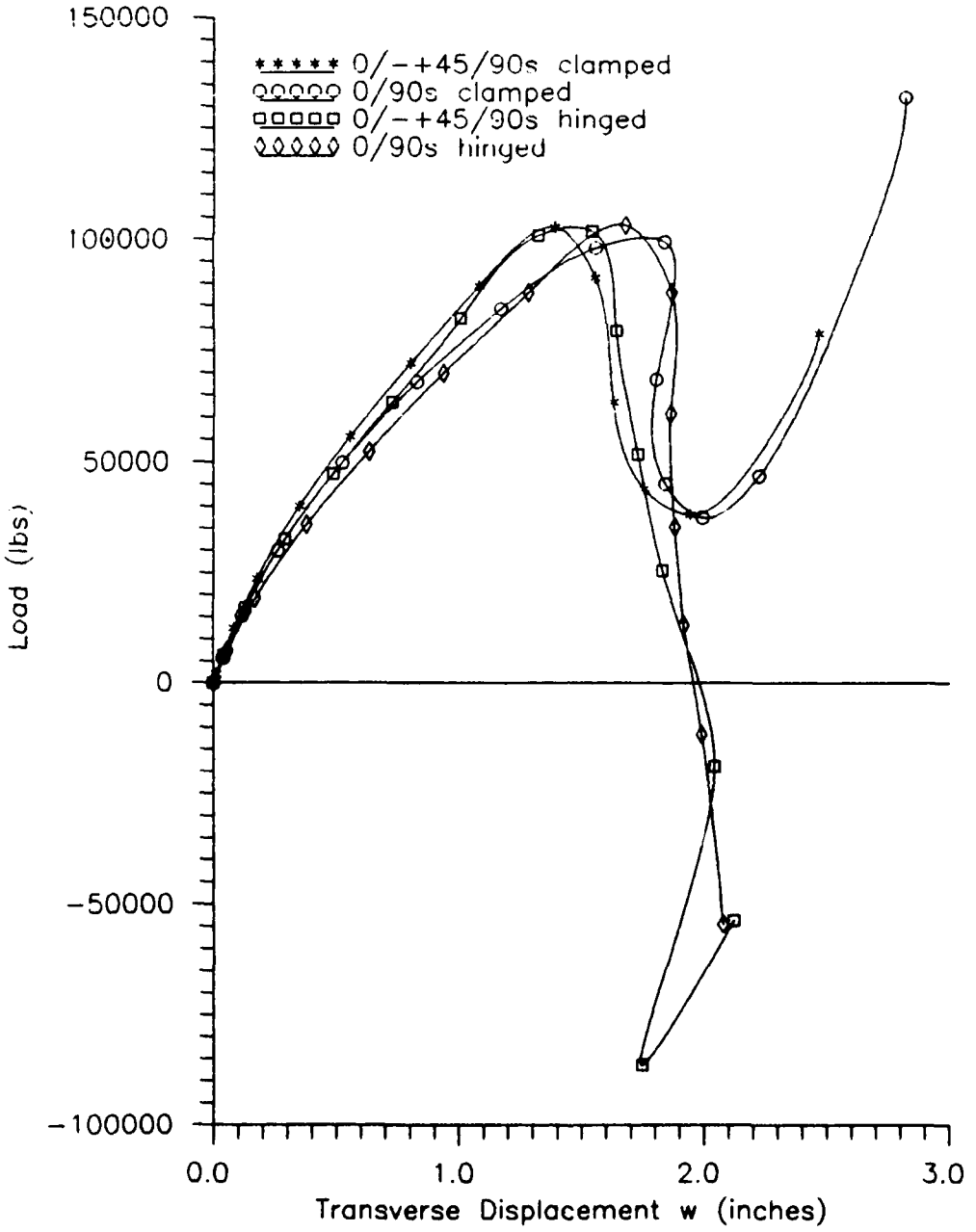

Figure A-12. Load vs Displacement, 96 Ply 1 Radian Shell

Appendix B: Plots of Thickness Variance

The response of each of the geometries at the four thicknesses analyzed is presented. The load values have been normalized by dividing by $(\text{thickness})^3 \times 10^6$, equivalent to normalizing to bending stiffness. This normalization is most appropriate to the least shallow geometry, which exhibits the most bending, but it allows comparison of the features of the shallower shells as well.

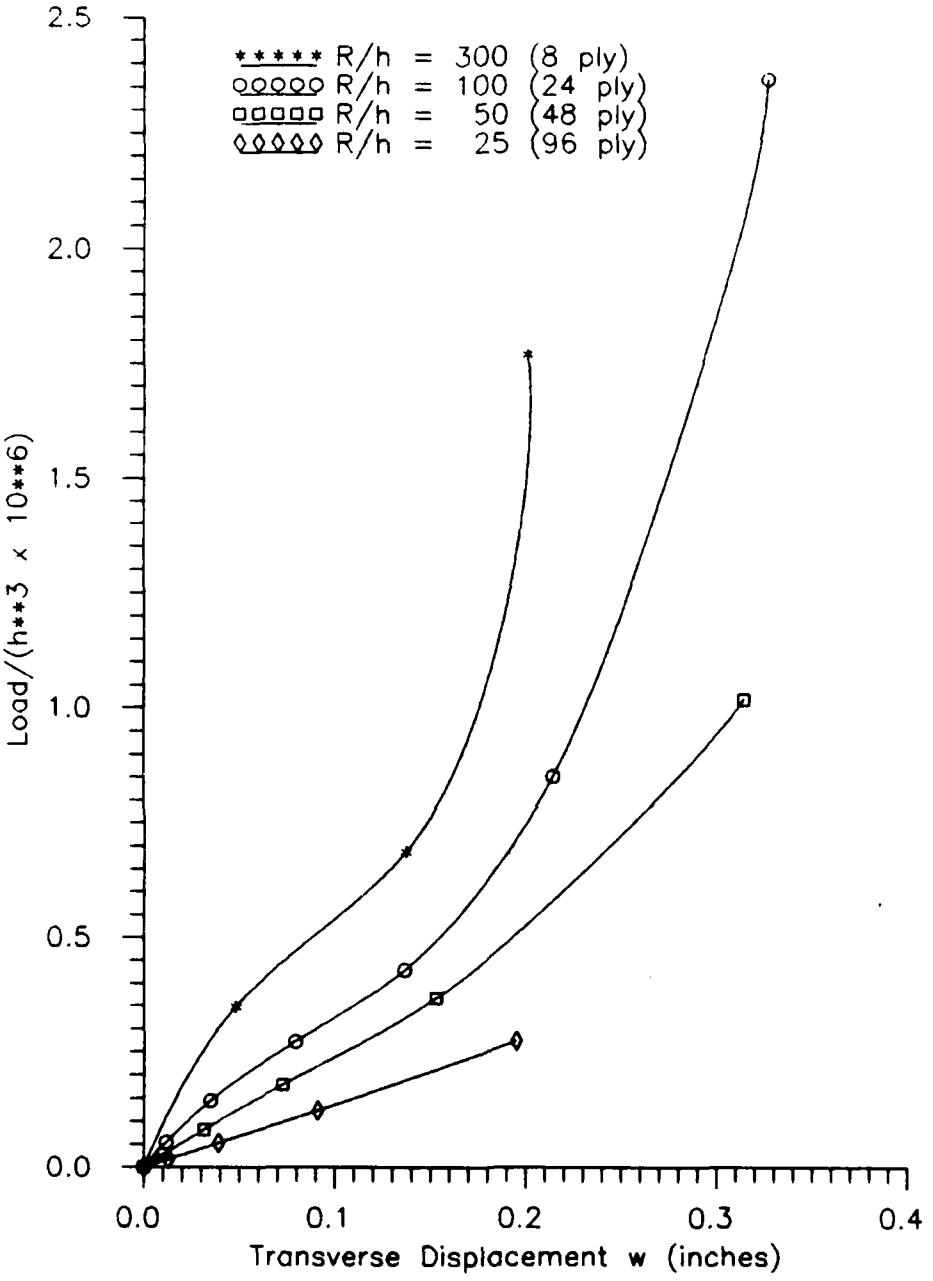

Figure B-1. Effect of Thickness, Clamped [0/∓45/90]$_s$ 1/4 Rad

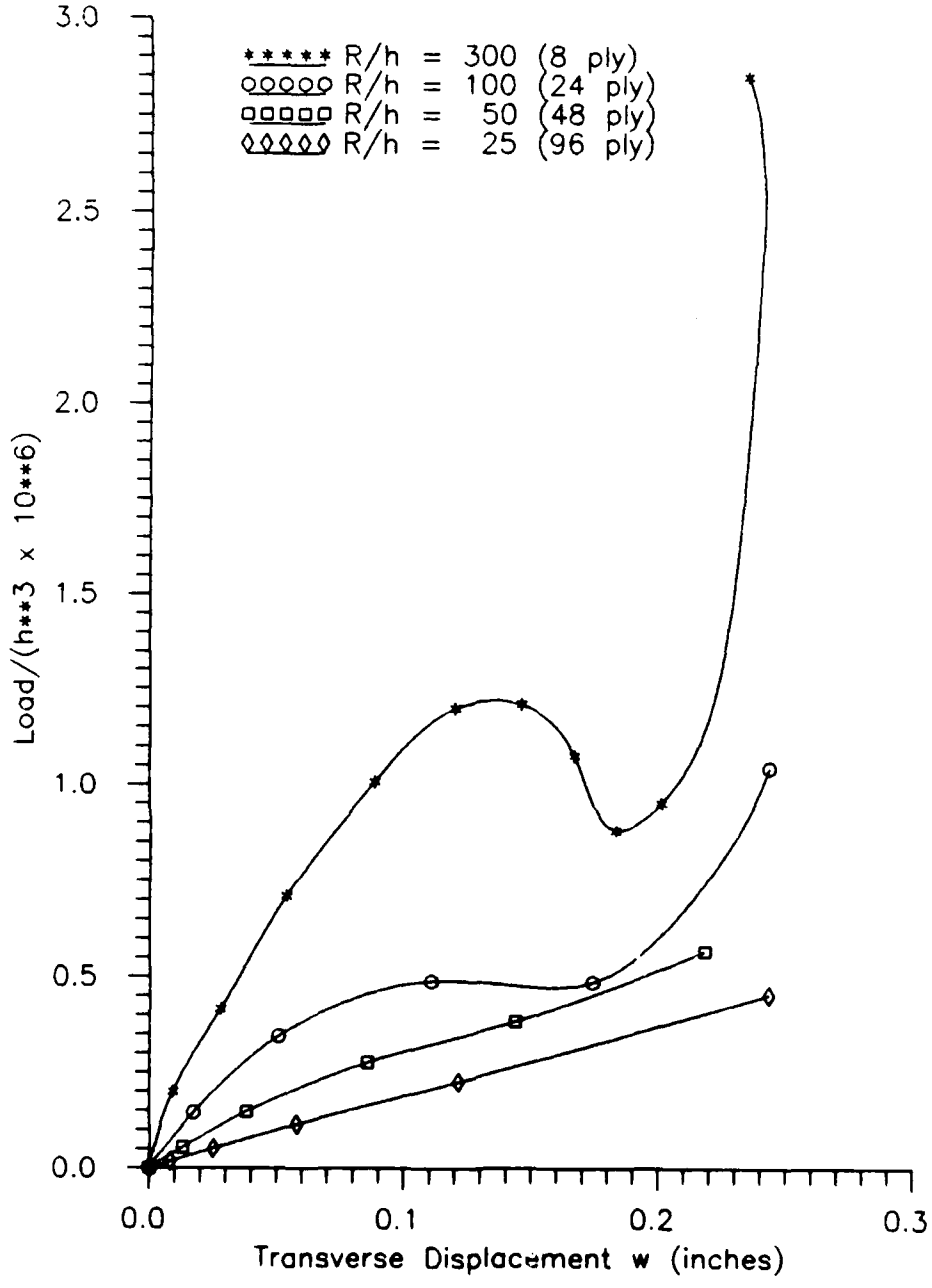

Figure B-2. Effect of Thickness, Hinged $[0/\mp 45/90]_s$ 1/4 Rad

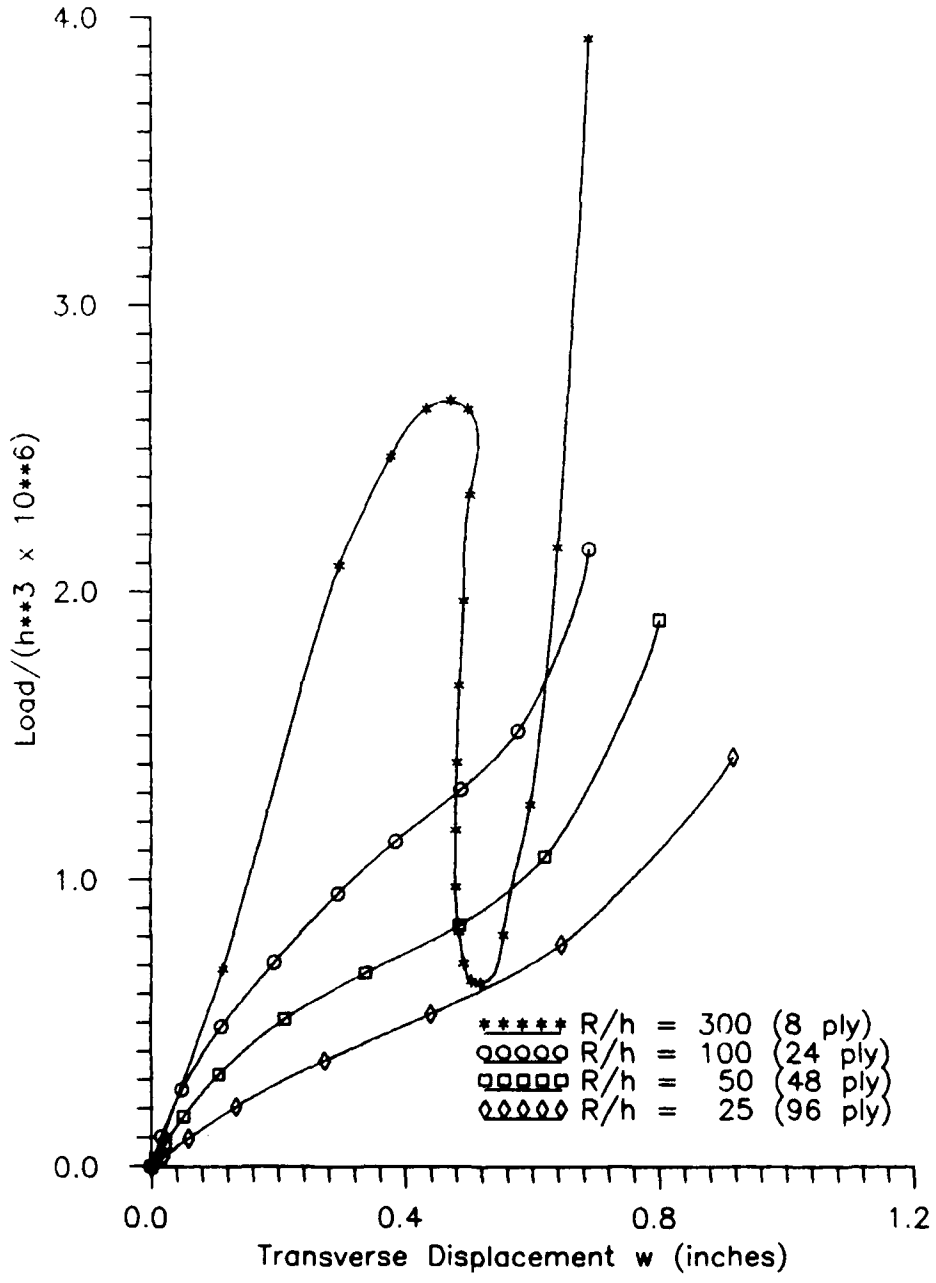

Figure B-3. Effect of Thickness, Clamped [0/90]$_s$ 1/2 Rad

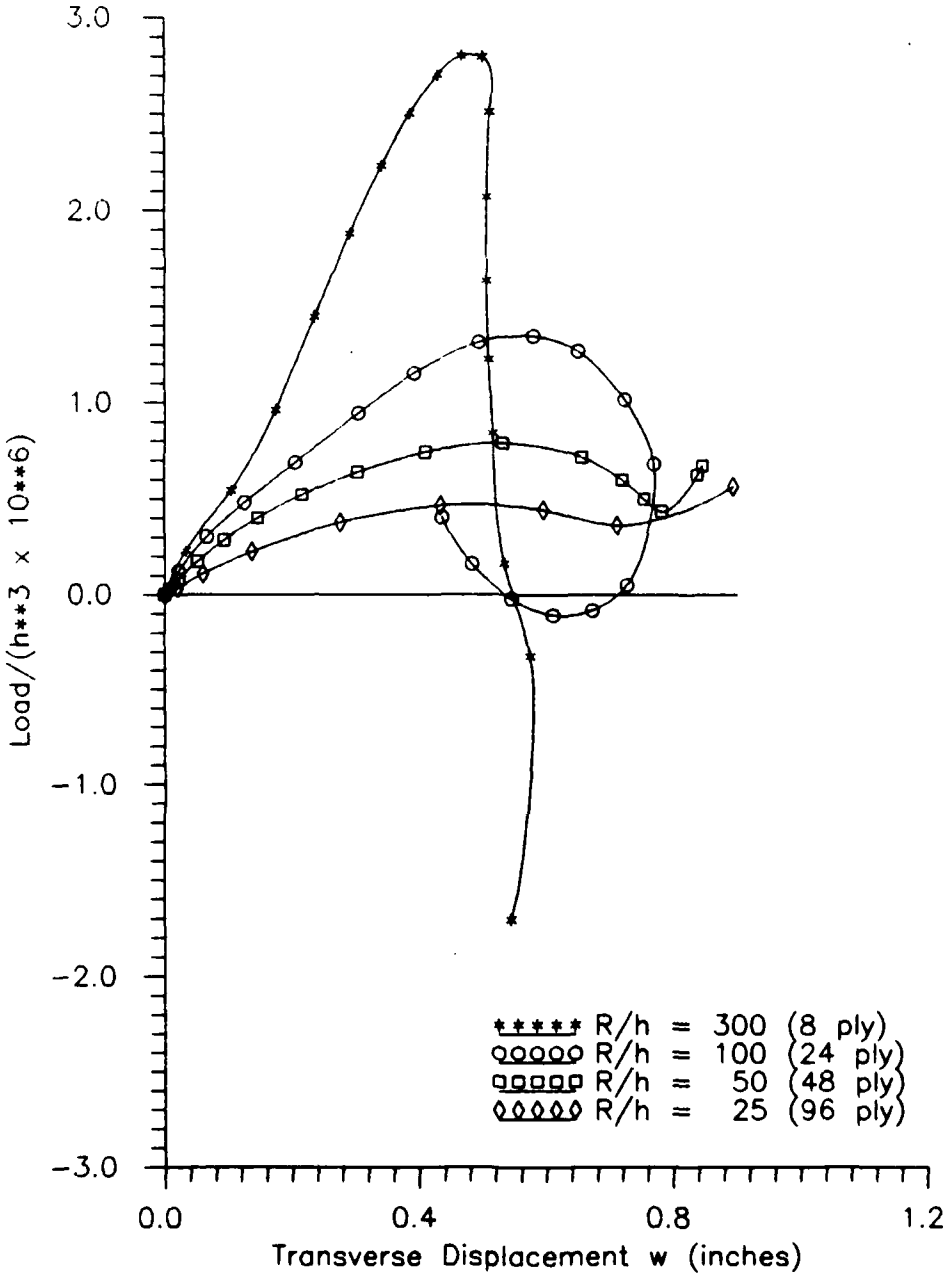

Figure B-4. Effect of Thickness, Hinged [0/90]$_s$ 1/2 Rad

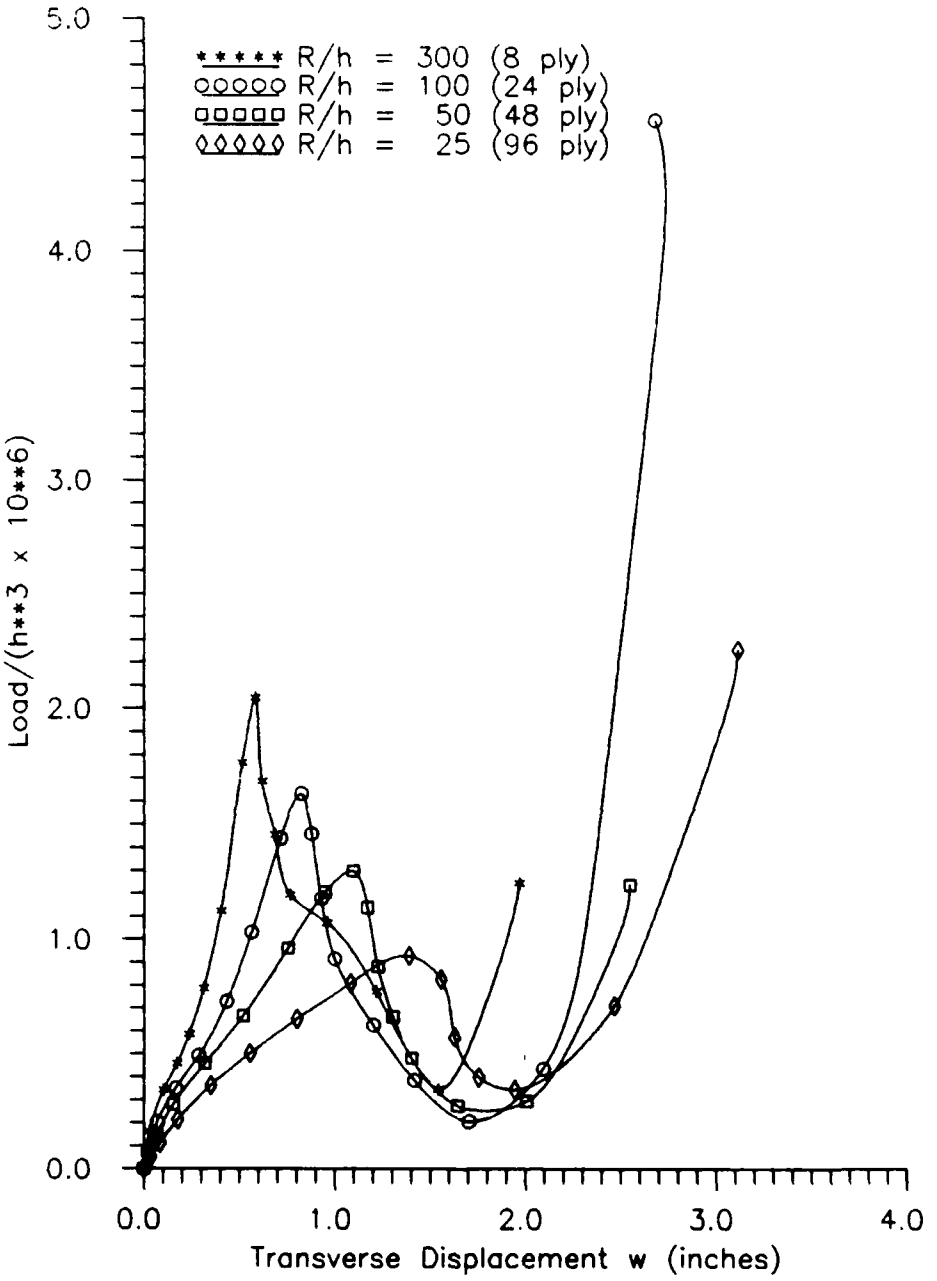

Figure B-5. Effect of Thickness, Clamped [0/∓45/90]$_s$ 1 Rad

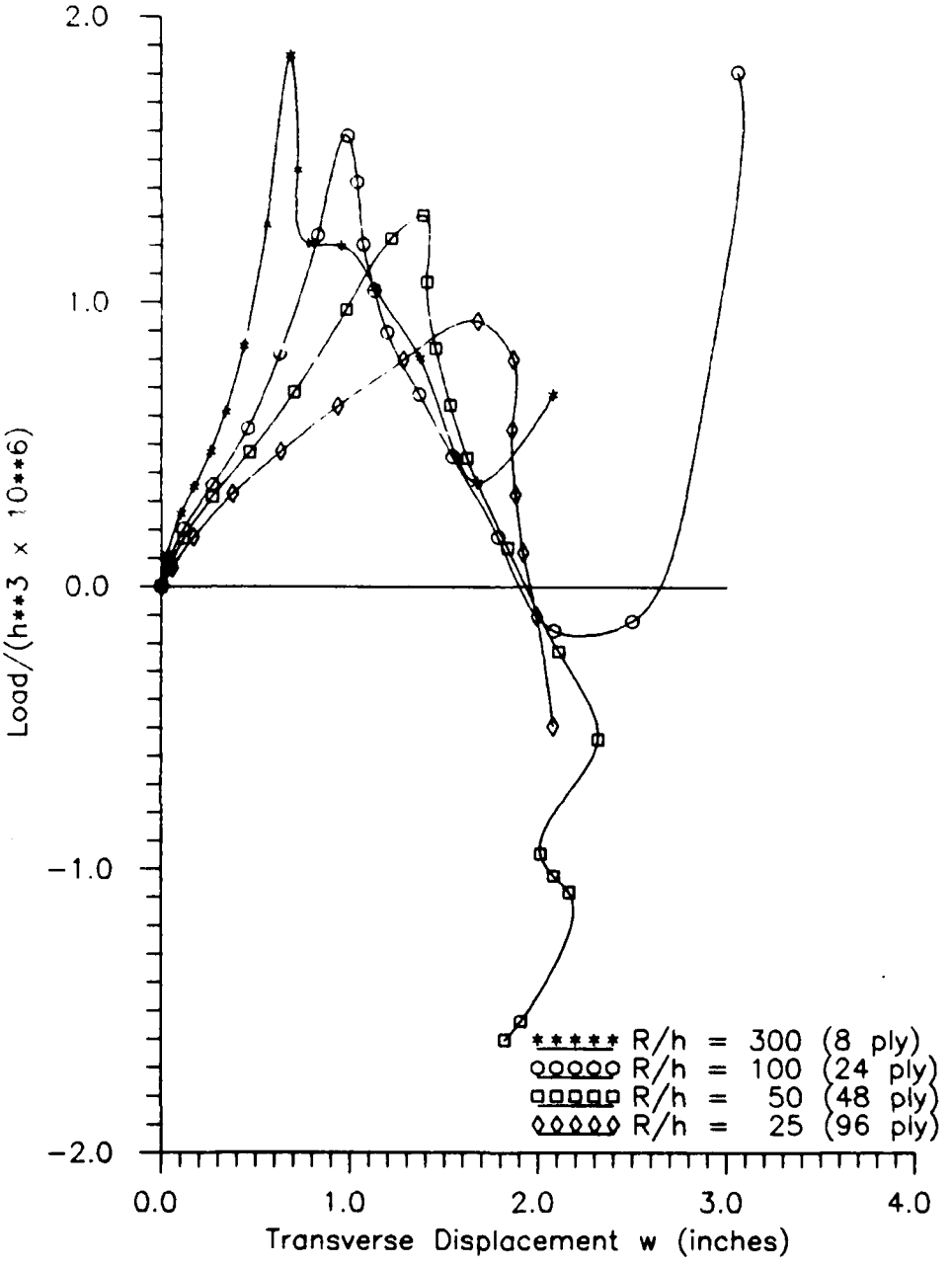

Figure B-6. Effect of Thickness, Hinged [0/90]$_s$ 1 Rad

Appendix C. Deformation Histories

This appendix contains the deformed contours at key points ofthe load - displacement curves of selected cases. Each type of response is represented here, to give a physical understanding of the shell deformation corresponding to each type of load curve. Contours for both layups are included for a couple of the cases to allow for qualitative comparison of the responses.

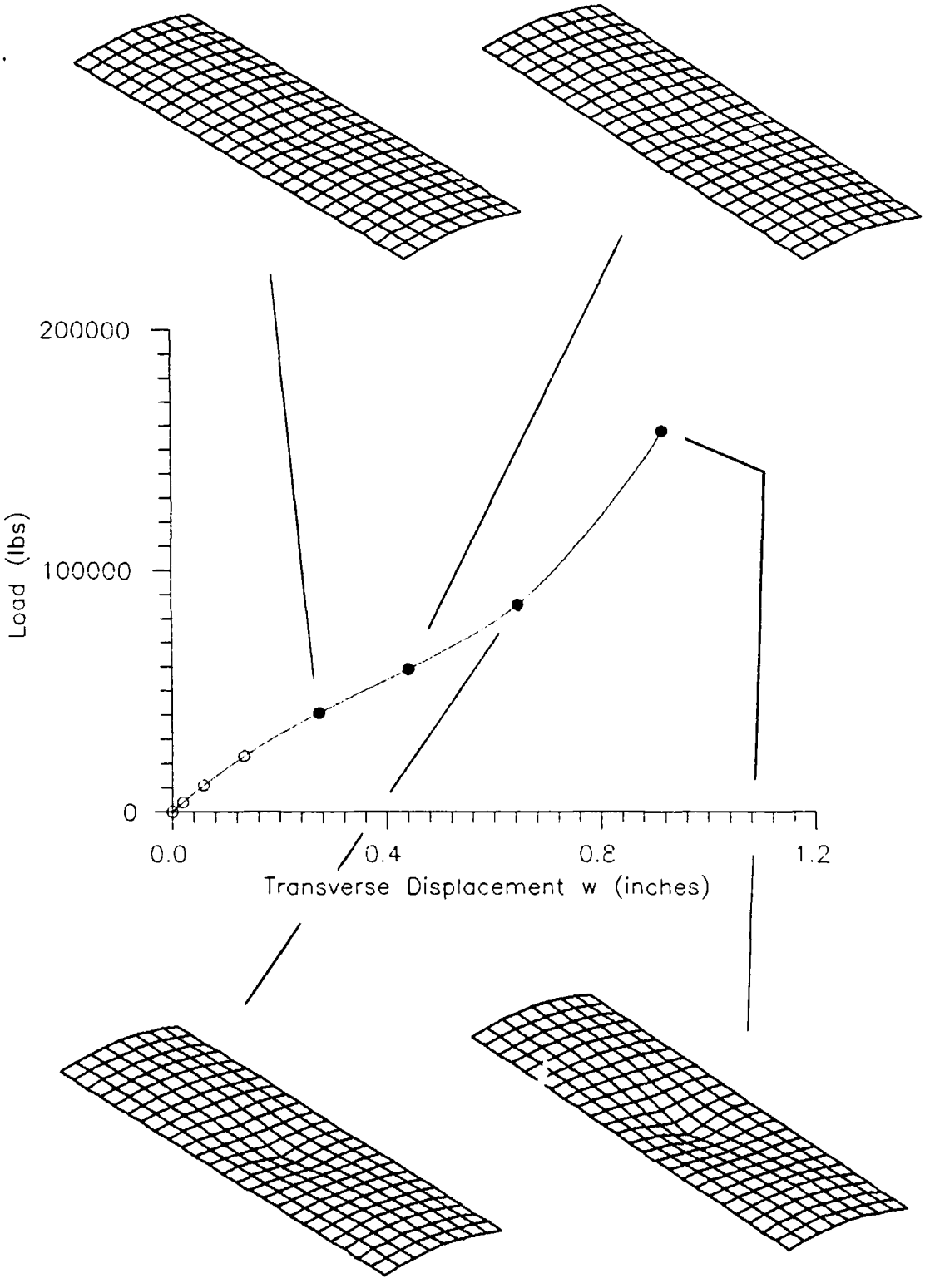

Figure C-1. Contours, $[0_{24}/90_{24}]_s$ Clamped 1/2 Radian Shell

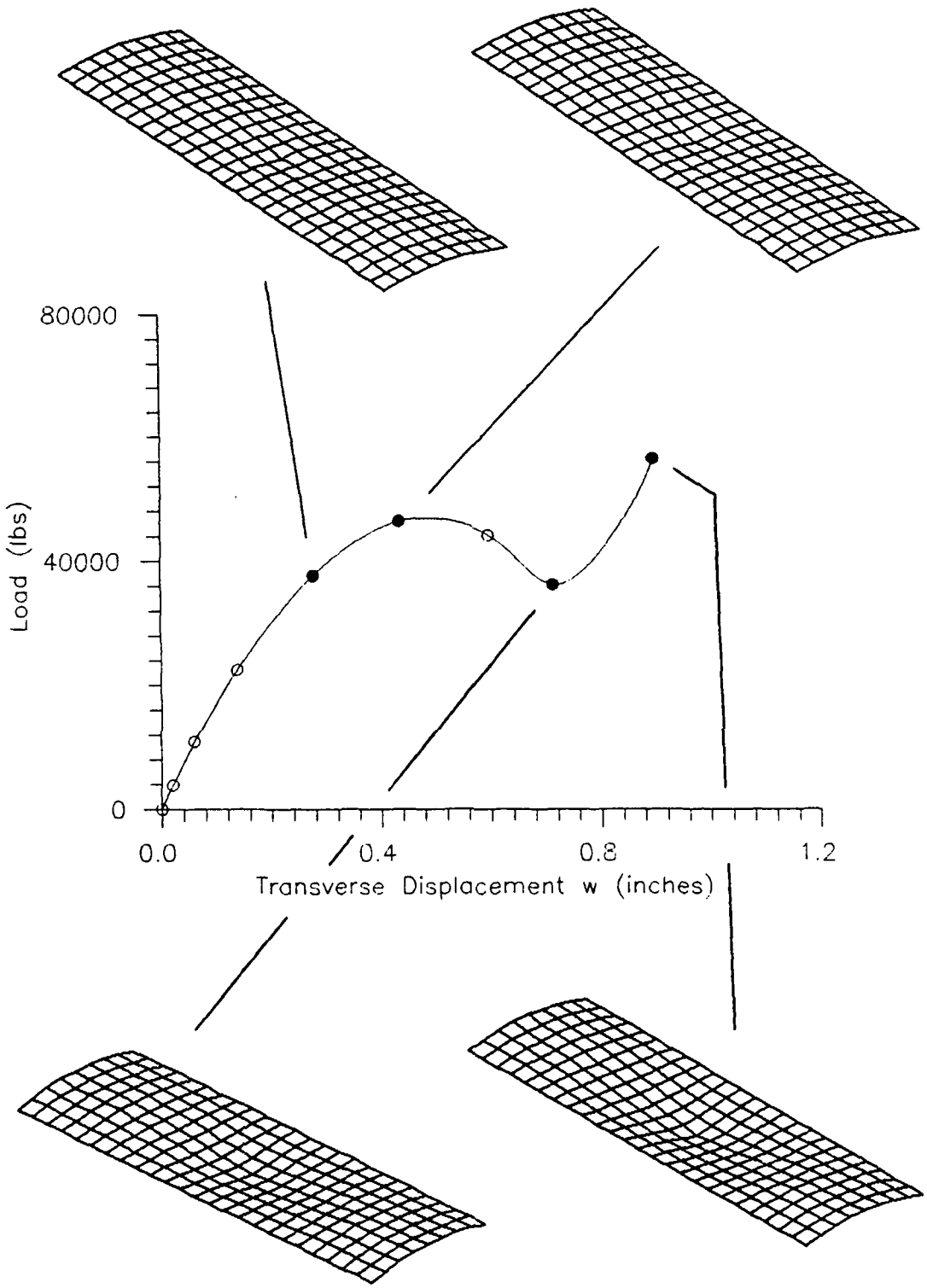

Figure C-2. Contours, $[0_{24}/90_{24}]_s$ Hinged 1/2 Radian Shell

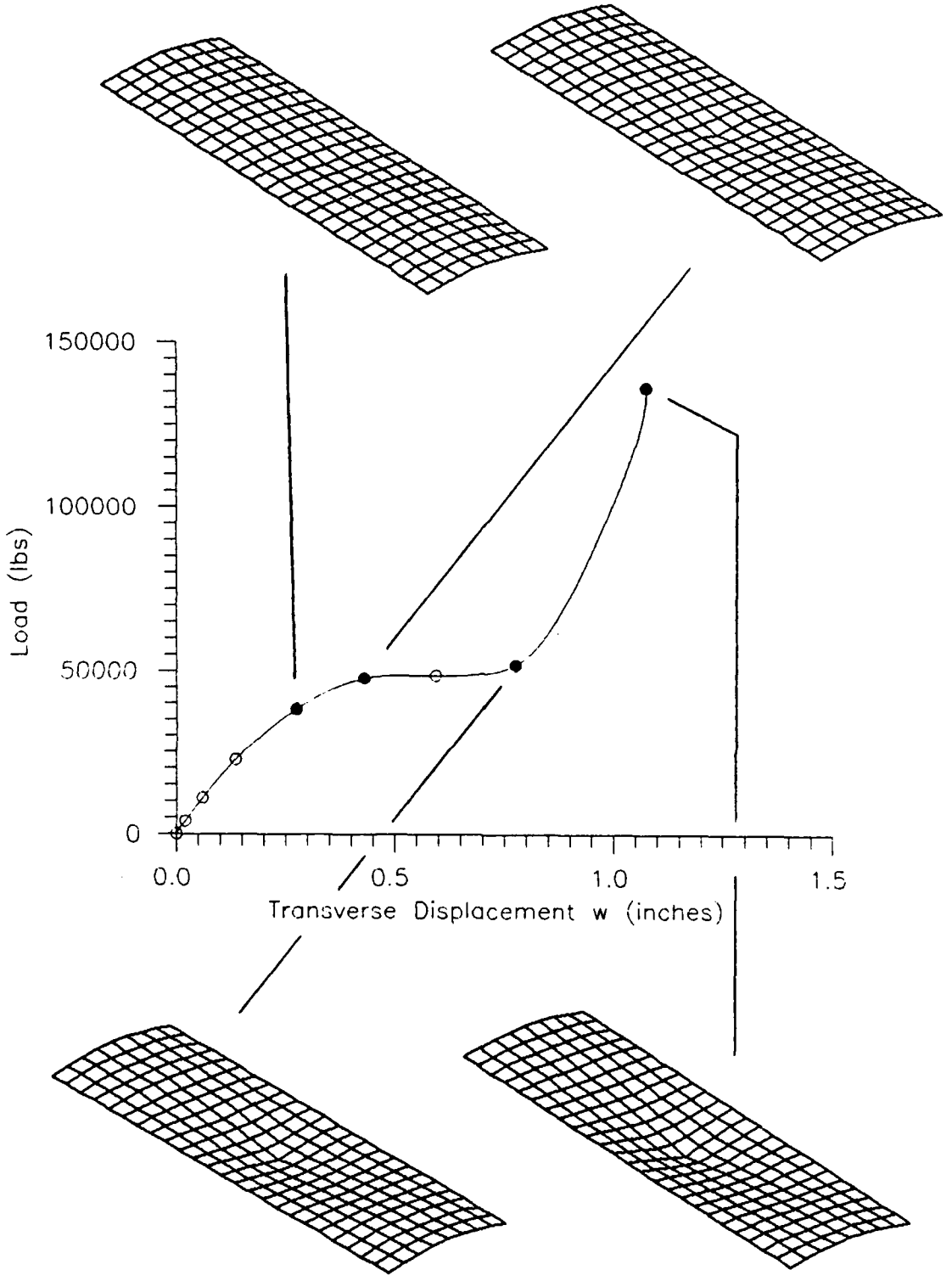

Figure C-3. Contours, $[0_{12}/\mp45_{12}/90_{12}]_s$ Hinged 1/2 Radian Shell

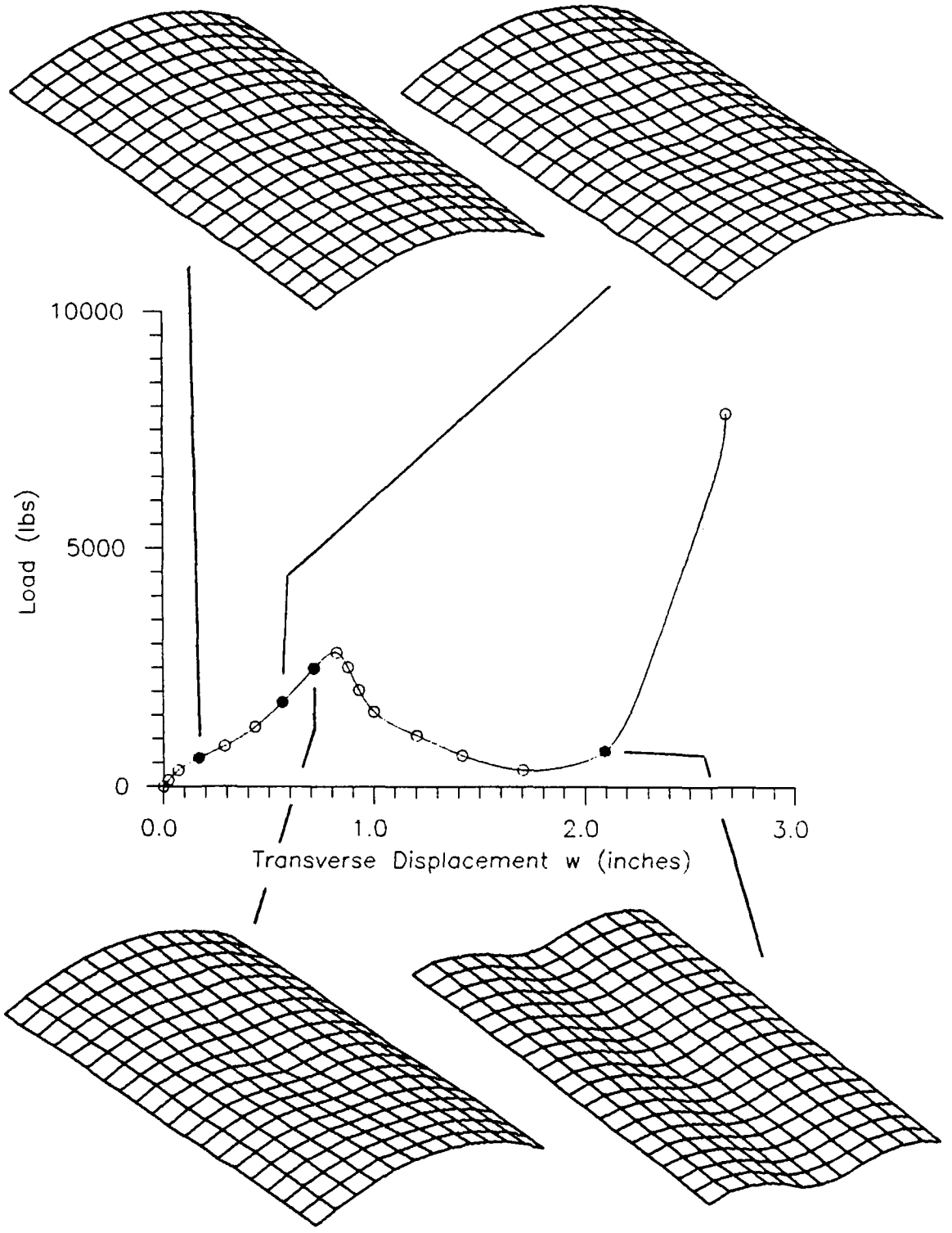

Figure C-4. Contours, $[0_3/\mp45_3/90_3]_s$ Clamped 1 Radian Shell

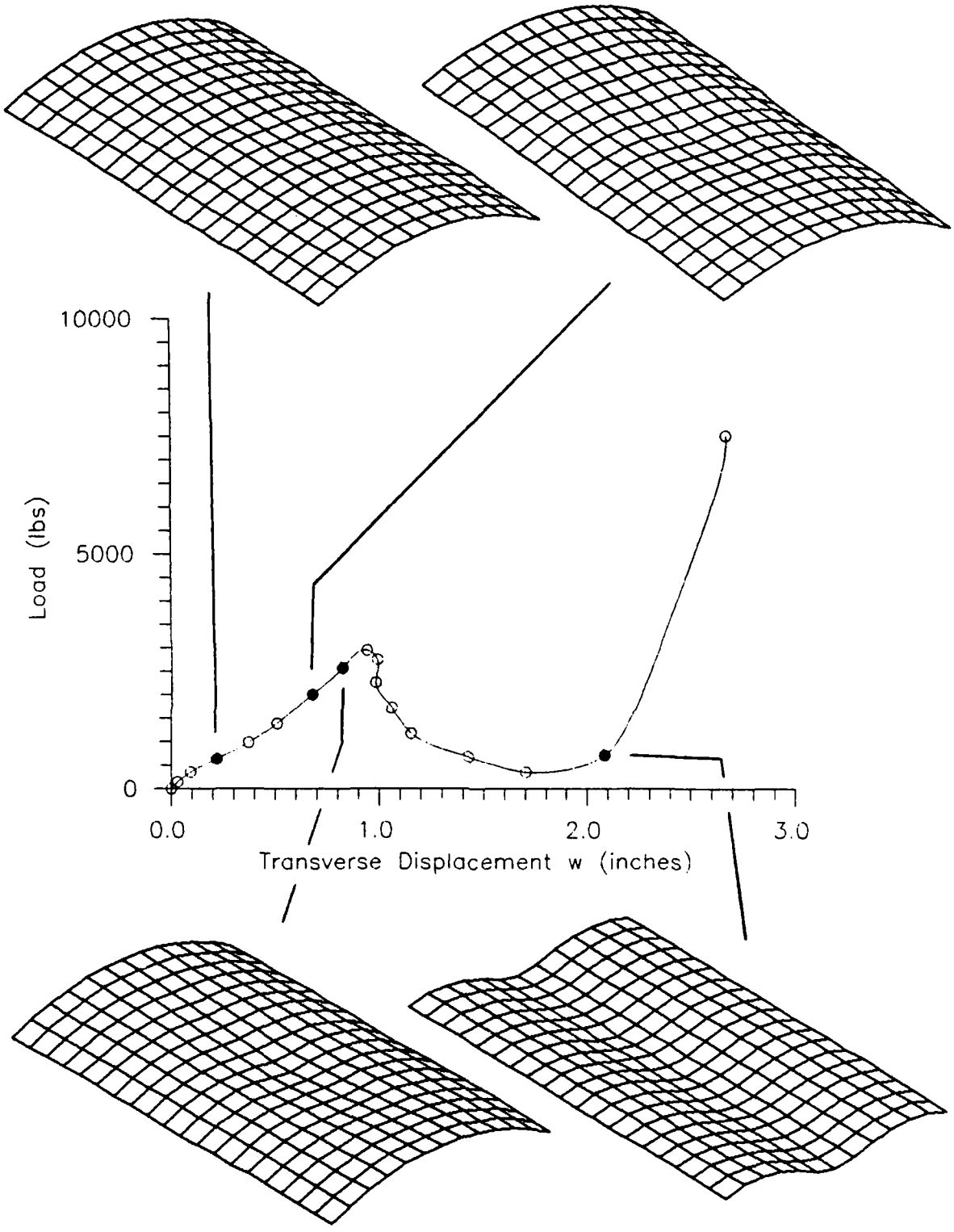

Figure C-5. Contours, $[0_6/90_6]_s$ Clamped 1 Radian Shell

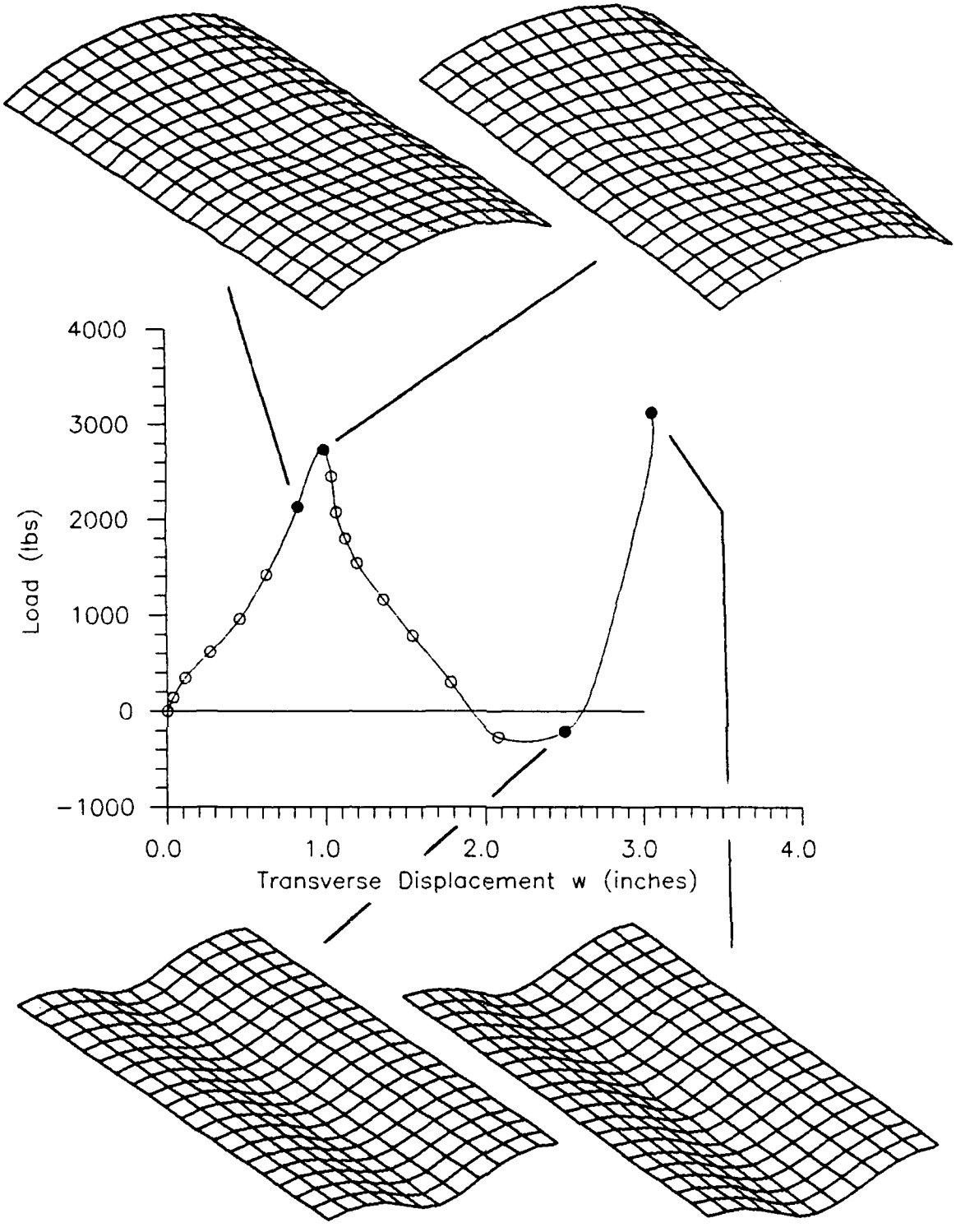

Figure C-6. Contours, $[0_6/90_6]_s$ Hinged 1 Radian Shell

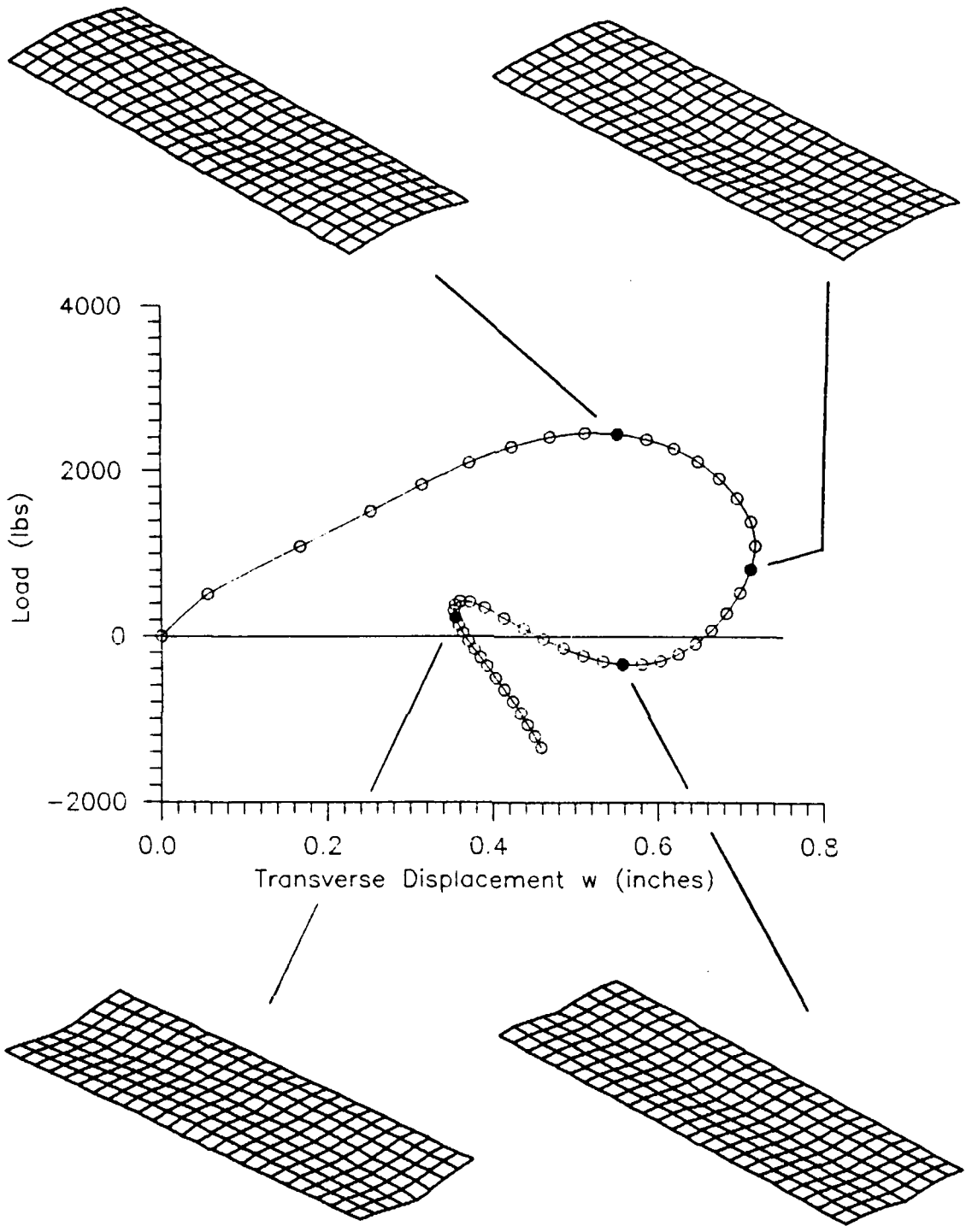

Figure C-7. Contours, $[0_3/\mp 45_3/90_3]_s$ Hinged 1/2 Radian Shell

BIBLIOGRAPHY

1. Ahmad, S. B.M. Irons and O.C. Zienkiewicz. "Analysis of Thick and Thin Shell Structures by Curved Finite Elements," International Journal of Numerical Methods in Engineering, 2: 419-451 (1970).

2. Bathe, K. J. and L. W. Ho. "Some Results in the Analysis of Thin Shell Structures," Nonlinear Finite Element Analysis in Structural Mechanics, ed. W. Wunderlich, E. Stein, and K. J. Bathe, 1981, Springer - Verlag Berlin, Heidelberg, NY, pp. 122-150.

3. Bergan, P.G., G. Horrigmoe, B. Kråkeland and T.H. Søriede. "Solution Techniques for Non-Linear Finite Element Problems," International Journal of Numerical Methods in Engineering, 12: 1677-1696 (1978).

4. Chang, F. and Z. Kutlu. "Strength and Response of Cylindrical Composite Shells Subjected to Out- of-Plane Loadings," Journal of Composite Materials, 23, 1: 11-31 (January 1989).

5. Chernyshev, G. "On the Action of Concentrated Forces and Moments on an Elastic Thin Shell of Arbitrary Shape." Journal of Applied Mathematics and Mechanics, 27, 1: 172-184 (1963).

6. Chung, S. and O. Widera. "A Theory for Non-Homogeneous Anisotropic Cylindrical Shells," Journal of Composite Materials, 6: 14-30 (January 1972).

7. Cook, R.D. Concepts and Applications of Finite Element Analysis, Second Edition, New York: John Wiley and Sons, 1981.

8. Crisfield, M.A. "A Fast Incremental/Iterative Solution Procedure That Handles 'Snap-Through'," Computers and Structures, 13: 55-62 (1981).

9. Dennis, Capt S.T. Large Displacement and Rotational Formulation for Laminated Cylindrical Shells Including Parabolic Transverse Shear. Ph.D dissertation. School of Engineering, Air Force Institute of Technology (AU), Wright - Patterson AFB, OH, June 1988.

10. Dennis, S.T. and A.N. Palazotto. "Large Displacement and Rotation Formulation for Laminated Shells Including Parabolic Transverse Shear," to appear in Nonlinear Mechanics.

11. Donnell, L.H. Stability of Thin-Walled Tubes Under Torsion. NACA Report 479, 1933.

12. Flügge, W. and R. Elling. "Singular Solutions for Shallow Shells," International Journal of Solids and Structures, 8, 2: 227-247 (February 1972).

13. Hinrichsen, R.L. and A.N. Palazotto. "Use of a Cubic Spline Function in Finite Elements," Mathematical Computer Modelling, 10, 1: 37-47 (1988).

14. Hoff, N.J. "The Accuracy of Donnell's Equations," Journal of Applied Mechanics, 22: 329-334 (1955).

15. Jahanshahi, A. "Force Singularities of Shallow Cylindrical Shells," Journal of Applied Mechanics, 30, 3: 342-346 (September 1963).

16. Jones, R.J. Mechanics of Composite Materials. Hemisphere Publishing Co, 1975.

17. Koiter, W.T. "A Consistent First Approximation in the General Theory of Thin Elastic Shells," Proceedings of the Symposium on the Theory of Thin Elastic Shells, 24-28 August 1959, pp. 12-33.

18. Knowles, J.K. and E. Reissner, "A Derivation of the Equations of Shell Theory for General Orthogonal Coordinates," Journal of Mathematics and Physics, 35: 351-358 (1959).

19. Morley, L.S.D. "An Improvement on Donnell's Approximation for Thin-Walled Circular Cylinders," Quarterly Journal of Mechanics and Applied Mathematics, 12: 89-99 (1959).

20. Moser, K. and A. Schmid. "Composite Structures - Modelling, Finite Element Analysis and Evaluation," Composite Structures, 11, 1: 33-55 (1989).

21. Palazotto, A.N., R.L. Hinrichsen and W.P. Witt. "Through - the - Thickness Considerations for Composite Plates with Large Displacements," Recent Advances in Structural Dynamics, 124: 47-53 (1987).

22. Palazotto, A.N. and W.P. Witt. "Formulation of a Nonlinear Compatible Finite Element for the Analysis of Laminated Composites," Computers and Structures, 21, 6: 1213-1234 (1985).

23. Ramm, E. "Strategies for Tracing The Non-Linear Response Near Limit Points," Nonlinear Finite Element Analysis in Structural Mechanics, ed. W. Wunderlich, E. Stein, and K. J. Bathe, 1981, Springer - Verlag Berlin, Heidelberg, NY, pp. 63-89.

24. Reddy, J.N. "Exact Solutions of Moderately Thick Laminated Shells," Journal of Engineering Mechanics, 110, 5: 794-809 (1984).

25. Reddy, J.N. and C.F. Liu. "A Higher Order Shear Deformation Theory of Laminated Composite Shells," International Journal of Engineering Science, 23, 3: 319-330 (1985).

26. Ren, J.G. "Exact Solutions for Laminated Cylindrical Shells in Cylindrical Bending," Composites Science and Technology, 29: 169-187 (1987).

27. Ren, J.G. "Analysis of Simply Supported Laminated Circular Cylindrical Shell Roofs," Composite Structures, 11, 4: 277-292 (1989).

28. Riks, E. "The Application of Newton's Method to Nonlinear Theories of Solids," Journal of Applied Mechanics, 39, 4: 1060-1065 (1972).

29. Riks, E. "An Incremental Approach to the Solution of Snapping and Buckling Problems," International Journal of Solids and Structures, 15: 529-551 (1979).

30. Saada, A.S. Elasticity, Theory and Applications. Krieger Publishing Co, 1987.

31. Sabir, A.B. and A.C. Lock. "The Application of Finite Elements to the Large Deflection Geometrically Non-linear Behaviour of Cylindrical Shells," Variational Methods in Engineering, ed. C. Brebbia and H. Tottenham, Southampton University Press, 1973, pp. 7/66-7/75.

32. Sanders, J.L. An Improved First-Approximation Theory for Thin Shells. NASA TR-24, 1959.

33. Sanders, J.L. "Singular Solutions to the Shallow Shell Equations," Journal of Applied Mechanics, 37, 2: 361-366 (June 1970).

34. Sanders, J.L. and J.G. Simmonds. "Concentrated Forces on Shallow Cylindrical Shells." Journal of Applied Mechanics, 37, 2: 367-373 (June 1970).

35. Simmonds, J.G. "A Set of Simple, Accurate Equations for Circular Cylindrical Elastic Shells," International Journal of Solids and Structures, 2: 522-541 (1966).

36. Tisler, Capt T. Collapse Analysis of Cylindrical Composite Panels with Large Cutouts Under Axial Load. MS Thesis, AFIT/GA/AA/86D- . School of Engineering, Air FOrce Institute of Technology (AU), Wright-Patterson AFB, OH, December 1986

37. Tsai, S.W. and H.T. Hahn. Introduction to Composite Materials. Technomic Publishing Co, 1980. (pp. 280-286)

38. Tsai, C.T. and A.N. Palazotto. "A Modified Riks Approach to Composite Shell Snapping Using High-Order Shear Deformation Theory," submitted for publication (1989).

39. Wempner, G.A. "Discrete Approximations Related to Nonlinear Theories of Solids," International Journal of Solids and Structures, 7: 1581-1599 (1971).

Vita

Captain Kevin J. Silva [redacted] accepted an appointment to the United States Air Force Academy in Colorado Springs, Colorado. After earning his Bachelor of Science degree in Engineering Sciences in May 1981 he served the Air Force as a mechanical engineer on the F-15 launched Anti-Satellite Missile development project at Air Force Space Division in Los Angeles, California, and later with the Peacekeeper Intercontinental Ballistic Missile Site Activation Task Force at F. E. Warren Air Force Base in Cheyenne, Wyoming. Captain Silva entered the Air Force Institute of Technology, School of Engineering in May 1988.

[redacted]

UNCLASSIFIED

SECURITY CLASSIFICATION OF THIS PAGE

REPORT DOCUMENTATION PAGE

Form Approved
OMB No. 0704-0188

1a. REPORT SECURITY CLASSIFICATION UNCLASSIFIED	1b. RESTRICTIVE MARKINGS
2a. SECURITY CLASSIFICATION AUTHORITY	3. DISTRIBUTION/AVAILABILITY OF REPORT Approved for public release; distribution unlimited.
2b. DECLASSIFICATION/DOWNGRADING SCHEDULE	
4. PERFORMING ORGANIZATION REPORT NUMBER(S) AFIT/GAE/ENY/89D-35	5. MONITORING ORGANIZATION REPORT NUMBER(S)
6a. NAME OF PERFORMING ORGANIZATION School of Engineering 6b. OFFICE SYMBOL (If applicable) AFIT/ENY	7a. NAME OF MONITORING ORGANIZATION
6c. ADDRESS (City, State, and ZIP Code) Air Force Institute of Technology (AU) Wright-Patterson AFB, OH 45433-6583	7b. ADDRESS (City, State, and ZIP Code)
8a. NAME OF FUNDING/SPONSORING ORGANIZATION AFOSR 8b. OFFICE SYMBOL (If applicable)	9. PROCUREMENT INSTRUMENT IDENTIFICATION NUMBER
8c. ADDRESS (City, State, and ZIP Code) Bolling AFB, Washington D.C.	10. SOURCE OF FUNDING NUMBERS PROGRAM ELEMENT NO. / PROJECT NO. / TASK NO. / WORK UNIT ACCESSION NO.

11. TITLE (Include Security Classification)
(U) FINITE ELEMENT INVESTIGATION OF A COMPOSITE CYLINDRICAL SHELL UNDER TRANSVERSE LOAD WITH THROUGH THICKNESS SHEAR AND SNAPPING

12. PERSONAL AUTHOR(S)
Kevin J. Silva, Captain, USAF

13a. TYPE OF REPORT	13b. TIME COVERED	14. DATE OF REPORT (Year, Month, Day)	15. PAGE COUNT
MS Thesis	FROM _____ TO _____	1989 December	135

16. SUPPLEMENTARY NOTATION

17. COSATI CODES			18. SUBJECT TERMS (Continue on reverse if necessary and identify by block number)
FIELD	GROUP	SUB-GROUP	composite structures, laminates, shells, cylindrical, transverse, shear
11	04		
20	11		

19. ABSTRACT (Continue on reverse if necessary and identify by block number)

Thesis Advisor: Dr Anthony N. Palazotto
Professor of Aerospace Engineering

ABSTRACT ON BACK

20. DISTRIBUTION/AVAILABILITY OF ABSTRACT ☒ UNCLASSIFIED/UNLIMITED ☐ SAME AS RPT. ☐ DTIC USERS	21. ABSTRACT SECURITY CLASSIFICATION UNCLASSIFIED
22a. NAME OF RESPONSIBLE INDIVIDUAL Dr Anthony N. Palazotto	22b. TELEPHONE (Include Area Code) (513) 255-3517 22c. OFFICE SYMBOL AFIT/ENY

DD Form 1473, JUN 86 *Previous editions are obsolete.*

SECURITY CLASSIFICATION OF THIS PAGE
UNCLASSIFIED

Block 19 Abstract

The static response of a laminated graphite/epoxy circular cylindrical open shell subjected to an inward point load is numerically investigated. The analysis uses a quasi two-dimensional thin shell finite element which incorporates parabolic transverse shear stress through the thickness, and uses either large displacement/rotation kinematics or a simpler Donnell formulation. A Riks solution algorithm enables tracking through critical load and displacement points during snap through. Ply layup, thickness, central angle and boundary conditions are independently varied. A comparison of Donnell and exact solutions is included.